Mixture Analysis by Metastable Mapping

by

Martin John Farncombe

Submitted to the University of Warwick in partial fulfilment of the degree of Doctor of Philosophy.

Department of Chemistry and Molecular Sciences
University of Warwick
Coventry
CV4 7AL

September 1983

To my parents,

and Peter,

and Alan.

Table of Contents

Acknowledgements

I acknowledge the financial support of the Science and Engineering Research Council and I.C.I. Petrochemicals and Plastics Division under the Co-operative Awards in Science and Engineering (CASE) Award scheme. I also thank the Department of Chemistry and Molecular Sciences, University of Warwick, for a travel grant.

Most projects are team efforts: I should first like to thank the heads of the teams involved in this work - Professor Keith Jennings and Dr. Jim Scrivens - for their help and constant encouragement. I should thank the members of the Warwick group (Roger Greathead, John Headley, Colin Moore, Mol Passman, Inder Katyal, Jim Laramee, Anil Shukla, David Brown, Willem Bouma etc.) and all those who helped me at Wilton (Norman Moore and his Merry Men, the programmers and Dr. Angus Hearmon). I also gratefully acknowledge the help of Alex Colburn, Ron Fathers, Eric Burgess and their respective staffs, and Iain, Deena and Bill from the Computer Unit. I am indebted to Ian Gregor, Graham Cooks, Derek Nelson, Dr. David Hirst and Prof. John Beynon for useful discussions. I should also like to thank Urs Schlunegger, Paul Cload and David Hutchinson for providing samples, and Sensei Mike Brown for showing me a gentler way. Last, but by no means least, I should like to thank Dr. Rod Mason (il miglior fabbro) for always being there to tell me how I should have done it.

"In the pursuit of learning, every day something is acquired.
In the pursuit of Tao, every day something is dropped."

Lao-Tzu: Tao Te Ching, Chapter 48.

Declaration

Parts of the work contained in this thesis have been published or accepted for publication. They are:-

G.A.Warburton, R.S.Stradling, M.J.Farncombe, R.S.Mason,
Org.Mass Spectrom., 16 (1981) 507

M.J.Farncombe, R.S.Mason, K.R.Jennings, J.Scrivens,
Int.J.Mass Spec.Ion Phys., 44 (1982) 91

R.S.Mason, M.J.Farncombe, K.R.Jennings, J.Scrivens,
Int.J.Mass Spec.Ion Phys., 48 (1983) 415

S.A.McLuckey, S.Verma, R.G.Cooks, M.J.Farncombe, R.S.Mason,
K.R.Jennings, Int.J.Mass Spec.Ion Phys., 48 (1983) 423

R.S.Mason, M.J.Farncombe, K.R.Jennings, R.G.Cooks,
Int.J.Mass Spec.Ion Phys., 43 (1982) 327

M.J.Farncombe, K.R.Jennings, R.S.Mason, U.P.Schlunegger,
to be published in Org.Mass Spectrom.

J.Scrivens,R.A.Hearmon, M.J.Farncombe,
to be published in Anal.Chem.

Parts of this work have also been presented at the 12th and 13th meetings of the British Mass Spectrometry Society (Cambridge 1981 and Coventry 1983), the 9th International Mass Spectrometry Conference (Vienna 1982).

The work described in chapters 2-7 was carried out with Dr. R.S. Mason and Prof. K.R. Jennings at the University of Warwick. The work described in chapter 8 was carried out with Dr. R.A. Hearmon and Dr. J. Scrivens at I.C.I. Petrochemicals and Plastics Division, Wilton.

List of Abbreviations

A	Kinetic energy release amplification factor
ARMS	Angle-resolved mass spectrometry
B	Magnetic sector field strength
CI	Chemical Ionization
CID	Collision-induced decomposition
CNL	Constant Neutral Loss linked scan
d.c.	Direct current
DIOP	Diisooctylphthalate
DOP	Dioctylphthalate
E	Electric sector field strength
EI	Electron Ionization
FA	Factor analysis
FAB	Fast atom bombardment
GC	Gas Chromatography
IE	Imbedded Error
IND	Indicator function
LC	Liquid chromatography
MS/MS	Mass Spectrometry/Mass Spectrometry
NMR	Nuclear Magnetic Resonance
PFK	Perfluorokerosene
RE	Real Error
r.f.	Radio frequency
T	Kinetic energy release
V	Accelerating voltage
XE	Extracted Error

List of Figures

List of Tables

Summary

This thesis describes a technique of practical use for the analysis of mixtures and the determination of organic ion structures which relies on the study of metastable and collision-induced decompositions which occur in the first field-free region of a forward-geometry double-focussing mass spectrometer. The technique, which is known as metastable mapping, works by scanning the magnetic field of the mass spectrometer in the usual way and decreasing the electric sector field slightly at the end of each magnetic field scan. The data are collected by a standard commercial data system and may be processed to produce simulated linked scans or a 'map' of parent ion mass against daughter ion mass. A theoretical explanation of the shapes of the peaks is given and the resolution, sensitivity, and susceptibility of the technique to artifact peaks are discussed. The metastable maps of a number of compounds and mixtures are presented to illustrate the use of the technique for mixture analysis and the differentiation of isomeric ions. A study of some ions scattered off the optical axis of the mass spectrometer is also discussed. A computer program, based on the statistical method of factor analysis, which can be used to deconvolute the mass or carbon-13 NMR spectra of mixtures has also been developed. A description of the program, which has been implemented on a small laboratory microcomputer is given and some results are presented which show the practicability of the technique.

1. Introduction

Mass spectrometry has for many years provided a sensitive tool for the determination of gas phase organic ion structures, but the technique has been less successful at identifying the components of mixtures because the signals from a minor species are often masked by fragment peaks for the major components. Methods such as chemical ionization, field desorption and mass spectrometry/mass spectrometry, as well as the traditional on-line chromatographic techniques, have all been used to overcome this problem. This thesis describes two methods of analysing mixtures which do not involve the prior separation of the components: the data for the entire mixture (or set of mixtures) are obtained and the components are identified from these. The first method, known as metastable mapping, involves the collection of some, or all, of the metastable or collision-induced decomposition products in a field-free region of a double-focussing mass spectrometer by a standard commercial data system. Software has been written which can process the data to simulate linked scans or two- or three-dimensional maps which can show how ions from the components of the sample fragmented.

The second method of mixture analysis described in this thesis is based on the multivariate statistical technique of factor analysis. A program has been written for a laboratory microcomputer which analyses the dissimilarities of different mixture spectra of the same components and extracts the spectra of the pure components and their concentrations in the various mixtures. The technique has been applied to the mass and carbon-13 NMR spectra of a number of mixtures of organic compounds. A new method of determining the number of components in a mixture is also described.

Chapter 2 describes some of the techniques which have been used to analyse mixtures, and discusses the types of ions observed in a mass spectrometer and the methods of detecting them. Chapter 3 sets out the theory of linked scans and metastable mapping, and chapter 4 describes how the maps were acquired and processed. Chapter 5 discusses the metastable maps of some simple compounds and gives an explanation for the shapes of the peaks on the map and in linked scans. A formula is derived which allows the determination of the amount of kinetic energy released during the decompositon from the degree of uncertainty in the mass of the parent ion. Chapter 6 describes a method, based on the electrostatic deflection of the beam, of observing ions which have been scattered off the optical axis of the mass spectrometer. Metastable maps of a number of compounds of both biological and industrial interest are presented and discussed in chapter 7: for example, a pair of phthalate isomers are distinguished and the amino-acid sequences of three simple peptides are determined. This chapter also contains an assessment of metastable mapping and some suggestions as to how the technique might be improved. Chapter 8 describes the statistical analysis of some mixture spectra by factor analysis.

2. Methods of Mixture Analysis

2.1 The Need for Mixture Analysis

It has been pointed out {1} that as we pollute the world we live in the need for mixture analysis becomes greater. Indeed, most of the work of the analytical chemist is concerned with the identification and quantification of the components of mixtures. For example, many industrial products will be multicomponent mixtures, by accident or design, and the price obtainable for them will often depend on the type and amount of the components present. Biological samples will almost certainly be mixtures, and here the rapid identification of trace impurities can be especially important.

2.2 Alternatives to Mass Spectrometry

Methods of mixture analysis can be divided into two general classes. Methods of the first type attempt to separate the mixture into its components and analyse them individually and those of the second type attempt to extract information about the components from the results for the entire mixture. The techniques described in this thesis fall into this second catagory.

Examples of techniques which fall into the first catagory are the chromatographic methods. Once a sample has been received for analysis, it is important that it be kept

free from further contamination. Chromatographic techniques fail to do this, because the sample is deliberately contaminated with large amounts of stationary and mobile phases which must be subsequently removed. In addition, some components of a mixture might not be amenable to chromatographic separation because, for example, they are insoluble or involatile. Chromatographic techniques are cheap and sensitive, but they can offer little information about the structure of individual components unless they are coupled to expensive detectors such as NMR instruments, or mass or infra-red spectrometers. Chromatography can also be very slow and can require extensive sample work-up, and if the analysis needs to be very rapid one must turn to a technique such as mass spectrometry {2}.

Amongst the second class of techniques - those which attempt to extract information about the components from the data for the entire mixture - lie methods such as computer data base searching {3} and multivariate statistical methods such as Factor Analysis {4}, which are known by the generic name of chemometrics {5}. An example of a statistical technique applied to the NMR and mass spectra of a set of mixtures is described in Chapter 8.

2.3 Basic Mass Spectrometry

Every mass spectrometer can be divided into three parts; it will have some method of producing ions, some means of separating them according to their mass-to-charge ratios, and some means of detecting them.

2.3.1 Ion Production

The most commonly-used means of producing ions in a mass spectrometer is electron ionization (EI), where the ionization is caused by high-energy electrons, produced from a hot metal filament, colliding inelastically with a molecule in the gas phase. The electrons' energies are large when compared to the ionization energy of an organic molecule, which is usually about 10 eV, and the ion can be formed with a large amount of energy which may be channelled into bond cleavage and rearrangement reactions and give rise to fragment ions. The daughter ions so produced may contain enough internal energy to fragment further, thus producing the complex spectra typical of EI {6}.

2.3.2 Ion Separation

It is assumed throughout this section that ions leaving the source have been accelerated by a potential of several thousand volts. The mass-analyser of a mass spectrometer has two purposes: it must be able to separate the ions according to their mass-to-charge ratios and must obtain the maximum resolved ion intensities. The first action is dispersive while the second is focussing.

An ion moving through a magnetic field experiences a force perpendicular to both the field and the ion's direction of flight, and it will describe a circular

path through such a field. The radius of the path followed is dependent on the mass and the velocity of the ion, and so the field disperses ions according to their momenta. An electromagnet used as a mass disperser also has the property of bringing an angularly divergent beam to focus at a single point {7} and may thus be said to be direction-focussing.

An important property of a dispersing field is its ability to separate ions of similar mass, M and $M+\Delta M$. A popular definition of the resolving power, known as the 10% valley definition, is the value of $M/\Delta M$ at which the height of the valley between two peaks of equal height is 10% of their intensity {12}.

The resolution of a magnetic sector is governed by the radius of the ions' path, the sizes of any slits at the entrance and exit of the sector, the aberrations in the ion optical system and the energy spread of the ion beam {7}. Of these, the only factors which can be altered without changing the geometry of the instrument are the slit dimensions and the energy spread of the incoming ion beam. Although the former improves resolution at the cost of beam intensity, the resolution can be helped considerably by placing an electric sector before or after the magnetic sector without major losses in sensitivity.

A radial electrostatic field between two sector-shaped coaxial cylindrical electrodes will act as

an energy dispersing device because the centripetal acceleration of an ion is dependent on its kinetic energy. An electric sector is velocity-dispersing because ions of slightly greater velocity than the norm will be deflected less and slightly slower ions will be deflected more. The sector can be used as an energy filter because ions of a certain energy will be focussed at a particular point after the electric sector, and all others can be filtered out by means of a suitably placed slit. This monoenergetic beam of ions may then be transmitted to the magnetic sector and high mass resolution will be obtained. If there was a considerable spread in the energies of the ions leaving the source a very sharp loss in intensity would be noted, however, because most of the ion beam would be filtered out. Ions leaving the source will have a distribution in both direction and velocity, and when they enter an electric sector, ions of different velocities will be focussed at different points on a plane perpendicular to the direction of flight. The magnetic sector will focus ions of the same mass, regardless of their position on this plane, at a single point, where they may be detected. Such a double-focussing mass spectrometer combines high mass resolution and high sensitivity. The instruments used for this work were of the Nier-Johnson geometry {8} where the electric sector precedes the magnetic sector (see Figure 2.1). Machines of reversed geometry, where the magnetic sector precedes the electric sector, will be discussed later.

Figure 2.1 A Diagram of a Forward-geometry Mass Spectrometer.

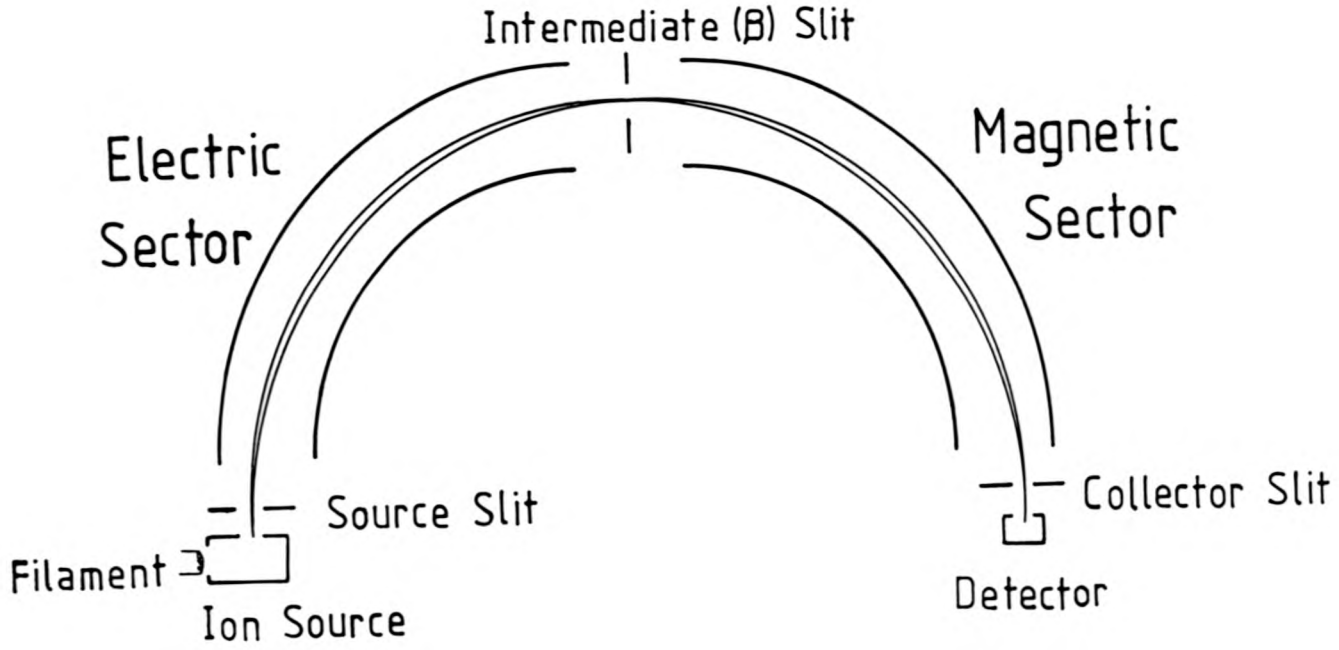

Apart from the magnetic field, other devices can be used as mass-analysers if they exploit some property of an ion which is dependent on its mass. For example, in an Ion Cyclotron Resonance spectrometer {9}, the ions absorb energy from a radio-frequency (r.f.) electric field perpendicular to a magnetic field when its frequency is equal to the cyclotron frequency of the ion (w). This is related to the strength of the magnetic field (B) and the mass-to-charge ratio (m/e) of the ion by $w = eB/m$ and a mass spectrum may thus be generated by measuring the r.f. absorbance while scanning the magnetic field. Ion Cyclotron Resonance instruments have recently become popular because of the use of Fourier transform techniques and the advent of large computers, and instruments with very high mass resolution can now be obtained {10}.

Ions of different mass-to-charge ratios accelerated from an ion source will acquire the same kinetic energy but will have different velocities. This can be exploited by measuring the arrival time of the ions at the detector of a time-of-flight mass spectrometer {11}. Such machines have again enjoyed a recent revival in popularity because of their theoretically unlimited mass range.

In a quadrupole mass spectrometer, the ions are trapped in an electric field generated by d.c. and r.f. potentials applied between opposite pairs of cylindrical or hyperbolic rods. Only ions of a particular

mass-to-charge ratio will be transmitted by the field. Such instruments have a relatively low mass range and resolution when compared to sector instruments, but they are cheap and comparatively easy to use. They may also be readily controlled by computers and very fast field scan rates may be obtained.

2.3.3 Ion Detection

Perhaps the simplest way of detecting the ions is to use a Faraday cup, where the ions hit a metal 'bucket' and the resulting charge is amplified and recorded. The detector is sensitive only to the number and charges of the ions which reach it. The more sensitive electron multiplier has a series of curved plates which emit electrons when struck by a charged particle. An ion hitting the first plate will cause a cascade of electrons to reach the end of the detector. The electron multiplier has a much faster response than the Faraday cup, but its output is dependent on the kinetic energy of the ions. Photomultipliers are similar to electron multipliers, but the ions strike a scintillator plate which emits photons, and these cause a cascade of electrons to be detected. These detectors are much less sensitive to the ions' kinetic energy, however.

Once amplified, the signal may by passed to a pen recorder or an ultra-violet recorder (12) or to a computer. Such computers can collect the data and

digitize them, and in some cases, control the mass spectrometer. Most large data systems record the time, measured from the start of the scan, at which the ions are detected, and an acquired spectrum can be compared to that of a suitable reference compound and converted from a table of time-vs.-intensity to a mass spectrum. The calibrated scan can be stored on a magnetic medium such as a disk or tape and processed later {13}.

2.4 Mass Spectrometry in Mixture Analysis

A conventional mass spectrum consists of a large number of peaks, each of which is the result of a chemical reaction occurring somewhere in the mass spectrometer. If the sample is a mixture, the situation is more complicated, because it can be difficult to tell which of the low mass ions came from which, if any, of the higher mass ions. The molecular ion of one component may even be completely obscured by fragments from another. This section will attempt to review some of the techniques used to overcome these problems, and some other mass spectrometric techniques used for mixture analysis.

2.4.1 High-resolution Mass Spectrometry

The principal advantage of spectra taken under conditions of high mass resolution and accurate mass measurement over those taken under low resolution conditions is that the elemental composition of ions may be determined. Components of mixtures which give ions at

the same nominal mass (isobaric ions) may often be distinguished by increasing the resolution of the instrument and thus separating the peaks. The technique cannot be used to separate isobaric peaks from isomers.

2.4.2 On-line Chromatographic Techniques

These techniques involve chromatographic separation of a mixture and the analysis of its components by mass spectrometry. Three separative techniques have been used: gas chromatography (GC), liquid chromatography (LC) and thin-layer chromatography (TLC). Of these, the one most commonly used is GC. The sample, which must be fairly volatile, is injected into a stream of carrier gas (usually helium) which is flowing over a liquid stationary phase suspended on a solid support or coated on the walls of the column. Good peak separation and sensitivity may be obtained, especially with capillary columns, although problems may be encountered at the interface between the chromatograph and the mass spectrometer {12} because of the pressure differences between the column and the mass spectrometer.

Liquid chromatography can be useful when the samples are thermally labile or involatile but, again, the weak point is the interface because the pressure differences present in GC-MS are worse for LC-MS: both capillaries {14,15} and moving belts {16,17} have both been used as interfaces, however.

Compounds separated on thin polyamide layers have been introduced into an ion source via a standard probe and good spectra obtained {18} although each spot on the TLC plate had to be examined individually. Entire chromatograms have also been examined without further preparation by using secondary ion mass spectrometry (vide infra) although the sensitivity has been shown to be greater if the chromatogram is first transferred to a silver substrate {19}.

2.4.3 Soft Ionization Methods

Electron ionization is probably the most widely used form of ionization, but it does have limitations. Firstly, some polar compounds are too involatile to be studied. Secondly, the amount of energy imparted to the molecule during the ionization process means that a large amount of fragmentation results. A molecule may dissociate without giving rise to a molecular ion {20} even if low-energy electrons are used. The result is that EI mass spectra often carry a great deal of the total ion current concentrated in the fragment ions, which can be confusing if the spectrum is that of a mixture. One way to overcome this is to use an method of ionization which does not supply much excess energy to the ion. Perhaps the best known form of 'soft' ionization is chemical ionization (CI) {21}.

Consider, for example, an ion source containing a high partial pressure of methane and a much lower

partial pressure of the sample. Most of the ions generated by electron bombardment will be those from methane, some of which will act as Bronsted acids and will protonate the sample molecules: for example,

$$CH_5^+ + M \rightarrow MH^+ + CH_4 \ .$$

The energy supplied to the sample molecule (M) during the reaction, which controls the degree of fragmentation, is determined by the difference between the proton affinities of the sample and the conjugate base of the reagent gas (methane, in this case). The most widely used reagent gases are methane, isobutane and ammonia, although others have been used [23-25]. The degree of fragmentation will thus be greater for a given molecule protonated by methane, which has a proton affinity of 530 $kJmol^{-1}$, than it will be for the same molecule protonated by ammonia (865 $kJmol^{-1}$). If the components of the mixture have widely differing proton affinities, it may be possible selectively to ionize one of them by choosing a suitable reagent gas. The reagent ion may also be captured: for example, adduct ions are common in ammonia CI. Ions can be generated with precise amounts of energy by charge transfer processes, where the internal energy of the ion is determined by the difference between the ionization potential of the sample molecule and the recombination energy of the ionizing species [12].

Under chemical ionization conditions, the electrons emitted by the filament may be slowed down considerably and captured by the sample molecule to form negative

ions {26}. If the sample has a positive electron affinity the technique can be an extremely fast process {27}. Negative ion CI may also be used to form quasimolecular sample ions: attachment of chloride ions to the sample molecule and the extraction of protons by (for example) hydroxide ions {26,28} are possible.

It is also possible to use electric fields to ionize molcules. Intense fields can be generated at metallic edges, points and wires, and they can induce electrons to tunnel out of the molecule. This technique is known as field ionization {29} and the resulting ion has very little excess internal energy. Consequently, molecular weight information can be obtained, but little structurally revealing fragmentation occurs. A related technique is that of field desorption {30}, where the sample is coated onto, and ionization occurs on, the surface of a wire covered in small carbon fibres. Molecules may be similarly desorbed by the use of Californium fission fragments {31}, lasers {32}, or by the bombardment of the sample with ions (secondary ion mass spectrometry {33,34}) or atoms (fast atom bombardment {35-37}).

2.5 Metastable and Collision-induced Decompositions

2.5.1 Metastable Ions

Metastable ions are defined to undergo unimolecular decompositions which occur after the parent ion has left the source and before it reaches the collector. Their existence can be predicted from the quasi-equilibrium theory {6} by considering the ions formed in the source to have a range of internal energies which can lead to decompositions a few microseconds after excitation: it will take an ion of m/z 100 approximately fifteen microseconds to reach the detector of an MS-50 if it is accelerated by a potential of 8 kV. Such ions would have an internal energy range of 0.1 to 1 eV above decomposition threshold {6}. Ions formed with more energy would probably decompose in the source, and ions with energies below the decomposition threshold will reach the detector intact.

There are three field-free regions in a double-focussing mass spectrometer: one lies before the first analyser, the second between the analysers and the third before the collector. The products of metastable decompositions in the second of these field-free regions in a forward-geometry mass spectrometer may be observed in a normal mass spectrum as broad peaks of low intensity at non-integral masses, a phenomenon first

explained by Hipple and Condon in 1946 {38}. The peaks will appear at an apparent mass, m^*, given by

$$m^* = m_2^2 / m_1$$

where m_1 is the mass of the parent ion and m_2 is the mass of the daughter ion. The peaks are broad because some of the internal energy of the fragmenting species is released as excess translational energy of the fragments leaving the daughter ions with a range of velocities which results in an apparent uncertainty in the momentum of the peak. The magnitude of this kinetic energy release is small - it is usually less than 1 eV - but the peaks observed have substantial spectral widths because the energy is released in the centre-of-mass coordinate system and the fragments are observed in the laboratory coordinate system. When converting from one system to the other, a large amplification factor, A, results {39}. For singly charged ions, this is given by

$$A^2 = 16(eV/T).((m_1-m_2)m_2)/m_1^2.$$

It may be observed that the factor is inversely proportional to the magnitude of the energy release (T). Very small kinetic energy releases may thus be observed because they result in large amplification factors.

2.5.2 Collision-induced decompositions

If ions do not undergo unimolecular dissociation it is possible to induce decomposition by supplying them with excess energy by a process known as collision-induced decomposition (CID). If the ion beam passes through a collision chamber containing a gas,

usually located at, or close to, a focal point the ions will undergo collisions which convert some of their translational energy to internal energy. If the ions have energies of several thousand electronvolts, glancing collisions are sufficent to change their internal energy by up to 10 eV, but if they are moving more slowly, for example, in a quadrupole mass spectrometer, then 'head-on' collisions are required for activation and the fragments must be gathered together by an electric field {40}. For high-energy ions, very little energy is transferred to the target molecule, and thus the amount of translational energy lost by the ion will be approximately equal to the amount of internal energy it gains. The change of velocity of the ions results in a shift in the centre of the resulting peak from what would be expected for a metastable transition, and this shift can be used to determine the amount of energy deposited in the ion during the collision {6}.

An ion which undergoes a metastable decomposition has less energy available to it than one which has been collisionally activated, and both the fragmentation pattern from subsequent decomposition and the amount of the kinetic energy released during them can be different. There is a smaller proportion of peaks due to rearrangement reactions in a CID spectrum than in a metastable spectrum because there is much more energy available to the decomposing ion. The proportion of fragments which result from simple bond cleavages, rather than rearrangements, will thus be higher from

ions have been collisionally activated than from those which undergo metastable decompositions. The range of energies deposited in an ion by a collision is similar to that deposited by an impacting electron, and CID spectra are similar to those produced in the source under electron ionization conditions, and can be compared to libraries of EI spectra. Because the ion has more energy available to it after collisional activation, more internal energy may be released as translational energy and so the velocity spread of the daughter ions after the fragmentation may be larger and thus broaden the peak, because the activation of the ion by collision is much faster than a bond vibration. CID may be regarded as a two-stage process: the activation of the ion followed by its unimolecular decomposition.

2.5.3 Uses for Mixture Analysis

In a mass spectrometer of Nier-Johnson geometry, the products of decompositions in the first field-free region would not normally be observed because the electric sector would filter them out. The product of a second field-free region decomposition will be observed in the normal mass spectrum as a broad peak. The products of decompositions in the third field-free region cannot be distinguished from their parent ions unless a special detector is used [41].

The situation is similar for instruments of reversed geometry for decompositions in the first and

third field-free regions, but ions may be mass-selected by the magnetic sector and their second field-free region decomposition products may be examined by altering the electric sector field.

Metastable and collision-induced decompositions are useful for mixture analysis because the means of detecting their products allow access to both the parent ion mass and the daughter ion mass. For a first field-free region decomposition in a forward-geometry mass spectrometer the ratio by which the electric sector field must be decreased to allow the daughter ion to pass through and the apparent mass at which it appears after traversing the magnetic field are both dependent on these masses.

2.6 Various Methods of Scanning

There are three participants in the unimolecular decomposition of an ion: the parent ion, the daughter ion and the neutral fragment. This section studies ways in which one of these may be regarded as constant during a series of decompositions and the other two studied.

2.6.1 Constant Parent Scans

Methods of scanning the mass spectrometer which lead to a spectrum of all of the daughters of a selected ion are discussed here. The simplest of these may only be used on reversed geometry mass spectrometers: the

magnetic sector may be used to select ions of a certain mass and their second field-free region metastable or collision-induced decompositions may be studied by scanning the electric sector field {42}. The observed peaks arise from the collection of the daughter ions and are broadened by the release of internal energy during the decomposition. Such a scan has been called {43} a Mass-analysed Ion Kinetic Energy scan. The MIKE scan will be further discussed in section 2.7.1

It has been shown {44,45} that if the magnetic sector field (B) and the electric sector field (E) are scanned such that the ratio B/E remains constant then the daughter ions which are detected all arise from a selected parent ion. This scan is discussed further in section 3.1.1.1.

It is also possible to achieve the same result by scanning the accelerating (V) and electric sector (E) fields in such a manner that the ratio of V/E^2 remains constant {46,47}. The magnetic field is set to transmit the parent ion and the V and E are scanned upwards. Because the momentum of the ions collected is constant, the resulting data do not constitute a mass spectrum, but form an energy spectrum of the daughter ions of a chosen parent ion. Because the sensitivity of an ion source is dependent on the accelerating voltage the mass range of this scan is limited to a factor of about two, and the scan has been largely replaced by the B/E scan.

2.6.2 Constant Daughter Scans

The methods of scanning discussed here allow the masses of all of the parent ions of a given daughter ion to be deduced. If the magnetic field is adjusted to transmit a specific daughter ion from decompositions in the source, the parent ions of decompositions which give that ion in the first field-free region can be detected by raising the kinetic energy of the parent ions - i.e. by increasing the accelerating voltage {48-50}. Again, the mass range is limited by the performance of the instrument when the accelerating voltage is changed. The peaks observed in the spectrum are broadened by the release of internal energy during the decompostion.

Similar results may be obtained without the limitations on the mass range by a scan of the magnetic and electric sector fields such that the ratio B^2/E remains constant {51}. The peaks observed are again broad. This scan is discussed further in section 3.1.1.2.

A spectrum of all the ions which decompose to give a certain ion in the second field-free region of a reversed geometry mass spectrometer can be obtained from a scan where the value of B^2E is constant. The peaks observed in this scan are very narrow.

2.6.3 The Constant Neutral Loss Scan

A scan in which the peaks detected are all due to decompositions in which a neutral fragment of constant mass is lost has been performed {54,55}. The magnetic and electric sector fields are scanned such that the ratio $B^2/E^2(1-E)$ remains constant. Another form of this scan has been suggested {56}, but it seems to offer little advantage over the previous one. The peaks in a constant neutral loss (CNL) linked scan are fairly narrow.

2.6.4 The Effects of Energy Release

The reason for the shape of the peaks in the scans described above can be seen by considering the velocity distribution of the daughter ions after the decomposition. The direction of flight of the ions can be defined as the x-direction, the direction of the magnetic field as the z-direction, and the direction of the electric sector field as the y-direction. The products of a decomposition after the ion has left the source will spread out as an exploding sphere and because the magnetic sector acts as a momentum filter, in scans where only one of the three fields (B, E and V) is altered, ions with components of velocity in the x- and y-directions will pass through the collector slit even after the appropriate field has been adjusted to transmit a slightly different mass and will cause an apparent mass broadening {53}.

If more than one field is being scanned simultaneously, the width of the peaks depends on the velocity discrimination of the combination of the fields used. The deflection of an ion in a magnetic sector is dependent on its momentum, and thus its velocity, whereas its behaviour in the other two fields is related to its kinetic energy, and thus to the square of its velocity. If the two parameters in the linked scan do not have the same velocity dependence, only ions of a certain velocity will be transmitted and the peak will be sharp. If their velocity dependence is the same, however, the full range of velocities will be transmitted and the peak will be broad. Broad peaks from metastable or collision-induced decompositions will thus be observed in the B^2/E linked scan and in normal mass spectra, accelerating voltage and MIKE spectra. This is discussed further in section 5.3.

The shape of a metastable peak in the normal mass spectrum can be altered by improving the mass and energy resolution of the mass spectrometer {57}. The magnitude of the kinetic energy release can also be calculated from the width of the peak in such a scan {39,58}.

2.7 Mass Spectrometry/Mass Spectrometry

This section is concerned with a technique known as mass spectrometry/mass spectrometry (MS/MS) in which the decomposition products of an ion selected by one mass-analyser are studied with another mass analyser. The

role of the first mass analyser has been likened to that of a gas or liquid chromatograph in that it can separate out single components of a mixture for analysis {59}. The use of such instruments has been extensively reviewed {1,40,59-62}. Such techniques require the use of mass spectrometers with geometries other than the Nier-Johnson.

2.7.1 Reversed Geometry Instruments

The simplest, and perhaps the most popular, type of MS/MS instrument is the reversed geometry mass spectrometer, in which the magnetic sector precedes the electric sector. The peaks observed in a MIKE spectrum are broad due to the release of internal energy, and this 'can seriously limit the resolution of the spectrum' {62}, especially when collision-induced decompositions are being studied, where more internal energy is available for conversion into translational energy of the fragments. Such instruments can also achieve very good resolution for ions formed in the source {42,43,63}.

2.7.2 Triple Quadrupole Instruments

The first and second mass-analysers are both quadrupole filters in such instruments, and the central collision cell consists of a quadrupole with no d.c. voltage applied, which acts to contain the fragments {40,64-68}. Constant daughter, constant parent and CNL scans may all be simply and rapidly performed under

computer control. Unit resolution can be obtained from both mass spectrometers.

2.7.3 Multisector Instruments

In instruments where an electric sector follows a mass spectrometer of forward geometry, MIKE spectra of ions selected at high mass resolution can be obtained {69-73}. Instruments have been constructed which have four sectors, which can theoretically achieve both high parent ion and daughter ion resolution {74,75}.

The design of multisector instruments has been recently reviewed {76} and it was concluded that the best three-analyser combinations were that of a reversed geometry mass spectrometer followed by either another magnetic sector or a quadrupole mass filter. The latter offers either high-resolution parent ion selection followed by unit mass daughter ion resolution or a MIKE spectrum with improved resolution. The instrument with two magnetic sectors offers high resolution parent ion or daughter ion selection.

3. Theory of the Metastable Map

After every metastable or collision-induced decomposition the kinetic energy and momentum of the parent ion will be partitioned between the daughter ion and the neutral fragment. The daughter ion so produced may have to pass through kinetic energy or momentum filters, depending on where the decomposition occurs, and the resulting peak may not be observed in the same way as those arising from decompostions occurring in the ion source. These differences in observation methods may be used to determine uniquely the masses of both the parent and daughter ions in a transition. This chapter attempts to explain the theoretical background to the metastable map and three of the linked scans. The phrase 'metastable map' is used to refer to a set of peaks which represent the products of unimolecular or collision-induced decompositions displayed either as a plot of the magnetic field strength against the electric sector field strength or as a plot of parent ion mass vs. daughter ion mass.

3.1 Position of a Peak on the B,E′ Plane

When an ion enters the radial electric field present in the electric sector of a mass spectrometer, it experiences a force perpendicular to its direction of motion and follows a uniform circular path (assuming that it passes equidistant between the sector plates). The force on the ion is defined by $F = e.E$ where e is the ion's charge and E is the field strength {77}. The ion undergoes a centripetal acceleration, and we may thus write

$$F = m_1 v_1^2 / r = E_1 e$$

or $E_1 e = 2V/r$

because $Ve = (1/2)m_1 v_1^2$

where E_1 is the field between the sector plates, m_1 and v_1 are the ion's mass and velocity, V is the accelerating potential and r is the radius of the electric sector. The deflection of the ion is thus dependent on its kinetic energy. If a daughter ion from a decomposition in the first field-free region is to pass through the electric sector, the sector field must be reduced from the value required to transmit the parent ion, E_1, to a lower value, E_2, given by

$$E_2 = (m_2/m_1).E_1$$

thus $$E' = E_2/E_1 = m_2/m_1 \quad .$$

Ions passing through a uniform magnetic field experience a force given by F = Bev perpendicular to their direction of motion, where B is the field strength. Again, the path they follow will be circular, and thus

$$Bev = m_1 v_1^2/R \quad \text{or} \quad BeR = m_1 v_1$$

where R is the radius of the ions' path. The magnetic sector will thus act as a momentum filter. By considering the kinetic energy gained by the ions during acceleration, and by eliminating their velocity, it can be seen that

as $$Ve = (1/2)m_1 v_1^2$$

and $$BeR = m_1 v_1 \quad .$$

Thus $$2Vem_1 = B^2R^2e^2$$

or $$m_1/e = B^2R^2/2V \quad .$$

This equation is only true for ions formed in the source. If an ion decomposes after it has been accelerated, its momentum will be partitioned between the fragments in the

ratio of their masses, and a daughter ion, m_2, will not be observed at the same value of B as that required for the parent ion. If these daughter ions are transmitted at a field strength B^*, such that

$$m_2 v_1 = B^* eR$$

and if the mass of a hypothetical ion formed in the source and collected at this same field strength is m^*, then, by equating the momenta of the ions,

$$m^*/e = B^{*2}R^2/2V$$

$$2m^*eV = B^{*2}e^2R^2 = m_2^2 v_1^2$$

$$2m^*(1/2)m_1 v_1^2 = m_2^2 v_1^2$$

Thus $$m^* = m_2^2/m_1 \quad .$$

It is at this apparent mass that the peak will be observed.

It is thus possible to determine where the peaks arising from transitions in the various field-free regions of a double-focussing mass spectrometer will fall on a plane described by B (the magnetic field) and E (the electric field) by considering what combinations of electric and magnetic sectors the daughter ions must pass through before they are collected.

3.1.1 Three Linked Scans

This section considers in more detail the three linked scans which can be used on instruments of both geometries and which are simulated by the programs described later. All of these scans detect the daughter ions from decompositions in the first field-free region, but the ratio of B to E is different in each linked

scan. Scan laws have been derived {55,78,79} in which the ratio is dependent on the value of the mass of the parent ion (m_1), the daughter ion mass (m_2), or the mass of the neutral fragment (m_3). The peaks observed in such scans will then be due to decompositions which involve that particular ion or fragment.

3.1.1.1 The B/E Linked Scan

In this type of scan, the magnetic and electric field strengths, B and E, are altered simultaneously such that the ratio B/E is kept constant. If the instrument is adjusted so that the parent ion of a transition in the first field-free region is transmitted at values of the magnetic and electric field strengths B_1 and E_1, and if these fields are then altered to allow the daughter ion to be detected at $B=B^*$ and $E=E^*$, then the apparent mass, m^*, at which the daughter ion will be observed is given by {78}

$$m^* = B^{*2}R^2/2V = m_2^2/m_1$$

But since $E' = E^*/E_1 = m_2/m_1$

$$m^* = m_1E'^2$$

So $$B^{*2}R^2/2V = m_1(E^*/E_1)^2$$

Rearranging, $$B^*/E^* = \sqrt{2Vm_1}/RE_1$$

Because this constant is not dependent on m_2 where the ratio of B to E is kept constant will yield peaks which correspond to all the daughters of a given parent ion.

scan. Scan laws have been derived {55,78,79} in which the ratio is dependent on the value of the mass of the parent ion (m_1), the daughter ion mass (m_2), or the mass of the neutral fragment (m_3). The peaks observed in such scans will then be due to decompositions which involve that particular ion or fragment.

3.1.1.1 The B/E Linked Scan

In this type of scan, the magnetic and electric field strengths, B and E, are altered simultaneously such that the ratio B/E is kept constant. If the instrument is adjusted so that the parent ion of a transition in the first field-free region is transmitted at values of the magnetic and electric field strengths B_1 and E_1, and if these fields are then altered to allow the daughter ion to be detected at $B=B^*$ and $E=E^*$, then the apparent mass, m^*, at which the daughter ion will be observed is given by {78}

$$m^* = B^{*2}R^2/2V = m_2^2/m_1$$

But since $E' = E^*/E_1 = m_2/m_1$

$$m^* = m_1E'^2$$

So $$B^{*2}R^2/2V = m_1(E^*/E_1)^2$$

Rearranging, $$B^*/E^* = \sqrt{2Vm_1}/RE_1$$

Because this constant is not dependent on m_2 where the ratio of B to E is kept constant will yield peaks which correspond to all the daughters of a given parent ion.

3.1.1.2 The B^2/E Linked Scan

In this scan, the ratio of the electric field strength to the square of the magnetic field strength is kept constant. If the daughter ions from transitions in the source are transmitted at $B=B_2$ and $E=E_2$, and if B and E are then decreased to detect the transitions at $B=B^*$ and $E=E^*$, then

$$m^* = m_2^2/m_1 = m_2E'$$

where $E' = E^*/E_2 = m_2/m_1$

Thus $B^{*2}R^2/2V = m_2(E^*/E_2)$

$$B^{*2}/E^* = 2Vm_2/R^2E_2$$

A scan where this ratio is kept constant will thus detect the products of all transitions in which the mass of the daughter ion is m_2.

3.1.1.3 The Constant Neutral Loss Linked Scan

The peaks observed in this linked scan are due to decompositions which give rise to a neutral fragment of a specified mass. As before,

$$m^* = B^{*2}R^2/2V = m_2^2/m_1 = m_1E'^2$$

where $E' = m_2/m_1 = 1-(m_3/m_1)$

Thus $m_1 = m_3/(1-E')$

and $m^* = m_3E'^2/(1-E')$

Rearranging, $B^{*2}(1-E')/E'^2 = 2m_3V/R^2$

Thus a scan where B and E are varied so as to keep this ratio constant will only show peaks from transitions in the first field-free region where a

neutral fragment of mass m_3 was lost.

3.1.2 Forward Geometry Instruments

In mass spectrometers where the electric sector precedes the magnetic sector, the products of decompositions in the first field-free region must pass through both sectors, and so the resulting peak will not be seen at normal mass or E′ values. Peaks which result from decompositions in the second field-free region, however, only need pass through the magnetic sector before collection, and so will be observed at the same E′ value as those arising from decomposition in the source (i.e. E′=1). This is represented in Figure 3.1a, where it can be seen that only first field-free region decompositions give rise to peaks with values of E′ of less than one, and that the three linked scans described above will all detect this transition.

3.1.3 Reversed Geometry Instruments

In mass spectrometers where the magnetic sector precedes the electric sector, daughter ions formed in the first field-free region also pass through both sectors and the resulting peak appears on the plane in the same position as that for instruments of the other geometry (see Figure 3.1b). The daughter ions from decompositions in the second field-free region will be energy-analysed, but not mass-analysed, and thus appear at the same value of E′ as those from first field-free

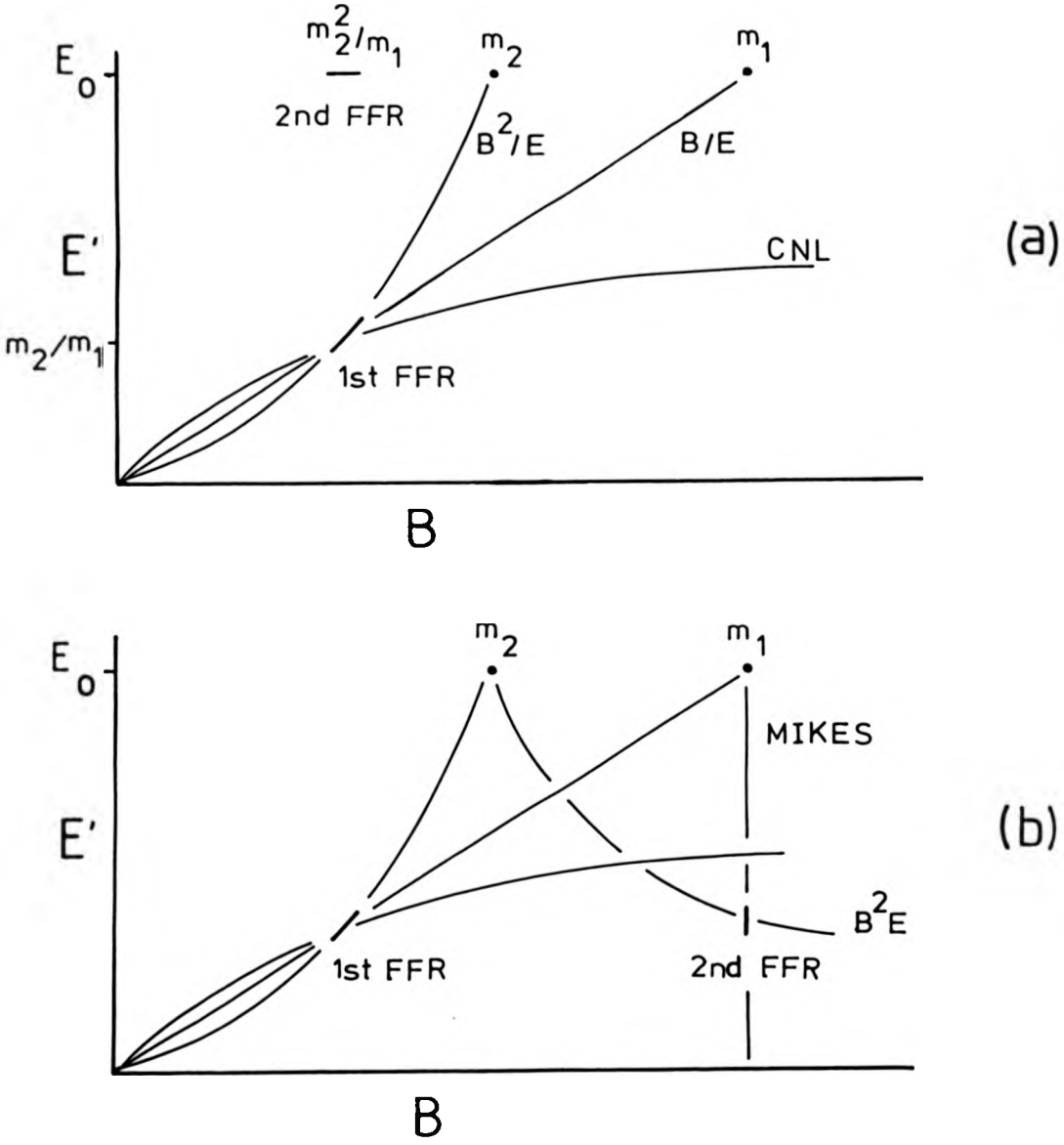

Figure 3.1 The positions of first and second field-free region metastable peaks on the B,E' plane, in
a) Forward-geometry mass spectrometers, and
b) Reversed-geometry mass spectrometers.

region transitions and at same value of B as the parent ion: these peaks may be detected by a MIKE scan or a B^2E linked scan {52}. Because there may be two peaks on the plane due to any given transition, linked scans designed to examine peaks from decompositions in the first field-free region might also detect peaks from second field-free region decompositions (and vice versa) thus giving rise to artifact peaks in the linked scans.

3.2 The History of Metastable Mapping

The phrase "metastable map" was first used in the literature in 1967 by Shannon et al. {80}, who produced a map using a mass spectrometer of Mattauch-Herzog geometry. On such an instrument, peaks over a wide mass range are detected simultaneously by a photoplate and the map was acquired by raising the accelerating potential. The experiment proved slow and the data difficult to extract from the photoplate, however.

Metastable ions have long been studied in double-focussing mass spectrometers either by raising the kinetic energy of the parent ions {81} (i.e. by increasing the accelerating potential), or by lowering the electric sector potential to allow the daughter ions to pass through {82,83}. Kiser has developed the latter method into a mapping technique {84} by scanning the magnetic field and decreasing the electric sector potential at the end of each scan, whereas Coutant and McLafferty {85} achieved the same end by scanning the magnetic field slowly and the electric

sector potential rapidly: this technique has also been used more recently {86-88}.

Lacey and Macdonald have acquired maps on forward- {89} and reversed-geometry {90} mass spectrometers and at high mass resolution {91}, and have studied the causes of artifact peaks on maps {92-94}. Their studies, however were of a more fundamental nature than those considered here, and were not primarily intended to produce maps of use in determining ion structures or the composition of mixtures.

Metastable mapping on double-focussing mass spectrometers has not been analytically useful until comparatively recently because the fast computers required for data acquisition and processing have not been commercially available. Another recent development is the introduction of triple-quadrupole mass spectrometers {64}, in which it is possible to perform constant-daughter, constant-parent and constant-neutral linked scans easily, and where it is also possible to select parent ions in turn with the first quadrupole, collisionally induce decompositions in the second, and obtain a mass spectrum of the daughter ions in the third, thus generating a metastable map {40}. The use of quadrupole filters and computer control makes it possible to acquire a map quickly. Such filters, however, suffer from the disadvantages of relatively low resolution and mass range. More recently, a metastable mapping experiment has been performed on a single sector instrument, involving the analysis of both the mass and arrival time of ions {95}.

4. Experimental Methods

4.1 The Method Used for this Work

The maps shown in this thesis were obtained by a metastable mapping system at the University of Warwick using MS-50 or MS-80 forward-geometry double-focussing mass spectrometers (Kratos Analytical Instruments Ltd.). The MS-50 has a 90° electric sector with a radius of 38.1 cm, a 90° magnetic sector with a radius of 30.5 cm, and can operate with accelerating potentials of up to 8 kV. The ions were detected by a photomultiplier tube. The MS-80 is similar, but the radius of the electric sector is 21.6 cm, the radius of the magnetic sector is 16.5 cm, it can only operate with accelerating potentials of up to 4 kV, and it was fitted with an electron multiplier instead of a photomultiplier. The fastest scan speeds available were three seconds per decade of mass for the MS-50 or one second per decade for the MS-80. Samples could be introduced via standard solids or liquids probes. Electron or chemical ionization methods were used. A collision cell, which was mounted in the isolation valve chamber between the source region and the electric sector of the MS-50, has been described previously [45]. The MS-80 did not have a collision cell fitted, and metastable maps obtained on that instrument were of unimolecular decompositions. It is possible that maps obtained under CI conditions on either instrument contained peaks formed by collision-induced decompositions, however. Mass spectra could be collected by

a Kratos DS-55 data system using standard software, or plotted on a chart recorder.

Three methods of mapping have been used previously for double-focussing mass spectrometers:-

1) Repetitively scan the magnetic field and slowly increase the accelerating voltage,
2) Scan the magnetic field slowly and repetitively scan the electric field downwards, or
3) Repetitively scan the magnetic field and slowly decrease the electric field.

Of these, the first is impracticable because the source conditions change during the scan, thus altering the sensitivity of the instrument. Both of the second and third methods have been used with some success, but the latter method was chosen because:-

1) The electric field is decreased slightly after each magnetic field scan, and so only one of the fields needs to be adjusted at a time,
2) The magnetic field scans on the mass spectrometers are reproducible and do not need to be controlled by a computer, and
3) The software needed to acquire mass-vs.-intensity data from the mass spectrometer during magnet scans was already written and tested.

It was thus decided to start and stop the magnetic field scans and collect the data using the DS-55 data system, and initially to use a microcomputer to decrease the electric sector potential slightly at the end of each scan.

4.2 Controlling the Mass Spectrometer

If the ion production and collection systems are ignored, the mass spectrometer may be regarded as having three components: an electric field which is used to accelerate the ions, another electric field which is used to energy-analyse them, and a magnetic field which is used to momentum-analyse them.

4.2.1 Manual Control of the MS-50

These three components are controlled in the MS-50 by means of reference voltages generated by a set of stable batteries, altered by the various controls of the mass spectrometer, and finally amplified to produce the appropriate field. In order to control the instrument by a computer, it is necessary to synthesize these voltages using a digital-to-analog (D/A) converter. Under normal operating conditions, the electric sector and magnetic sector references are generated from the batteries in Scan Control Unit 'C' (see Figure 4.1), and the accelerating voltage reference is generated from the electric sector reference in unit 'J'. The accelerating and energy-analysing fields are coupled to ensure that the ratio V/E remains constant so that the ions are transmitted by the electric sector. The accelerating voltage reference is then passed to the Source Supplies Unit 'B', where the voltage may be finely adjusted before being amplified to produce the accelerating field. The Metastable Unit 'M' can be used to generate

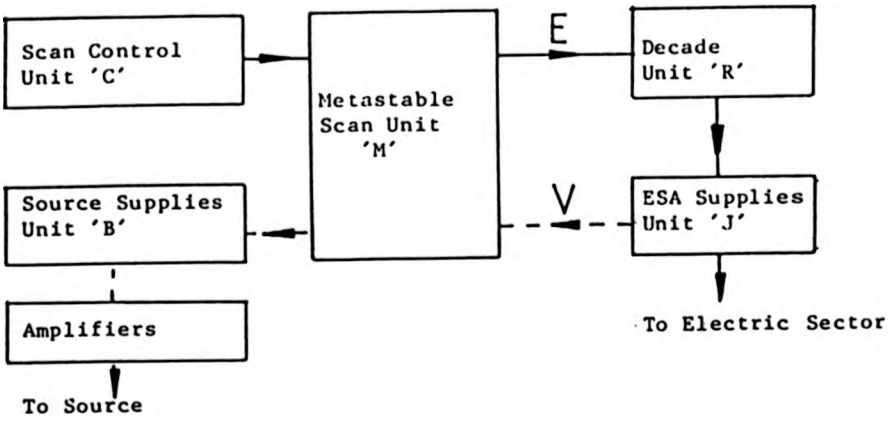

Figure 4.1 A diagram of the MS-50 reference voltages.

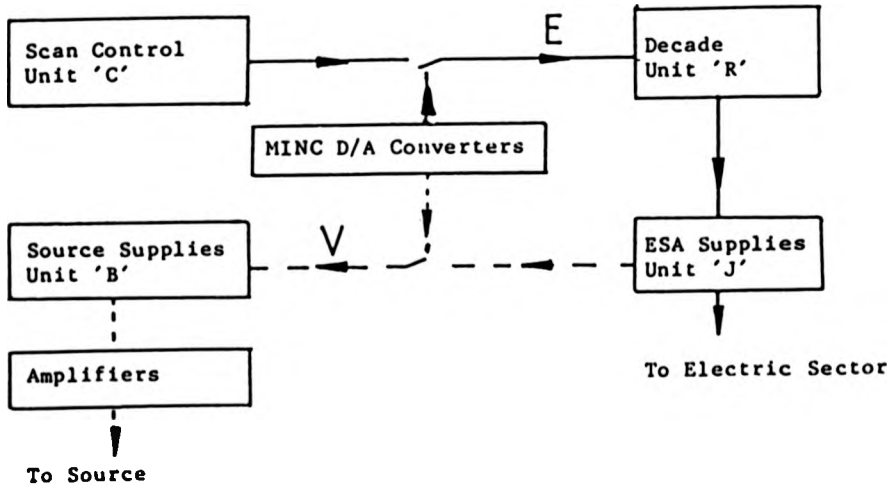

Figure 4.2 Control of the MS-50 reference voltages by the MINC.

V, E, or V/E^2 scans, and the Decade Unit 'R' can be used to accurately measure mass by high-resolution peak matching.

4.2.2 Control of the MS-50 by a microcomputer

The microcomputer used to control the reference voltages of the MS-50 was a MINC-11, manufactured by Digital Equipment Corporation (DEC). The MINC is based on an LSI-11 microprocessor functioning as a PDP-11/03 minicomputer. It is equipped with 32k words (1k=1024) of core memory, each of sixteen bits, two 5 Mbyte floppy disk drives, a DEC LA38 line printer, a DEC VT105 graphics terminal and a Hewlett-Packard 7225A graphics plotter. The operator can use either the RT-11 operating system (which supports FORTRAN IV and a macroassembler language) or a special operating system which incorporates a BASIC intepreter.

The MINC has a number of modules which can be used to receive data or to control external devices attached to the central processor. It has a 1 MHz clock module, modules which can accept or transmit 16-bit digital words, four 12-bit digital-to-analog (D/A) converters, sixteen 12-bit analog-to-digital (A/D) converters and interfaces conforming to the IEEE-488 and RS-232 standards to communicate with peripheral devices.

It was decided to use the MINC to control the electric and accelerating fields, and to leave the

control of the magnetic field during the scan to the electronics of the MS-50. A BASIC program was written {96} which supplied the appropriate electric sector reference voltage via one of the D/A converters. As this is usually linked to the accelerating voltage reference, it was also necessary to supply that via another D/A converter. A diagram of the MINC/MS-50 connections are shown in Figure 4.2. The D/A converters produce voltages in the range -5V to +5V or 0 to 10V. These had to be amplified to produce the correct voltages for the MS-50 (accelerating voltage reference: 0 to 8V; electric sector reference: 0 to 20V) by amplifiers whose circuits are shown in **Figure** 4.3.

Because the data system was to be used to acquire the individual scans which compose the map, it was decided to use it to start the magnet scan by sending a logic pulse to the electronics of the MS-50. On receipt of this "start" pulse, the electronic circuits of the MS-50 decreased the magnetic field until a low mass limit was reached (preset by a dial on unit 'C'), when the mass spectrometer sent a "stopped" pulse back to the data system which caused it to stop acquiring data. This pulse was also sent to a logic input on the clock module of the MINC, which triggered the output of a slightly decreased electric sector reference voltage.

The time-to-mass calibration of the data system was found not to be reliable during the first few magnetic field scans performed on the MS-50, and so the program

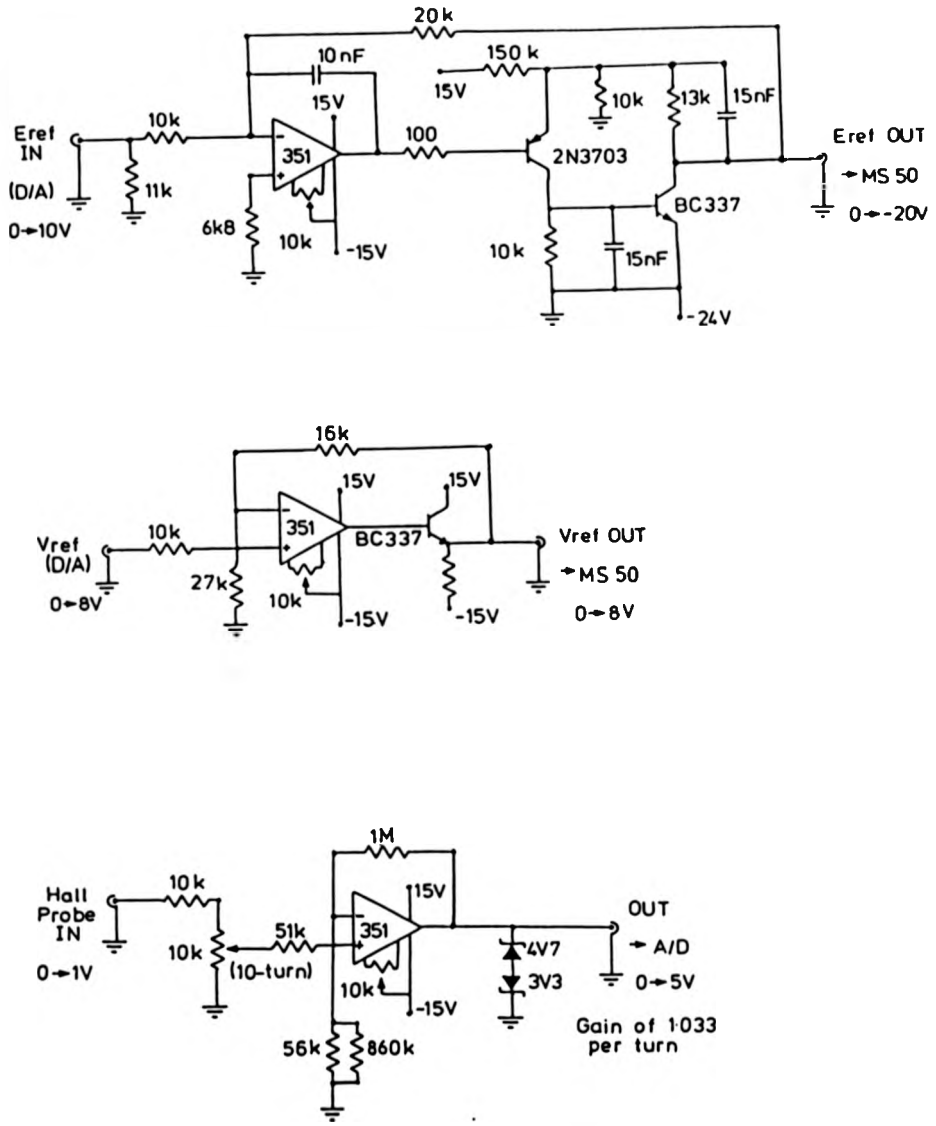

Figure 4.3 Circuit diagrams of the amplifiers used in between the MINC-11 and the MS-50

which controlled the reference voltages was adapted to allow a specified number of scans to be taken at the normal electric sector field (E′=1) before the electric sector reference voltage was decreased. The gain of the multiplier used to detect the ions was usually increased after the lead-in scans had been acquired. The size of the steps by which the electric sector reference voltage was decreased could also be selected by the user before the map was started. The number of scans which any map could contain was limited primarily by the lifetime of the sample, and so the program was further altered to allow the value of E′ at which the first scan (after the lead-in scans) was taken to be altered by the user. This allowed a large map to be constructed out of several smaller ones if the sample was particularly volatile or difficult to handle. The sequence of operations of the MINC program is shown below.

1. Generate the accelerating reference voltage.
2. Generate the electric sector reference voltage.
3. Read in the number of lead-in scans, the step size and the initial value of E'.
4. Wait for the operator to start the map.
5. Work out the electric sector voltage to be generated for the next scan.
6. On receipt of a "scan stopped" pulse from the MS-50,
7. Send out the new electric sector reference voltage,
8. If the map is not finished, then go to 6.
9. Reset the original reference voltages and stop.

4.2.3 Control by the data system

The electric sector field was decreased between magnet scans, when data were not being collected, and so it seemed sensible to use the data system to control the reference voltages. A problem with the MINC was found to be the limited resolution of the D/A converter: because it is only a 12-bit device, the minimum step size which could be used was 0.024% (1 part in 4096). A system was designed by KRATOS {97} which used a 16-bit D/A converter connected to the data system to produce the electric sector reference voltage. The step size and the number of lead-in scans were requested by the acquisition software before the map was collected. The

system was used on both the MS-50 and the MS-80.

The accelerating voltage reference was generated from the d.c. supplies of the mass spectrometer by a variable potential divider. The electric sector reference voltage, which was generated by the D/A converter, and the accelerating voltage reference were fed directly to the appropriate circuit board in the Source Supplies Unit 'B' of the MS-50. Changing between normal control of the reference voltage and control by the D/A converter was controlled by a switch installed on the console of on Source Supplies Unit 'C'. In the MS-80, the accelerating voltage reference and electric sector reference voltage were fed directly to the appropriate amplifiers. A switch on the rear of the MS-80 electric sector amplifier allowed the selection of externally-generated reference voltages.

The system was installed and found to have a much better electric sector resolution than the MINC (1 part in 65536) and proved much easier to use. It did not, however, allow the user to start at E' values of less than one, and any subsequent alteration of the programs will prove difficult as the KRATOS acquisition software is written in NOVA assembly language.

4.3 Data Acquisition

The data system used for this work was DS-55 (written by KRATOS Ltd.) operating on a NOVA 2 computer (Data

General Ltd.). The NOVA 2 has 32K words of core memory, each of sixteen bits, and it is equipped with a TEKTRONIX 4010 graphics terminal with a COMPLOT 8600 screen copier, two 5 Mbyte hard disk drives and an interface to a mass spectrometer. The acquisition software and some of the processing software were supplied by KRATOS Ltd.

Before the map was acquired, it was usual to collect a few time-vs.-intensity spectra of a reference compound, such as perfluorokerosene, and to use one of these to perform a time-to-mass calibration. Peaks in subsequent scans could then be mass-assigned by the standard data acquisition program. Spectra taken at low resolution were usually processed prior to storage to ensure that the peaks were rounded up (or down) to the nearest integral mass by a process called Hites-Biemann correction {98}, but because the metastable ion peaks collected would not necessarily fall at integral masses, this could not be used.

Maps were not taken at high resolution because those acquisition programs require that a suitable calibrant be mixed in with the sample, and, once the lead-in scans had been acquired, ions formed in the source would not be collected and the calibrant would be unrecognisable. In addition, a much finer step in the electric sector voltage and a much slower magnet scan would be needed, thus considerably increasing the time taken to perform the experiment.

4.4 Data Processing

Once the data have been collected, they must be displayed in a form that would help the user identify the composition of the sample. Although the data are stored in large mass files with an index to each {99}, it is convenient to regard them as being stored in separate disk files, each containing the data from one magnet scan. The scans are numbered consecutively, and if the step size (S) and the number of lead-in scans (L) are known, it is possible to compute the fractional electric sector value, E′, at which the Nth scan appears, by;-

$$E' = 1 - S(N-L).$$

The daughter ion from a decomposition in the first field-free region will appear, if that ion passes through a magnetic sector, at an apparent mass, m^*, which is given by;-

$$m^* = m_2^2/m_1$$

and it is the apparent mass of each peak which is stored in the files. The programs described here treat the data as if all the decompositions occur in the first field-free region and they would thus need adapting for use with reversed geometry mass spectrometers.

4.4.1 To Give Metastable Maps

The easiest form in which to present the data is a plot of apparent mass vs. scan number vs. intensity, and it was found that a program originally written (by KRATOS Ltd.) to generate GC profiles, GCMAP, could

produce these. In such a map (an example is shown in Figure 4.4) constant daughter (B^2/E) scans appear as straight lines because the apparent mass is proportional to the square of the magnetic field. Constant parent (B/E) scans appear as gentle curves and CNL scans appear as much steeper curves. Data in this format were not easy to interpret, and so it was decided to produce a map where the three axes represent the variables which were of most interest to the analyst: parent ion mass, daughter ion mass and peak height.

The program calculates the parent ion (m_1) and daughter ion masses (m_2) associated with each transition by using the fractional electric sector values and apparent masses of the observed peak to derive m_1 and m_2 by;-

$$m_2 = m^*/E' \quad \text{and} \quad m_1 = m_2/E'.$$

A map in this format can be seen in seen in Figure 4.5, and it can be seen that a B/E linked scan (all daughters of a given parent ion) can be represented by a line parallel to the m_2 axis. A B^2/E scan is equivalent to a line parallel to the m_1 axis and a CNL scan is equivalent to a line at forty-five degrees to both axes. A normal mass spectrum would be displayed on the map as a CNL scan with a neutral loss of zero but peaks in the normal spectra are much larger than those appearing on the map, and so they are suppressed. Intense peaks from the loss of one or two mass units may also be suppressed. The map is produced as an isometric projection by a plotting method similar to that used by

Figure 4.4 A plot of scan number vs. apparent mass vs. intensity for decan-1-ol

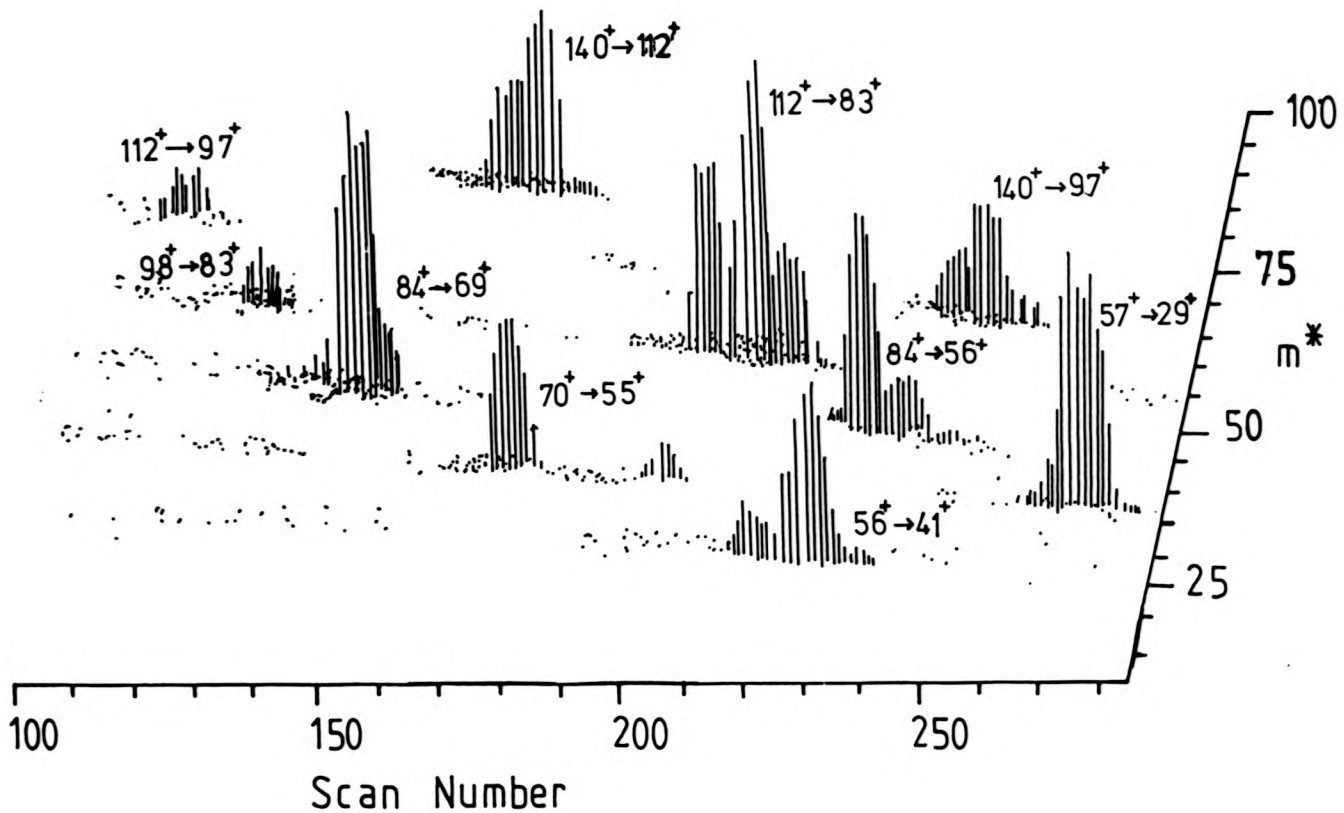

Figure 4.5 A plot of parent ion mass vs. daughter ion mass vs. intensity for decan-1-ol

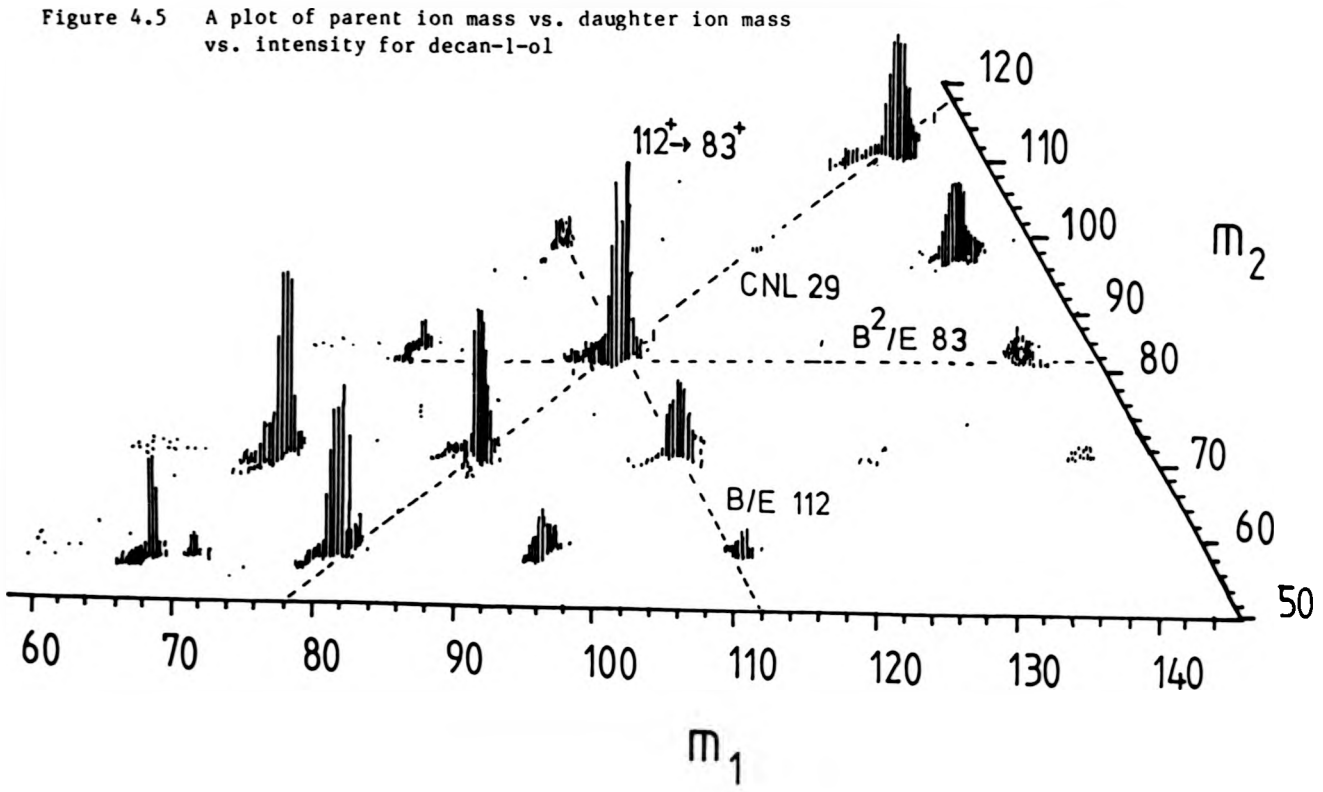

GCMAP. The program requests the user to specify mass and intensity ranges for the axes and then opens the disk files and reads the peaks' masses and intensities. The masses of the parent ions and daughter ions are then calculated, and if the peak falls within the specifed mass ranges and has a non-zero intensity, the intensity and masses are stored in a pair of arrays. Because of the limited core space in the NOVA a maximum of two thousand values can be stored in each of these arrays, and the user must ensure that the mass and intensity ranges which he selects do not produce more than this number of peaks to be stored.

The user specifies the horizontal and vertical angles at which he wishes to look at the map. To make the program compatible with GCMAP, the user is asked to choose the height-to-width ratio of the plot and the tangent of the angle between the daughter ion axis and the screen vertical. Using these, the program projects the positions of the peaks and axes from the three-dimensional map onto the two-dimensional screen and draws them.

4.4.2 To Give Linked Scans

It is often interesting to study the way a particular ion fragments to obtain information about its structure. It may also be useful to see which ions lose a certain neutral fragment or decompose to give a certain daughter ion. For this reason it was decided to

write a set of programs which could simulate the linked scans from data stored on disk.

The programs ask the user to specify which of the three linked scans he requires, and on what mass. The user is also asked to specify a 'window' parameter which is used to compensate for calibration errors caused by the absence of Hites-Biemann correction. Typical values of this parameter would lie between 0.1 and 0.5 Dalton. The disk files are then opened and the programs calculate the mass at which a peak appears in the linked scan, using;-

$$m^* = m_1(E')^2 \quad \text{for a B/E linked scan,}$$
$$m^* = m_2E' \quad \text{for a } B^2/E \text{ linked scan,}$$

and $$m^* = m_n(E')^2/(1-E') \quad \text{for a CNL scan.}$$

These formulae are derived in sections 3.1.1.1 to 3.1.1.3. If a peak with a mass difference of less than half the window width from the predicted apparent mass is found, it is assumed that that peak would appear in the linked scan and it is stored for output. A maximum of five hundred peaks can be stored, but this limit is rarely exceeded. Once all such peaks have been collected, the simulated scans may be produced by plotting parent ion mass vs. intensity for the B/E scan or daughter ion mass vs. intensity for the B^2/E and CNL scans. A simulated B/E linked scan for m_1=112 in decan-1-ol is shown in Figure 4.6 compared to one generated by conventional means.

write a set of programs which could simulate the linked scans from data stored on disk.

The programs ask the user to specify which of the three linked scans he requires, and on what mass. The user is also asked to specify a 'window' parameter which is used to compensate for calibration errors caused by the absence of Hites-Biemann correction. Typical values of this parameter would lie between 0.1 and 0.5 Dalton. The disk files are then opened and the programs calculate the mass at which a peak appears in the linked scan, using;-

$$m^* = m_1(E')^2 \quad \text{for a B/E linked scan,}$$
$$m^* = m_2E' \quad \text{for a } B^2/E \text{ linked scan,}$$

and $$m^* = m_n(E')^2/(1-E') \quad \text{for a CNL scan.}$$

These formulae are derived in sections 3.1.1.1 to 3.1.1.3. If a peak with a mass difference of less than half the window width from the predicted apparent mass is found, it is assumed that that peak would appear in the linked scan and it is stored for output. A maximum of five hundred peaks can be stored, but this limit is rarely exceeded. Once all such peaks have been collected, the simulated scans may be produced by plotting parent ion mass vs. intensity for the B/E scan or daughter ion mass vs. intensity for the B^2/E and CNL scans. A simulated B/E linked scan for m_1=112 in decan-1-ol is shown in Figure 4.6 compared to one generated by conventional means.

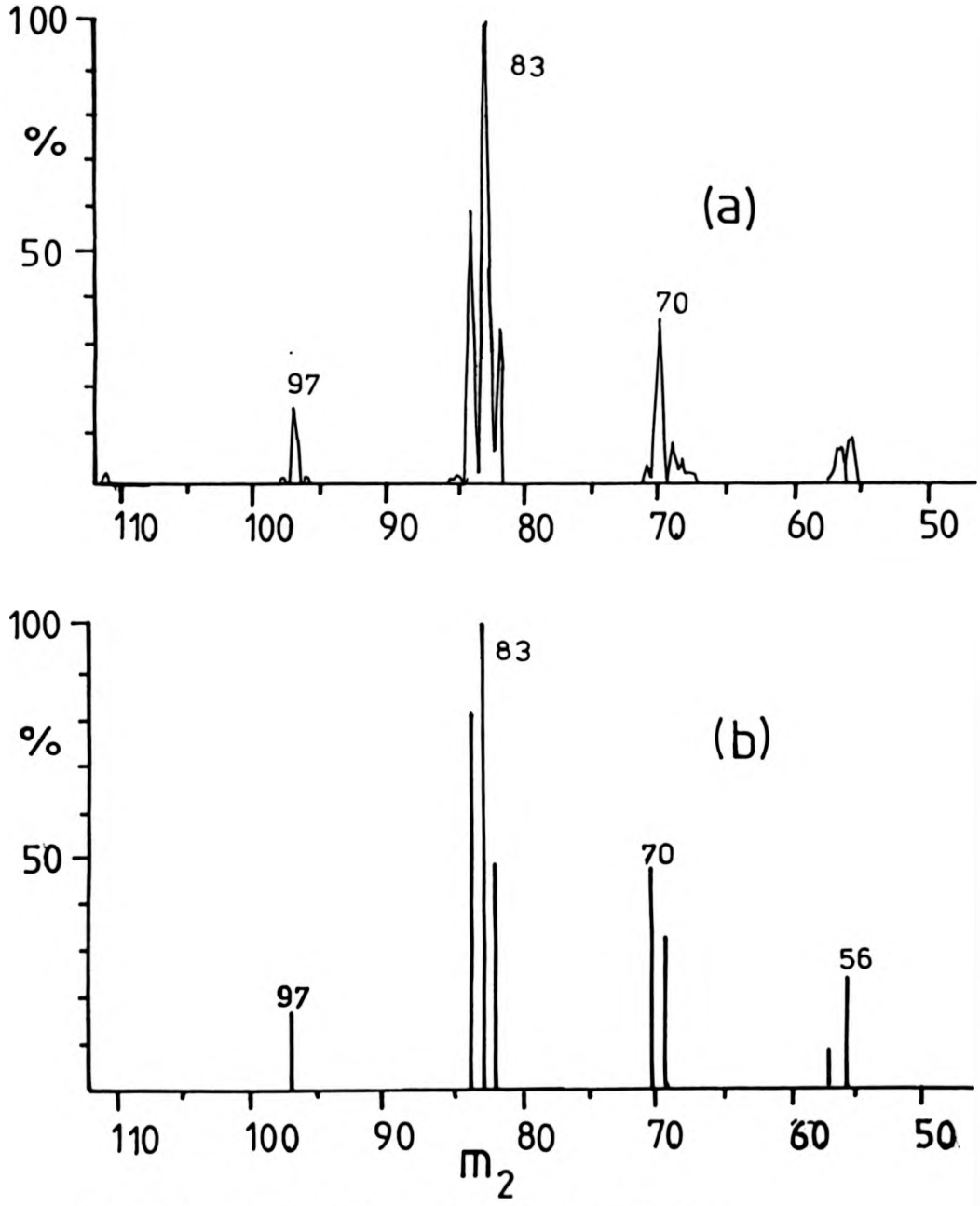

Figure 4.6 A comparison of B/E linked scans for $m/z\ 112^{+}$ from decan-1-ol, showing
a) a linked scan simulated from the metastable map (see Fig 4.5), and
b) a linked scan generated by conventional means

4.5 Computer-controlled Linked Scans

When only a few metastable (or collision-induced) decompositions are of interest, a metastable map can take too long to acquire, and so a set of programs was written to allow the MINC to control the three linked scans described in detail in the previous chapter. BASIC, which had been used for the metastable mapping control program, was found to be much too slow for these programs, and so FORTRAN IV was used.

With the accelerating voltage and electric sector references under control of the MINC, the mass spectrometer was tuned to the top of a peak of interest in the normal spectrum. This peak was the parent ion for the B/E spectrum, the daughter ion for the B^2/E linked scan, or any peak of known mass for the CNL linked scan. The output of the Hall probe was then read by an A/D converter. The gain of the amplifier (the circuit of which is illustrated in Figure 4.3) used to convert the output of the Hall probe (0 to 1V) to the 5V maximum input of the A/D converter was variable from 1 to 10 to allow the full resolution of the A/D converter to be used for peaks of relatively low mass.

The magnet scan was started and stopped by the MINC via a pair of leads between the MINC module used to send out digital words and a socket on the rear of the console usually used to carry "start" and "stop" commands from the data system. The lead carrying the "start" pulse was connected to bit 0 of the output on the MINC, and the

magnet scan could then be started by sending '1', which has the digital value 1, to the module. The lead carrying the "stop" pulse was connected to 'bit 1' of the module. The scan could thus be stopped by sending '2', which has the binary value 10, to the module.

Once the scan was started, the Hall probe voltage was sampled and the appropriate electric sector voltage could then be calculated and output from knowledge of the original electric and magnetic field values. The Hall probe voltage was then sampled again and the process repeated. This cycle was performed at about 200 times per second for the B/E and B^2/E linked scans, and about 150 times per second for the CNL linked scan, where the electric sector voltage to be produced corresponds to one of the roots of a quadratic equation. If very fast scan speeds were required, it would be necessary to re-write the appropriate subroutines in assembly language.

5. Analysis of some simple maps

In this chapter, some results obtained by using metastable mapping are presented, and two simple alcohols (methanol and decan-1-ol) will be used to illustrate how the maps may be interpreted. The shape of the peaks on the B,E′ plane is also discussed.

5.1 Methanol

Methanol was introduced into the EI source of the MS-50 via a reservoir probe. A metastable map of its unimolecular decompositions was acquired, where 15 scans were collected at the normal electric sector voltage and the voltage was decreased by 0.0477% of its original value after every subsequent scan. The mass range obtainable from a calibration obtained using PFK was unsuitable and so the data were calibrated against a methanol reference spectrum. Methanol was studied because its unimolecular decompositions are well known {100}. Part of the metastable map is presented in Figure 5.1. Intense peaks for the transitions $31^+ \rightarrow 29^+$ and $30^+ \rightarrow 29^+$, and a smaller peak for the $32^+ \rightarrow 31^+$ transition, can be seen. A very small peak for the $31^+ \rightarrow 30^+$ transition is not shown. The normal mass spectrum, which corresponds to a constant neutral loss of zero, is not shown either as it would obscure the peaks shown on the map.

A B^2/E linked scan for the 29^+ ion is shown in Figure 5.2. The $30^+ \rightarrow 29^+$ peak is almost gaussian in shape, but the $31^+ \rightarrow 29^+$ peak is much broader and

Figure 5.1 A metastable map of the unimolecular decompositions of methanol

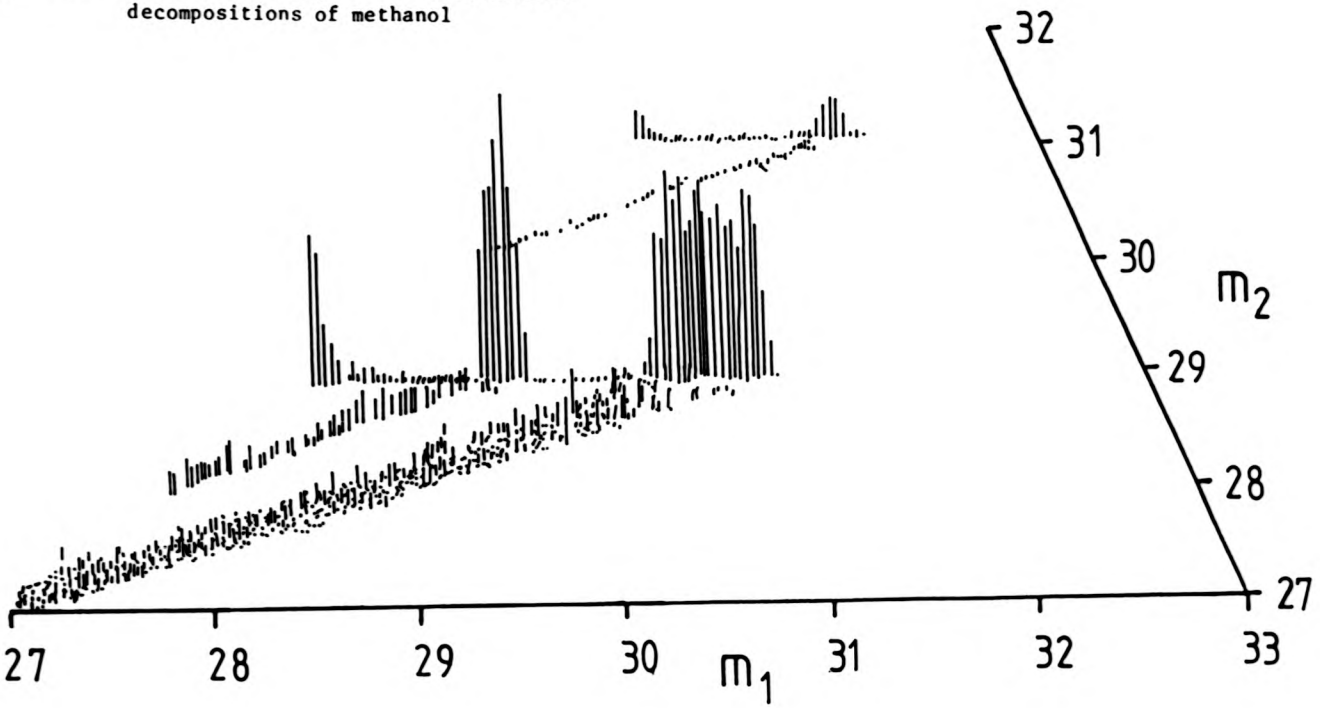

exhibits a slight decrease in intensity at the centre of the peak. The kinetic energy release of the latter transition can be calculated: the half-width of the peak at half-height is 0.24 Dalton, and the half-width at the most intense points of the peak is 0.2 Dalton, and from the formula for the kinetic energy release derived below, it can be calculated that these widths lead to values of 1.8 eV and 1.2 eV respectively. A value for the kinetic energy release of about 1.5 eV can thus be assumed, which is similar to the value of 1.42 eV obtained from the width of the metastable peak in the normal mass spectrum {100}.

The baseline of the spectrum shown in Figure 5.2 appears to be raised between the peaks and the left-hand axis. At this axis, any ions detected must be due to the products of decompositions occuring in the ion source, and so the raised baseline must result from decompositions occuring between the source and the first field-free region - i.e. while the parent ions are being accelerated. Similarly, the continua between the peaks in Figure 5.1 and the normal spectrum at an angle to the m_1 axis can be explained as the result of decompositions occurring between the first field-free region and the second field-free region. For the forward-geometry instruments used here, these decompositions occur in the electric sector. The products of these decompositions will only be observed if the daughter ion mass is not too different from the parent ion mass. The products of ions decomposing during their flight through the magnetic sector will be detected as a continuum between the second field-free region

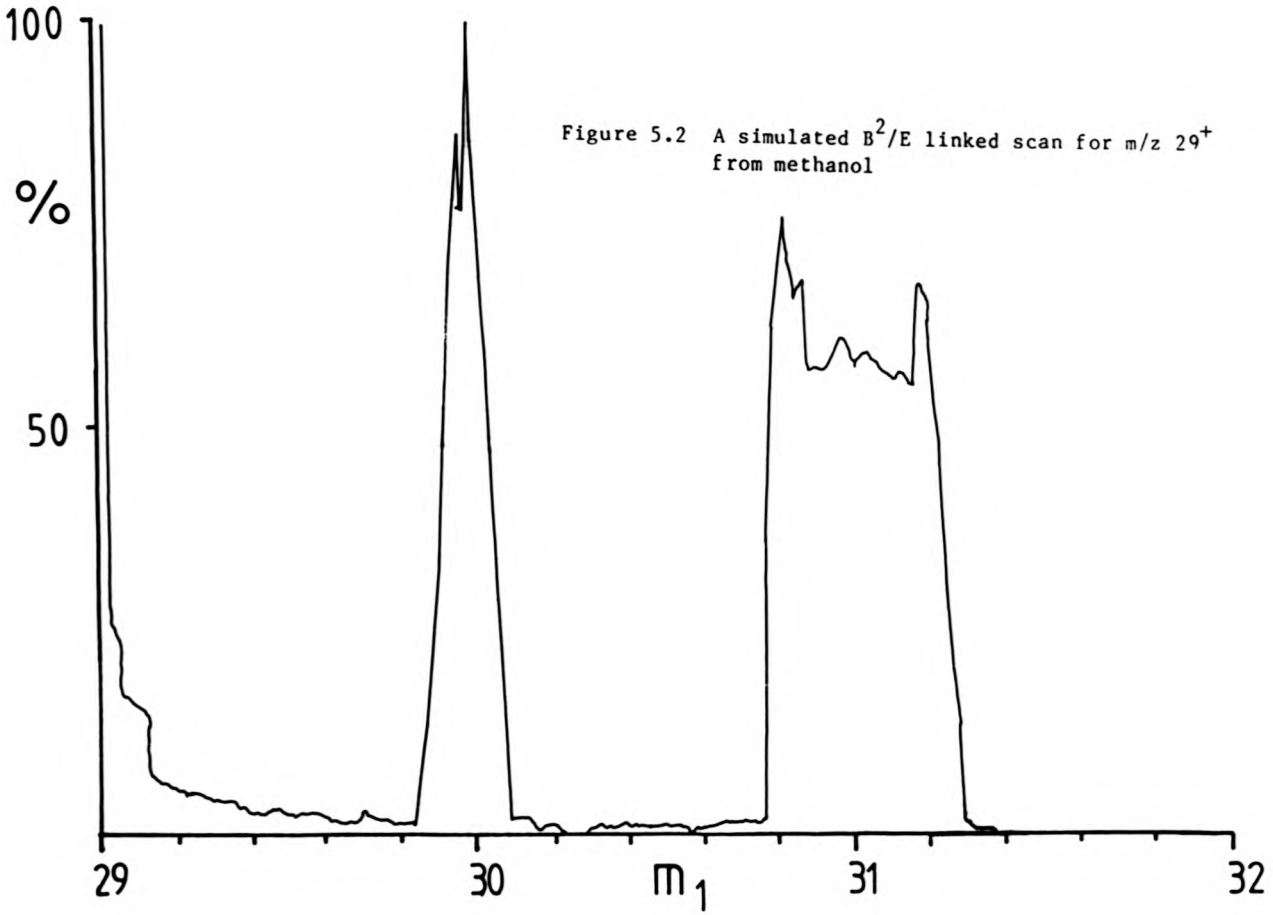

Figure 5.2 A simulated B^2/E linked scan for m/z 29^+ from methanol

decompositions and the parent ions in the normal mass spectrum.

It is possible to detect the products of these electric sector and accelerating region transitions in linked scans: for example, in the B/E linked scan of the 30^+ ion (see Figure 5.3) a large peak for the transition $30^+ \rightarrow 28.5^+$ can be observed. By examining the metastable map (Figure 5.1) it can be seen that this peak is due to the transition $31^+ \rightarrow 29^+$ occuring in the electric sector. Similarly, in the B/E spectrum of the 31^+ ion (see Figure 5.4) a peak at m/z 30 is about the same size as a peak at m/z 30.5, which is due to the transition $32^+ \rightarrow 31^+$ occuring in the electric sector.

5.2 Decan-1-ol

Decan-1-ol was introduced into the EI source of the MS-50 via the reservoir probe. A metastable map was acquired (10 lead-in scans, step size = 0.127%) and is displayed in Figure 5.5. A regular "chessboard" pattern, typical for the EI metastable maps of long-chain hydrocarbons, is evident: it is due to the losses of alkyl and alkene neutral fragments from the various ions formed in the source. No transitions from the molecular ion (m/z 158) can be seen because it is not formed [20]. The map is presented in three dimensions in Figures 4.4 and 4.5. It can be seen from the two figures that the products of decompositions in the electric sector and accelerating region do occur, but that they do not form continua between

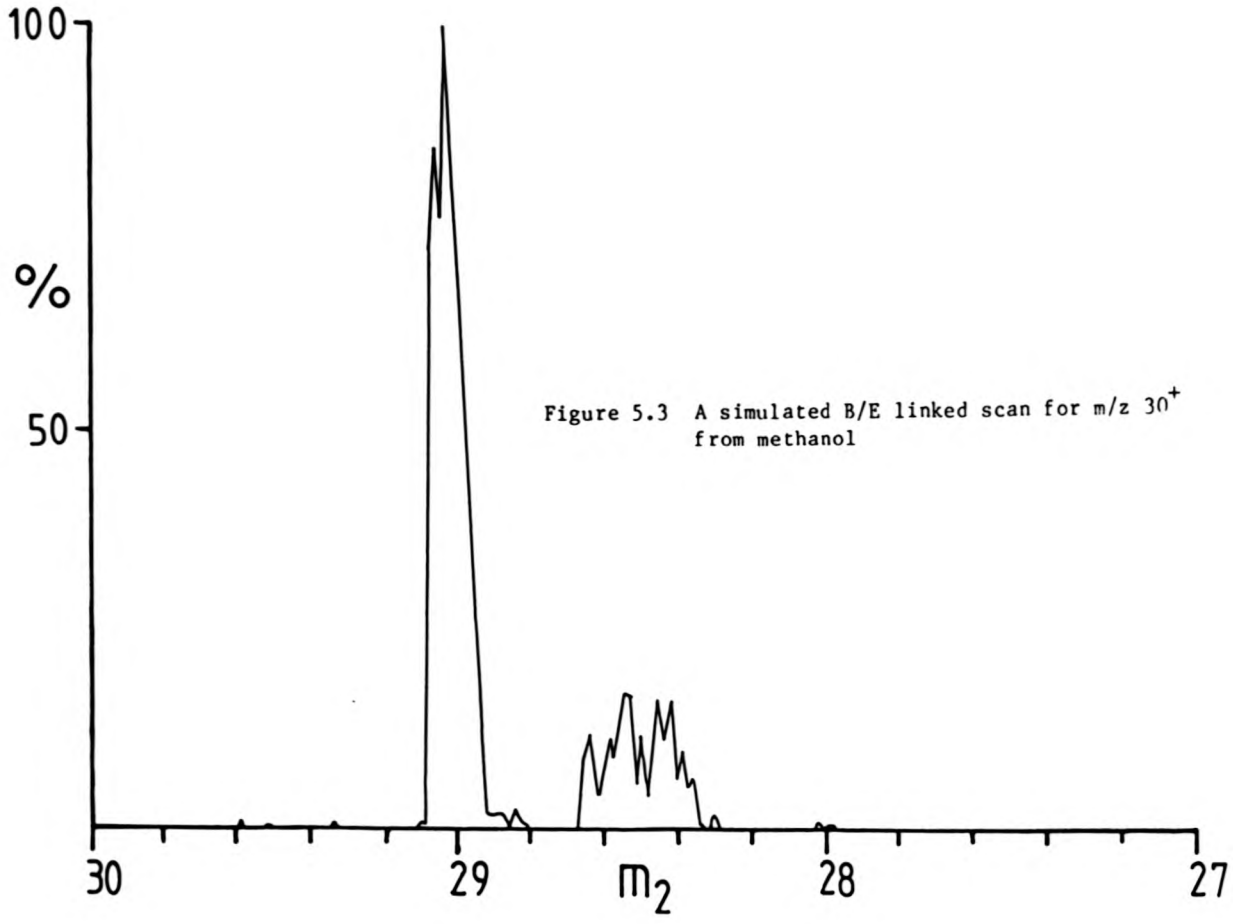

Figure 5.3 A simulated B/E linked scan for m/z 30^+ from methanol

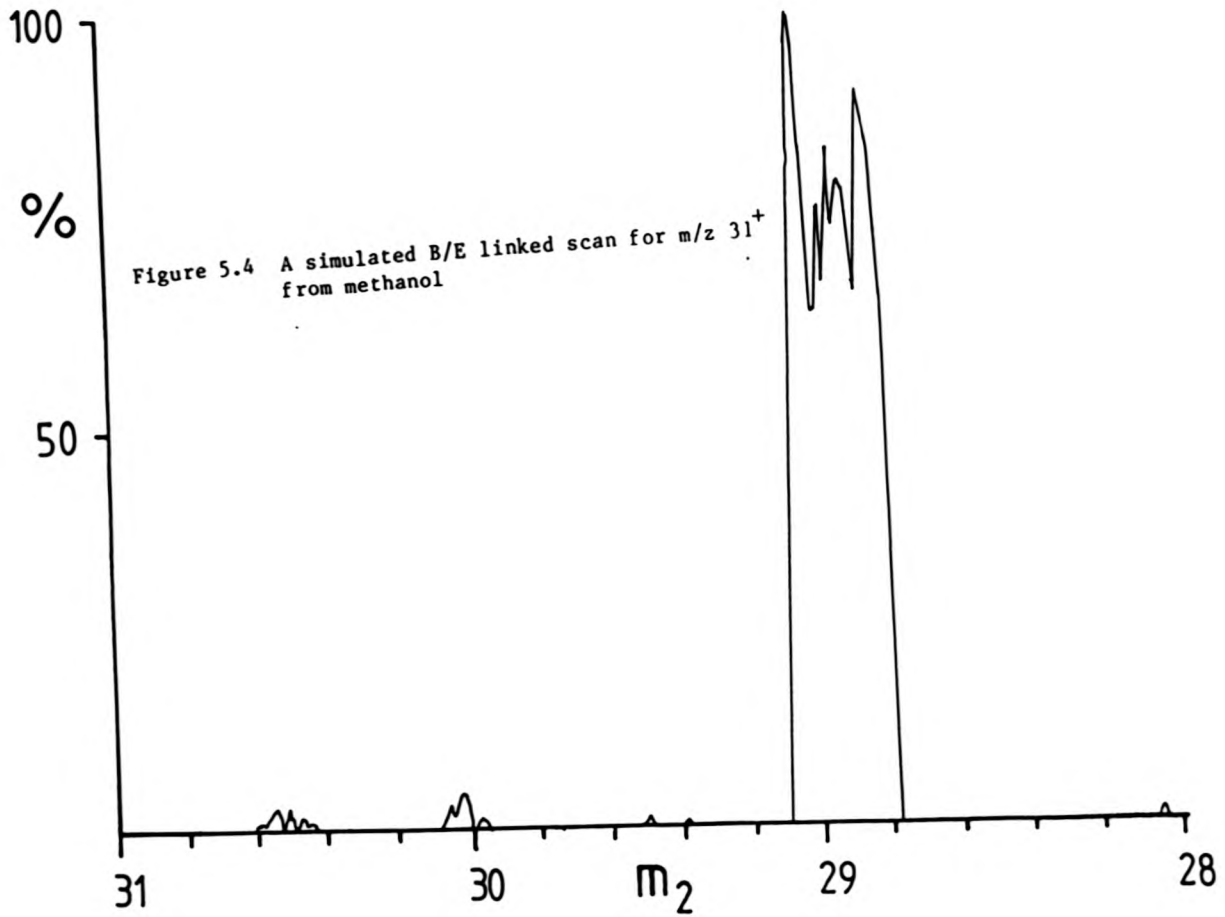

Figure 5.4 A simulated B/E linked scan for m/z 31^+ from methanol

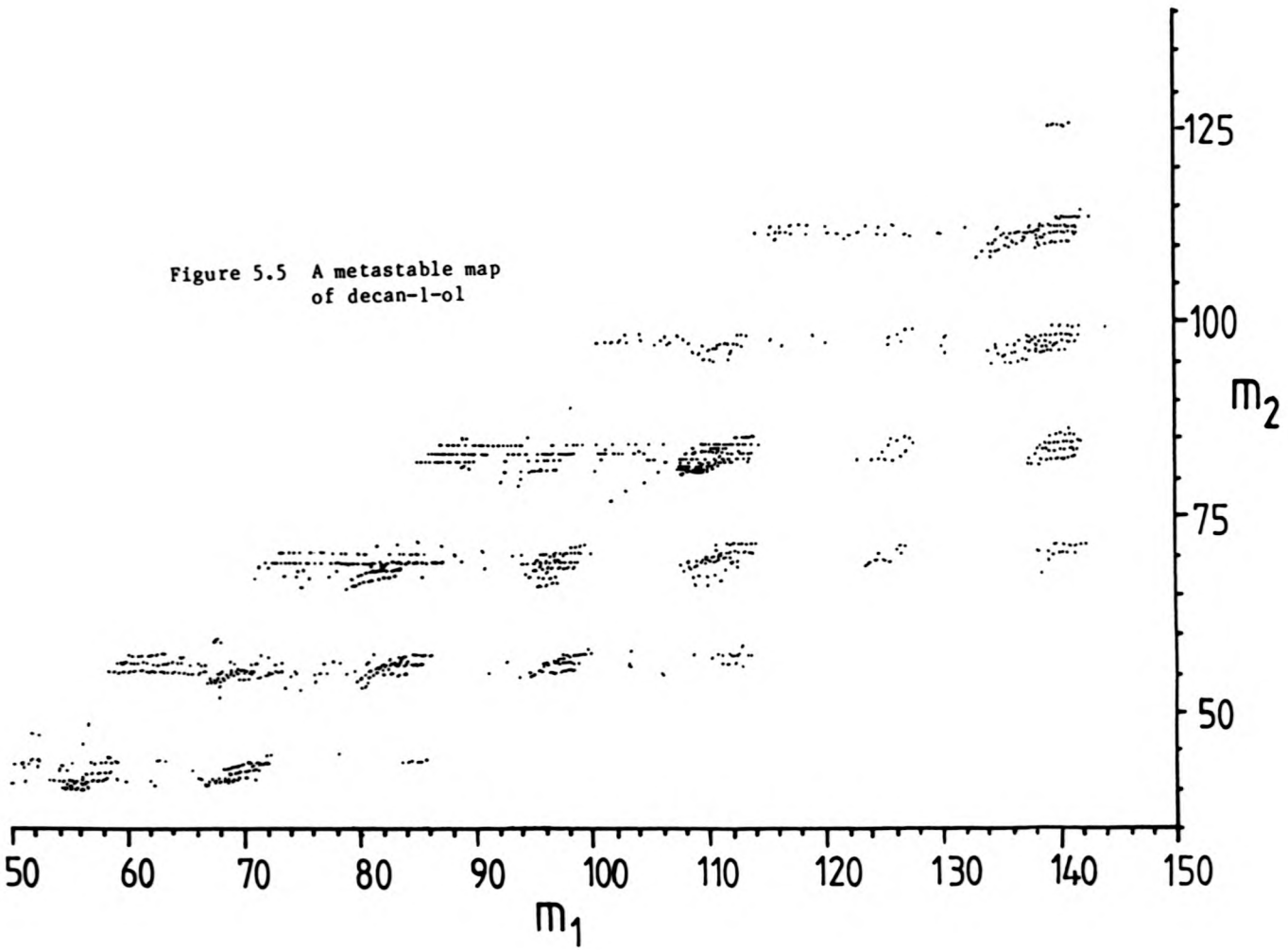

Figure 5.5 A metastable map of decan-1-ol

the peaks and the normal mass spectra as they did for methanol because the likelihood of such a decomposition product being detected decreases as the mass of the neutral fragment increases (vide supra). Consequently, only the products of decompositions close to the source or one of the field-free regions will be detected. A B/E linked scan extracted from the map is shown in Figure 4.6, and B^2/E and CNL linked scans are presented in Figure 5.6. The convention, suggested by Haddon {55}, that the daughter ion mass be shown in CNL linked scans has been adopted here.

5.3 The Shape of the Peaks on the B,E′ Plane

It will be noticed from the figures shown earlier that the peaks are broader in some directions than in others. It is well known that the effects of kinetic energy release significantly broaden metastable ion peaks in a normal mass spectrum, but its effect on peaks on the B,E′ plane is less well known.

5.3.1 Calculation of Peak Shapes

If we consider the fragmentation of an ion in the first field free-region of a double-focussing mass spectrometer, it will be apparent that the daughter ions will no longer have the same kinetic energy or momentum as the parent ion, and, if there is any energy transfer from the internal energy of the parent ion to the translational energy of the fragments, they will not have the same velocity either. If an ion of mass m_1 is

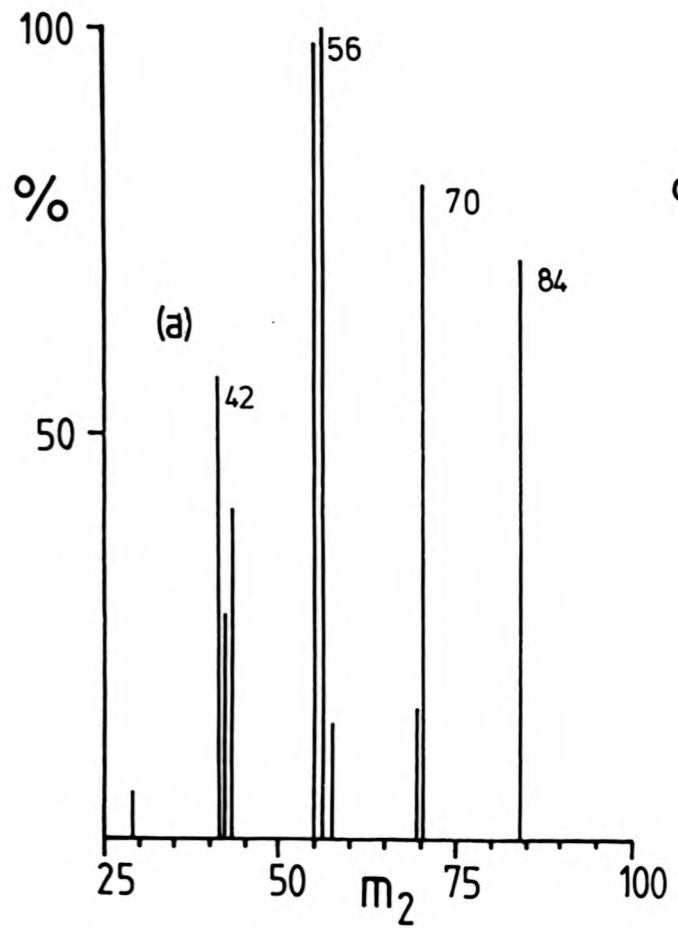

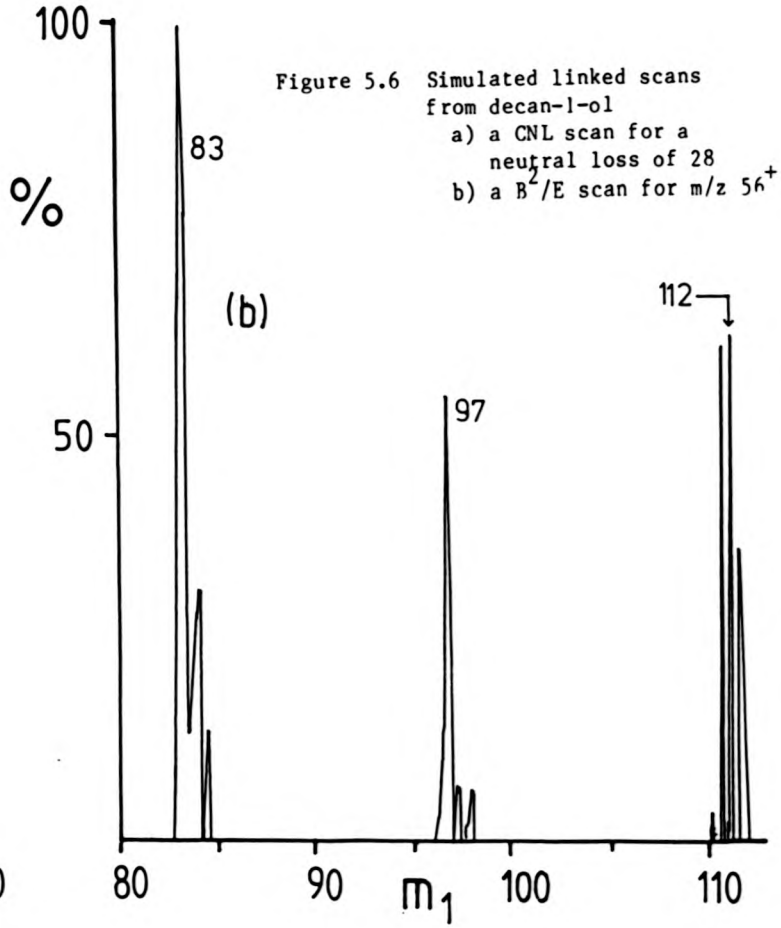

Figure 5.6 Simulated linked scans from decan-1-ol
a) a CNL scan for a neutral loss of 28
b) a B^2/E scan for m/z 56^+

accelerated through a potential V, it will gain a kinetic energy of;-

$$Ve = (1/2)m_1v^2$$

where e is the charge on an electron and v is the velocity of the ion. If the masses of the daughter ion and the neutral fragment from a decomposition in the first field-free region are m_2 and m_3 respectively, and if we assume that the fragmentation releases energy which causes a change in velocity of Δv, then the daughter ion will have a maximum velocity distribution of $(v \pm \Delta v)$ from the velocity components in the direction of flight. If the electric sector potential required to transmit the parent ion is E_1, and the potential required to transmit the daughter ion is E_2, then;-

$$E_1e = m_1v^2/r$$

where r is the radius of the electic sector. If we consider the daughter ion;-

$$E_2e = m_2(v \pm \Delta v)^2/r$$

and

$$E' = E_2/E_1 = (m_2/m_1)(v \pm \Delta v)^2/v$$

It should be emphasised that here E′ is not a constant, but a variable whose limits are defined by $(\Delta v/v)^2$.

If B_1 is the magnetic field required for the parent ion to pass through the magnet (radius R), and $(B_2 \pm \Delta B)$ is the range of field values which transmit the daughter ion, then;-

$$B_1eR = m_1v \quad \text{and} \quad (B_2 \pm \Delta B)eR = m_2(v \pm \Delta v)$$

At the centre of the peak, where we may assume that there was effectively no energy released in the direction of the flight of the ions, the mass at which

the daughter ion appears is given by;-

$$m^* = B_2^2 R^2 e/2v$$

thus

$$2m^* eV = ((B_2 \pm \Delta B)eR)^2 = m_2^2 (v \pm \Delta v)^2,$$

so

$$m^* = (m_2^2/m_1)(v \pm \Delta v)^2/v^2$$

Again, m^* is a variable whose spread is determined by the velocity distribution of the daughter ion.

The magnetic field strength at which the daughter ion will be transmitted is proportional to the square root of the apparent mass and thus to the first power of Δv. The electric sector field strength necessary to transmit the ion is dependent on the square of Δv. The velocity dependence of B and E′ are thus different, and the shape of the peak on the B,E′ plane will be curved and will lie along a line corresponding to a B^2/E linked scan of that ion.

5.3.2 The Peak Shape in Linked Scans

If there was no kinetic energy released during a decomposition, the daughter ion and parent ion masses could be found from the apparent mass and the value of E′: but if there was, m_2 is still given by $m_2 = m^*/E'$, since the velocity terms cancel, but the parent ion mass is no longer equal to m_2/E'. We thus have peaks on the plane with a well defined daughter ion mass but with a spread in the parent ion mass, which may be observed in the metastable maps presented here. Since the parent ion mass is poorly defined, a scan which studies all parent ions of a given daughter ion (i.e. a

B^2/E scan) will contain broadened peaks. Both of the other linked scans cut through the peak at an angle to the m_1 axis, and so the peaks in those scans will be narrow.

5.3.3 Determining the Kinetic Energy Release

If we define the half-width of the peak in the m_1 direction as Δm, and the upper and lower masses as m_H and m_L, then because the mass of the parent ion is given by m_2/E' :-

$$m_H = m_1+\Delta m = m_1v^2/(v-\Delta v)^2, \text{ and}$$
$$m_L = m_1-\Delta m = m_1v^2/(v+\Delta v)^2$$

Thus

$$(m_H-m_L)/m_Hm_L = [(v+\Delta v)^2-(v-\Delta v)^2]/m_1v^2$$
$$(m_H-m_L)/m_Hm_L = 4\Delta v/m_1v$$

If we substitute for m_H and m_L, and neglect $(\Delta m)^2$ when compared to m_1^2, we may conclude that;-

$$\Delta m/m_1 = 2\Delta v/v \ .$$

If the amount of kinetic energy released was T, and the velocities of the parent and daughter ions and the neutral fragment were v_1, v_2 and v_3 respectively, then from the laws of conservation of energy and momentum;-

$$T + (1/2)m_1v_1^2 = (1/2)m_2v_2^2 + (1/2)m_3v_3^2$$

and $m_1v_1 = m_2v_2 + m_3v_3$.

Substituting for v_3,

$$v_2^2(m_2^2 + m_2m_3) + v(2m_1m_2v_1) + (m_1^2v_1^2 - m_3m_1v_1^2 - 2Tm_3) = 0.$$

Solving the quadratic equation,

$$v_2 = v_1 \pm (2Tm_3/m_1m_2)^{(1/2)}$$

But if $v_1 = v$, and $v_2 = (v \pm \Delta v)$

$$\Delta v = (2Tm_3/m_1m_2)^{(1/2)}$$

This may be compared with the equation at the foot of page 58 of reference 39. We may now express T in terms of Δm.

$$\Delta v = v\Delta m/2m_1 = (2Tm_3/m_1m_2)^{(1/2)}$$

$$T = (\Delta m)^2 m_2 v^2/8m_1^2 m_3,$$

but since $v^2 = 2eV/m_1$,

$$T = (\Delta m)^2 m_2 eV/4m_1^2 m_3 .$$

Using this formula, we may calculate the kinetic energy released during a decomposition from the mass spread of the parent ion. It will be noted that this equation does not correspond to the one published previously {39} because that equation refers to metastable peaks observed in normal magnet scans, and the one derived above refers to peaks observed in a metastable map or in a B^2/E linked scan. A peak in such a scan may also be regarded as having a spread in E' (i.e. an uncertainty in the electric sector voltage) and if we express the half-width of the peak as ΔE, then;-

$$2\Delta m = m_2/(E-\Delta E) - m_2/(E+\Delta E)$$

$$2\Delta m = m_2[(E+\Delta E)-(E-\Delta E)]/(E-\Delta E)(E+\Delta E)$$

Since $E^2 >> (\Delta E)^2$,

$$2\Delta m = 2m_2 . \Delta E/E^2$$

$$\Delta m = m_2 . \Delta E . m_1^2/m_2^2$$

So

$$T = m_2 eV . (\Delta E)^2 m_1^4/4m_1^2 m_3 m_2^2$$

$$T = (\Delta E)^2 m_1^2 eV/4m_2 m_3$$

which corresponds to one of the published formulae.

It is thus possible to rationalize the shape of the peaks in B^2/E linked scans and on the metastable map, and to determine the magnitude of the kinetic energy released during the decomposition from the widths of these peaks, without interference from intense peaks in the normal mass spectrum. The accuracy of the value of T obtained depends on the uncertainty in the width of the peak, which is determined primarily by the size of the step taken in the electric sector field strength.

6. Angle-resolved Mass Spectrometry

6.1 Introduction

It was reported ten years ago {101} that an ion travelling through a collision cell could be deflected from its original path by colliding with a molecule of gas. Since then angle-resolved mass spectrometry (ARMS) has shown itself to be a potentially useful analytical tool because the fragmentation pattern of a collisionally-activated ion varies as its internal energy increases. If a plot of decomposition product ion intensities vs. parent ion internal energy is constructed, the resulting 'breakdown curve' can be useful when trying to determine ion structures.

The ratios of fragment ion intensities of an ion scattered from a molecule of collision gas have been observed to be correlated to both the kinetic energy of the ion (E) and the angle at which it is scattered (θ): the precise relationship is uncertain, but it has been expressed as $\Delta E \propto E^2\theta^2$ {102,112} for inelastic collisions and as $\Delta E \propto E\theta^2$ {102,103} for elastic collisions, where ΔE is a measure of the energy deposited by the ion. A breakdown curve obtained from a plot of θ^2 vs. intensity has been found to compare well with theoretical results {104} as well as with data obtainable from charge exchange experiments {104} and field ionization kinetics {105}. However, if the intensities of the

decomposition products of the molecular ion of n-butylbenzene are plotted against θ {114} and against the amount of energy deposited in the ion by a photon {180}, it can be seen {181} that these quantites are linearly related.

6.2 The Z-deflection Method

Angle-resolved experiments have been performed with high angular resolution on both forward- {104} and reversed-geometry {106} instruments by determining the angle of observation with a movable slit. This chapter describes simple angle-resolved studies performed on the MS-50 by a new technique involving the electrostatic deflection of the ions after collision. Ions produced in the source first pass through the y-plates, which deflect them in the direction of the electric sector field, and then through the z-plates, which deflect them in the direction of the magnetic sector field. The purpose of these plates is to align the ion beam along the optical axis of the mass spectrometer. The ions then pass through a cylindrical earthed tube and into the electric sector (see Figure 6.1). It was found to be possible to use these plates to deflect ions scattered at an angle back onto the optical axis: since ions scattered at all other angles will not be observed, this method provides a crude means of selectively observing the products of ions scattered at specific angles.

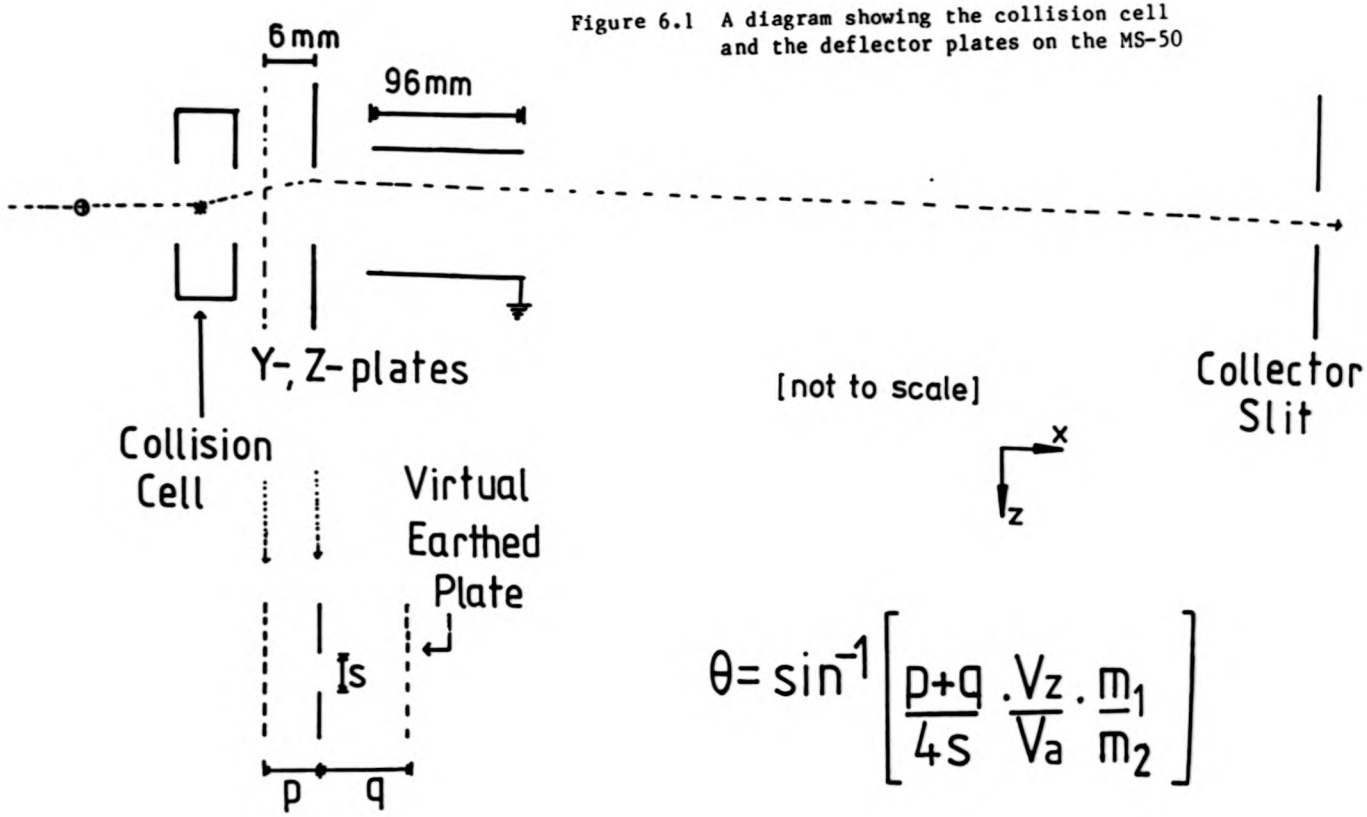

Figure 6.1 A diagram showing the collision cell and the deflector plates on the MS-50

$$\theta = \sin^{-1}\left[\frac{p+q}{4s} \cdot \frac{V_z}{V_a} \cdot \frac{m_1}{m_2}\right]$$

6.3 Results

6.3.1 Argon

Positive argon ions were accelerated from the EI source by a 7 kV potential, and argon was introduced into the collision cell so that the intensity of the parent ion was reduced by about 70%. An accelerating voltage scan was performed at several values of the z-deflection voltage and the data were collected on a Biomac 1000 signal averager. Each of the spectra shown in Figure 6.2 was an average of about 10-20 scans, taking less than a minute to collect. The data are very similar to those recorded previously {106-109}, although the signal-to-noise ratio was much better in these experiments and the resolution was worse. The peak labelled 'A' in Figure 6.2 is due to the elastic scattering of the ions, and peaks 'B','C' and 'D', which are observed at higher accelerating voltages, are due to inelastic processes occurring in the target atom which extract successively greater amounts of translational energy from the ions {109}: peak B is due to the target molecules becoming electronically excited by the deposition of 11.5 - 15.8 eV of energy, peak C is due to the target molecules losing an electron altogether, which requires 16 - 40 eV of energy, and peak D is due to the double ionization of the target, which requires energies in excess of 40 eV {109}.

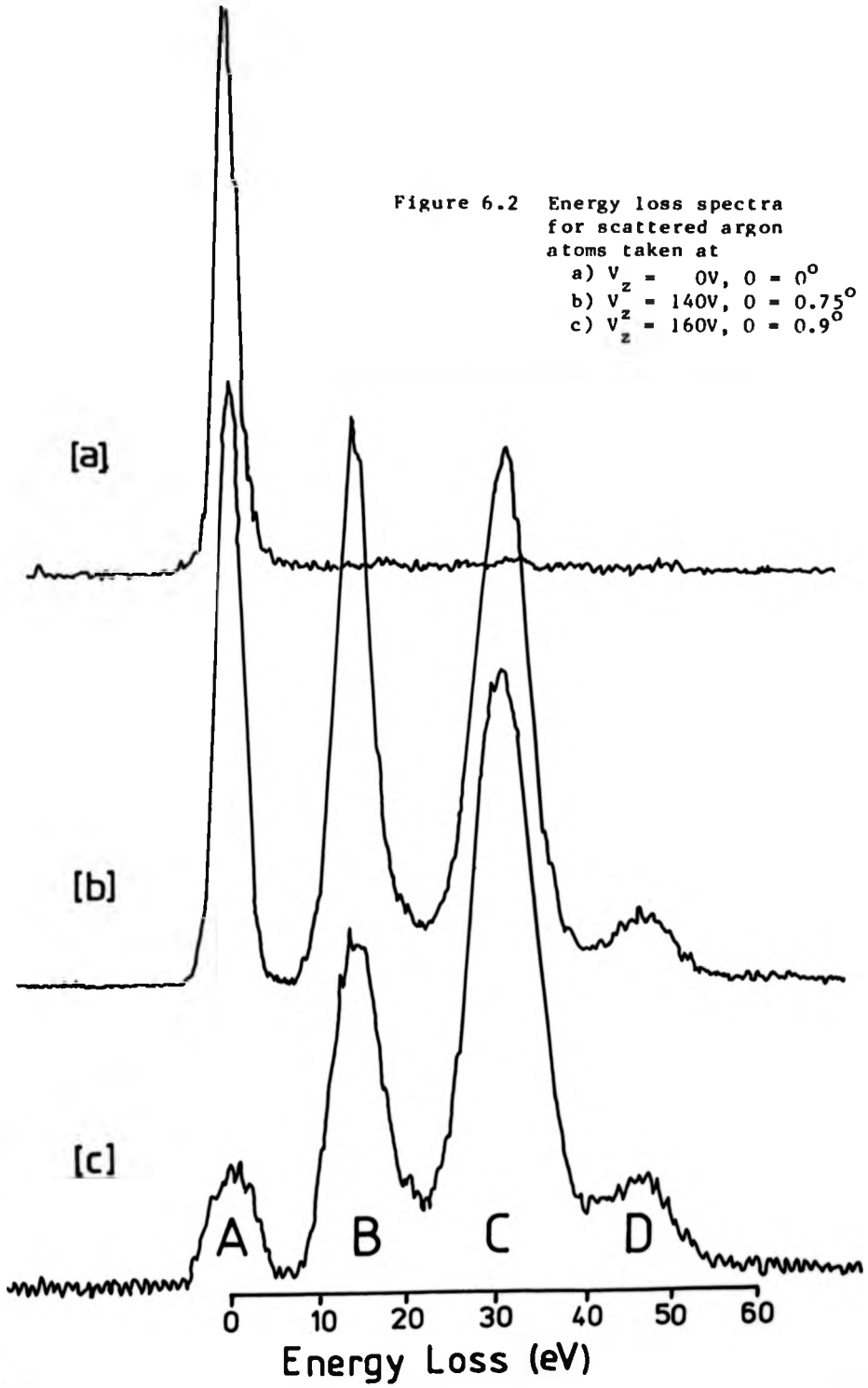

Figure 6.2 Energy loss spectra for scattered argon atoms taken at
a) V_z = 0V, 0 = 0°
b) V_z = 140V, 0 = 0.75°
c) V_z = 160V, 0 = 0.9°

6.3.2 Methanol

Methanol was introduced into the EI source of the mass spectrometer via a reservoir probe and a number of metastable maps were taken at different values of the z-deflection voltage. Ten lead-in scans were taken and a step size of 0.127% was used for each map. Argon was introduced into the collision cell so that the intensity of the parent ion was reduced to 20% of its original value. Figure 6.3 shows how the relative concentrations of the product ions from the collision-induced decomposition spectra of the molecular ion vary with the z-deflection voltage. The data were extracted from metastable maps because the inelastic collisions occuring at high angles would shift the position of the peak on the B,E′ plane and might make B/E linked scans unsuitable. The results compare well with previously published angle-resolved data {102,104} as well as with charge exchange experimental data and theoretical results {104}.

6.3.3 Carbon disulphide

Figure 6.4 shows a plot of daughter ion intensity from the molecular ion of carbon disulphide vs. z-deflection voltage. The sample was introduced into the EI source via a reservoir probe and argon was introduced into the collision cell so that the parent ion intensity was reduced to 20% of its original value. The data were not extracted from metastable maps because the large

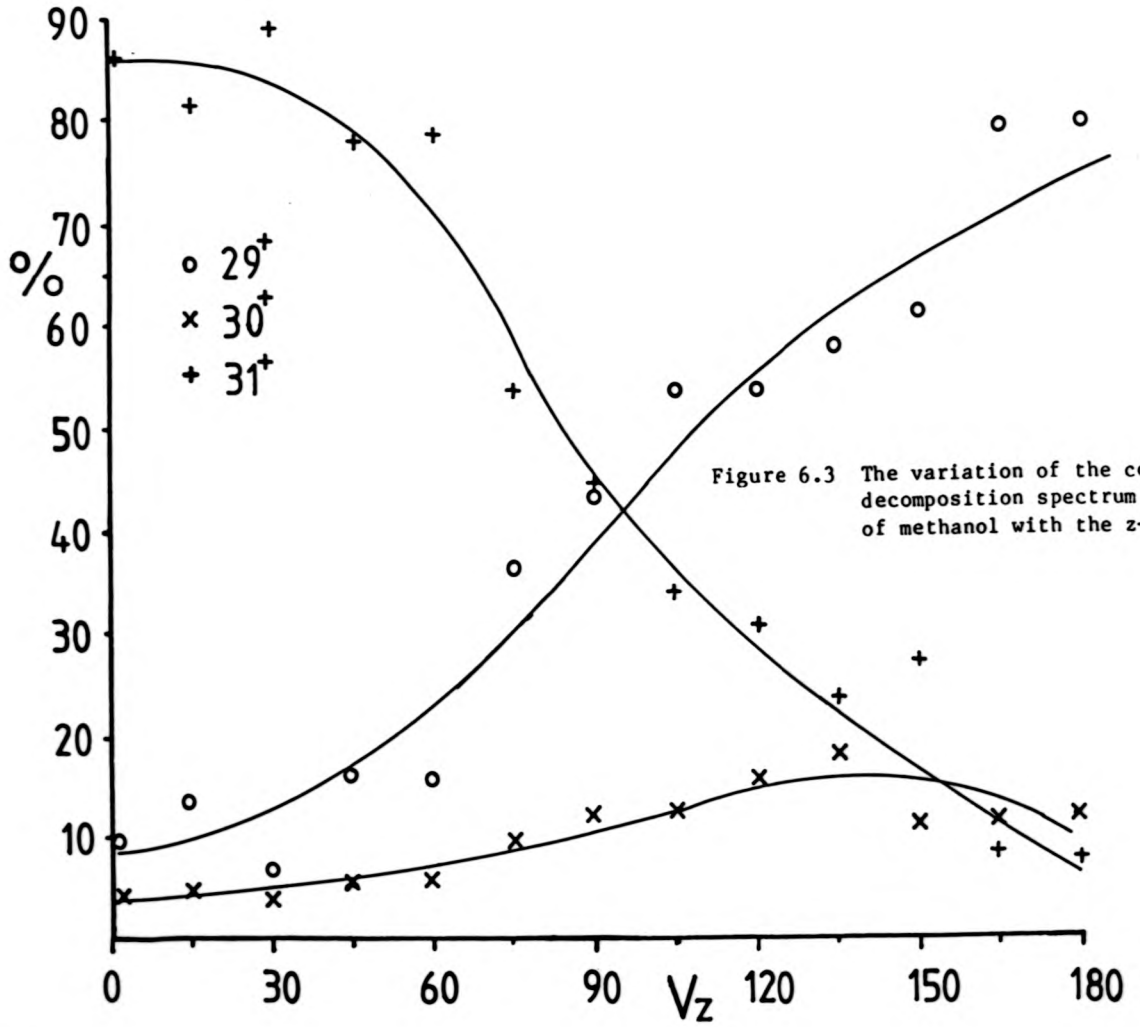

Figure 6.3 The variation of the collision-induced decomposition spectrum of the molecular ion of methanol with the z-deflection voltage.

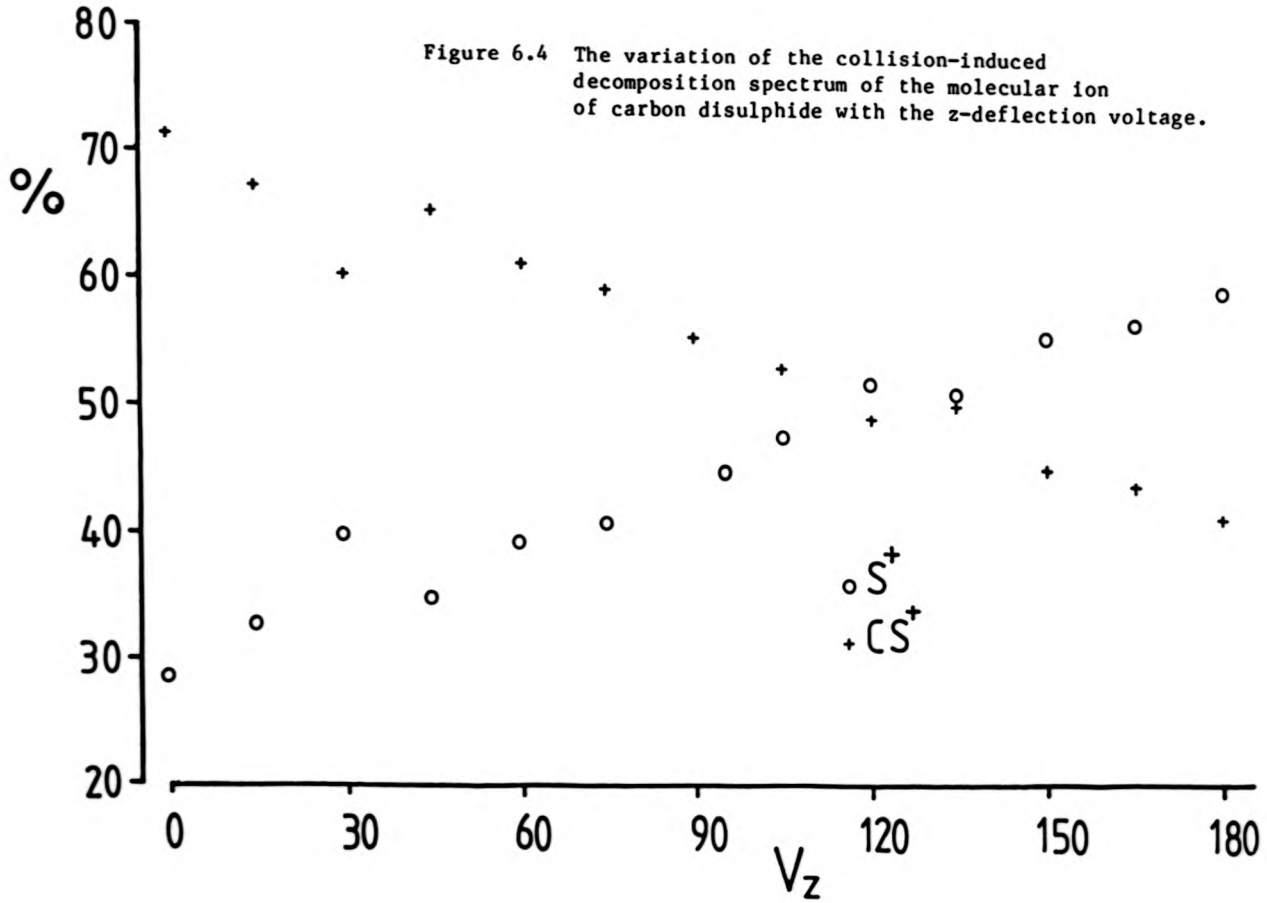

Figure 6.4 The variation of the collision-induced decomposition spectrum of the molecular ion of carbon disulphide with the z-deflection voltage.

mass separation of the daughter ions would have made the experiment too time-consuming. Instead, the accelerating voltage reference was held constant by the MINC-11, and the electric sector reference voltage was set to the correct value to transmit each daughter ion in turn by a Fluke 720A voltage divider. A short magnet scan was then performed and the daughter ion intensities were calculated from the heights of the peaks on an ultra-violet recorder trace. Each of the points shown in Figure 6.4 is the mean of three experiments, with an average variance of about 1.2% on each point. The spectra show a similarity to work published previously (cf. Figure 5 from Laramee et al. {104}), but they do not show a crossing point, where the 32^+ ion becomes more intense than the 44^+ ion, at low angle.

6.4 Determining the Angle

A relationship has been derived {110} between the z-deflection voltage and the angle at which the observed fragments were scattered. If the y-plates are assumed to be at earth potential (which they will be for a perfectly aligned ion beam) and the cylindrical tube is regarded as a virtual earthed plate q millimetre from the z-plates, and if the field generated by the z-plates decreases linearly towards both the y-plates and the virtual earthed plate, then the velocity, v_z, which is imparted to an ion passing between the y-plates and the virtual earthed plate is given by {110}

$$v_z = (eV_z/2mv_x).(p+q)/s$$

where p is the distance between the y-plates and the z-plates (6 mm), s is the separation of the z-plates (6 mm), V_z is the potential between each of the z-plates and earth, m/e is the mass-to-charge ratio of the ion and v_x is the ion's velocity in its direction of flight. If the ion passes through the y-plates at an angle θ and with velocity v, then

$$v_z = v.\sin\theta \quad \text{and} \quad v_x = v.\cos\theta \quad .$$

The ion will be collected if a potential is applied to the z-plates which causes an equal and opposite v_z to be imparted to the ion. Thus

$$v.\sin\theta = (eV_z/2mv.\cos\theta).(p+q)/s$$

For small values of θ, $v.\cos\theta = v$,

$$\sin\theta = (eV_z/2mv^2).(p+q)/s$$

For an ion of mass m_1 decomposing to give an ion of mass m_2 in the field-free region before the y-plates,

$$v^2 = (2eV_a/m_1)$$

where V_a is the accelerating potential,

and so the scattering angle (θ) at which the product of the decomposition is observed is given by;-

$$\theta = \sin^{-1}(p+q/4s).(V_z/V_a).(m_1/m_2)$$

The nature of q, the extent to which the field from the z-plates penetrates the earthed cylinder, is unknown, but if it is assumed to be about 11 mm, then the 29^+ ion becomes more intense than the 31^+ ion in the collision-induced decompositon spectrum of the molecular ion of methanol at an angle of about 0.52^o, a value which corresponds to that found previously {104}. The maximum observable scattering angle in the MS-50 if q = 11 mm, $m_1 = m_2$, and V_z = 200V, is about 1^o for 8 kV ions and

about 1.3^{o} for 6kV ions.

6.5 Angular Resolution

Figure 6.5 shows the arrangement and widths of the slits in the MS-50 which determine the angular resolution of a scattered ion beam which has been brought to focus by using the z-deflector plates. The most important of these are the collector slit and the z-restrictor slit next to the source. The latter controls the width of the ion beam before it passes through the collision cell and the former defines the angular acceptance of the collector. The experiments described above were performed with the slits fully open to achieve maximum sensitivity and the scattering angle was thus definable to about $\pm$ 0.11^{o}. This value is reducible to about 0.03^{o} with considerable loss of sensitivity, but neither value is comparable to experiments performed previously where an angular resolution of 0.01^{o} was obtained {108}. In practice, the values for the angular resolution obtained were probably worse than this.

The y-deflection plates may also be used to deflect scattered ions back onto the optical axis of the mass spectrometer, but because the electric sector focusses the ion beam in the y-direction, results obtained by this method showed a considerably worse angular resolution than those obtained from scattering in the z-direction.

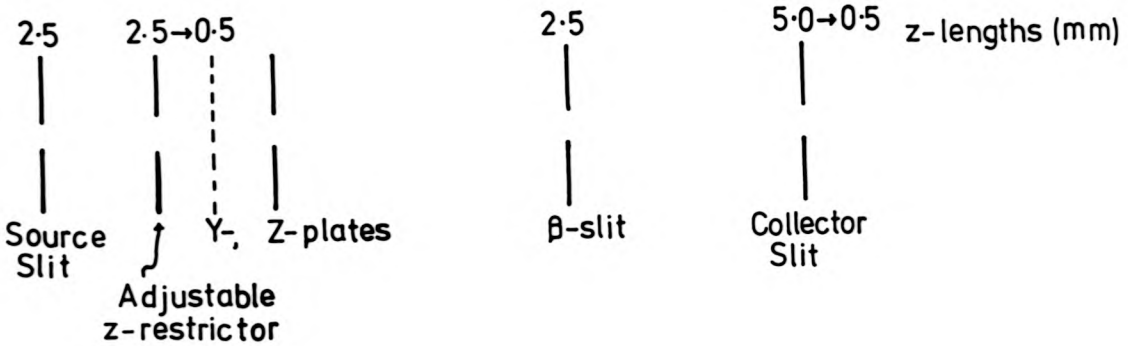

Figure 6.5 The arrangement of the slits in the MS-50

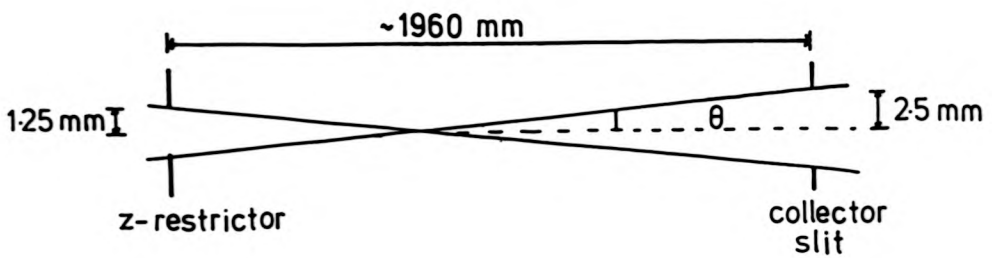

$\therefore \theta$ has a spread of $\pm 0.11^\circ$ [reducible to $\pm 0.03^\circ$]

6.6 Discussion

The results for argon and methanol compare very well with previously published results, but those for carbon disulphide do not. The double crossing point exhibited in the previous work {104} has been explained by postulating decompositions from isolated electronic states of the parent ion. The conditions used here are similar to those used in that work, but it might be possible that ions in such states were not being formed. More likely explanations for the poor quality of these results were the low angular resolution of the beam (if the observation angle was poorly defined the first crossing point (at $\theta=0.05^{o}$) might be obscured) and the mass dependence of the degree of deflection of the products by the z-plates. For methanol, where the masses of the daughter ions are similar, the degree of mass discrimination is likely to be small, but in the case of carbon disulphide, where the masses of the fragments differ radically, severe discrimination will occur. For example, when a z-deflection voltage of 180V was used in the experiment described in section 6.3.3, the 44^{+} ions observed (according to the equation quoted above) resulted from the fragmentation of parent ions scattered through about 1.6^{o}, while the 32^{+} ions arose from ions scattered through about 2.2^{o}.

It has been proposed that the observed angular distribution of the products is due largely to the kinetic energy released by the fragmentation, and not to the scattering of the parent ion {113}. Breakdown curves

calculated from the variation of the kinetic energy released with ion internal energy show good agreement with those derived from ARMS experiments for some compounds, but it can be argued that since normal mass spectra of scattered ions can be observed {108,181}, there must be some contribution to the observed angle of decompostion from the scattering of the parent ions. In addition, if the decompositions of the molecular ion of benzyl methyl ether are considered {114}, it can be shown that the intensity of the $122^+ \rightarrow 91^+$ transition increases relative to that of the $122^+ \rightarrow 92^+$ transition as the angle of observation increases. As the kinetic energy released in the former decomposition (T = 0.07 eV) is smaller than that in the latter (T = 0.3 ev), this observation supports the scattering theory. It is likely, however, that the angle of observation is dependent on both the scattering of the parent ions and the degree of kinetic energy released during the decomposition.

In conclusion, therefore, it can be seen that the z-deflection method offers an easy method of producing angle-resolved CID spectra when the masses of the daughter ions studied do not radically differ. Both the collimation of the ion beam, which has been shown to be important {115}, and the angular resolution were poor in these experiments and it would be more sensible to study ions that are deflected onto the optical axis of the mass spectrometer by the collision: such ions would have to enter the collision chamber at an angle, and a suitable swinging ion source is currently under construction.

calculated from the variation of the kinetic energy released with ion internal energy show good agreement with those derived from ARMS experiments for some compounds, but it can be argued that since normal mass spectra of scattered ions can be observed {108,181}, there must be some contribution to the observed angle of decompostion from the scattering of the parent ions. In addition, if the decompositions of the molecular ion of benzyl methyl ether are considered {114}, it can be shown that the intensity of the $122^+ \rightarrow 91^+$ transition increases relative to that of the $122^+ \rightarrow 92^+$ transition as the angle of observation increases. As the kinetic energy released in the former decomposition (T = 0.07 eV) is smaller than that in the latter (T = 0.3 ev), this observation supports the scattering theory. It is likely, however, that the angle of observation is dependent on both the scattering of the parent ions and the degree of kinetic energy released during the decomposition.

In conclusion, therefore, it can be seen that the z-deflection method offers an easy method of producing angle-resolved CID spectra when the masses of the daughter ions studied do not radically differ. Both the collimation of the ion beam, which has been shown to be important {115}, and the angular resolution were poor in these experiments and it would be more sensible to study ions that are deflected onto the optical axis of the mass spectrometer by the collision: such ions would have to enter the collision chamber at an angle, and a suitable swinging ion source is currently under construction.

7. Results and Discussion

In this chapter, some results obtained by using metastable mapping are presented and discussed. Both industrial samples and compounds of biological interest are considered. An assessment of the technique is also given and some suggestions are made for improvements to the technique.

7.1 A Phosphonate Ester

This section describes the use of a metastable map to study the decompositions of a phosphonate ester, tetraisopropylmethylenediphosphonate. Phosphonate esters are important in the life sciences, where they can be regarded as pyrophosphate analogues in the ATP-ADP cycle, and in synthetic organic chemistry, where they can be used to produce alkenes by the Wittig-Horner reaction {142,143}. The sample was provided by Dr D.W. Hutchinson and P.A.Cload (University of Warwick) and introduced into the source of the MS-80 via a solids probe. The intensities of the fragment ions from the protonated molecular ion (m/z 345) in the ammonia CI spectrum of the sample, which is shown in Figure 7.1, are much smaller than in a spectrum published previously {144}. A metastable map of the sample, taken under ammonia CI conditions, is shown in Figure 7.2 (15 lead-in scans, step size 0.15%). The number of transitions visible on the map may indicate that there was a degree of collision-induced decomposition caused by gas escaping from the ion source. The largest transition shown corresponds to the loss of ammonia from the adduct ion at m/z 362. This ion was approximately 1.5% as abundant as the protonated

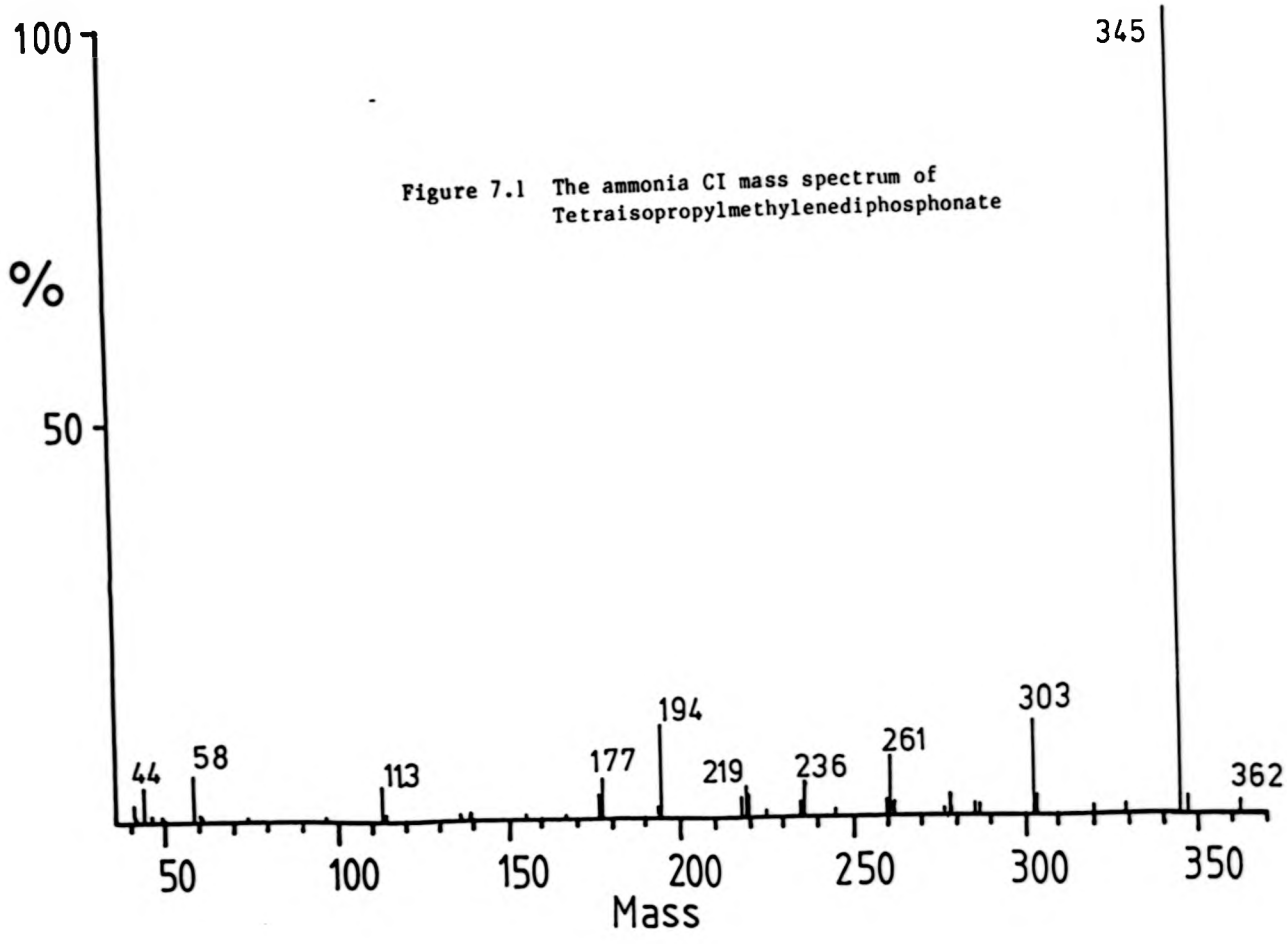

Figure 7.1 The ammonia CI mass spectrum of Tetraisopropylmethylenediphosphonate

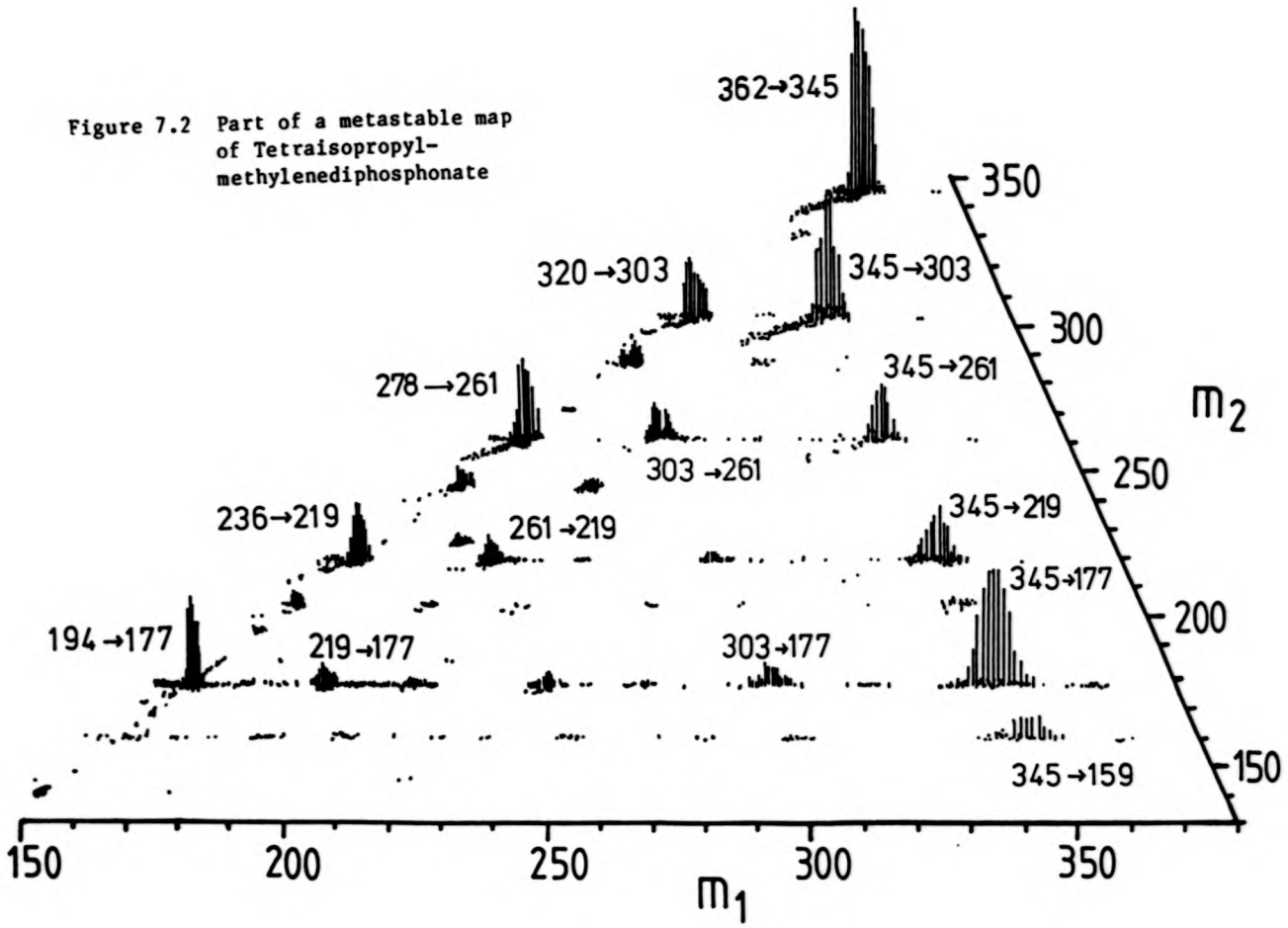

Figure 7.2 Part of a metastable map of Tetraisopropyl-methylenediphosphonate

molecular ion in the mass spectrum (Figure 7.1), and the size of this metastable peak may indicate that the adduct is formed in the source but that it quickly decomposes to produce the protonated species. The ions at m/z 320, 278, 236 and 194 can also be identified as adduct ions by examining the metastable map.

The map confirms the view {144} that the recurrent loss of a neutral fragment of mass 42 Daltons, corresponding to a rearrangement leading to the loss of propene from an isopropyl group, is the most common fragmentation pathway. All four isopropyl groups are successively lost from the protonated molecular ion, giving rise to the ions at m/z 303, 261, 219 and 177 (a map of the sample taken under EI conditions showed mainly losses of single propene units). The daughter ion of lowest mass (m/z 159) of the protonated molecular ion could be formed by the elimination of all the isopropyl groups and a rearrangement leading to the loss of a water molecule. The loss of a second water molecule to give an ion at m/z 141 was not observed. Structures for some of these ions can be postulated and are shown in Figure 7.3.

7.2 Industrial Surfactants

This section describes a study made on three mixtures of long-chain amines, known as synprolams (SYNthetically PROduced AMines), manufactured by I.C.I. Petrochemicals and Plastics Division for use as surfactants. They are known by code numbers denoting the number of methyl groups attached

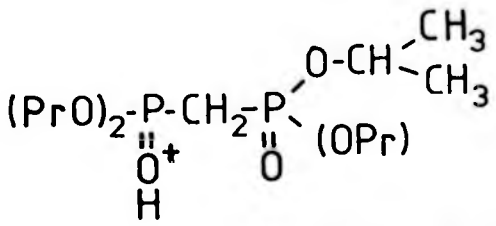

345+

where PrO= -O-CH(CH3)2

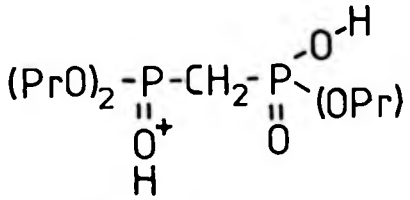

303+

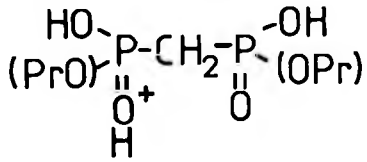

261+

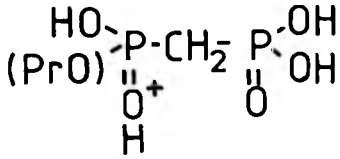

219+

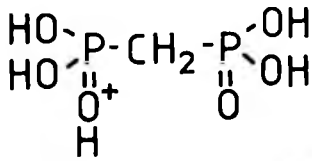

177+

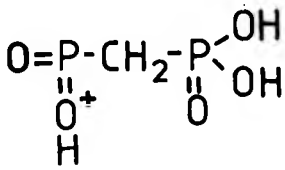

159+

Figure 7.3 Possible structures for some of the ions seen in Figure 7.1

to the nitrogen atom. The composition of the mixtures are given below:-

		MWt.
S35	$C_{13}H_{27}NH$	199
	$C_{15}H_{31}NH$	227
S35M	$C_{13}H_{27}NH(CH_3)$	213
	$C_{15}H_{31}NH(CH_3)$	241
S35DM	$C_{13}H_{27}N(CH_3)_2$	227
	$C_{15}H_{31}N(CH_3)_2$	255

The component of lower mass is present in the mixtures at approximately four times the concentration of the component of higher mass. Because of the similarity of the long chain alkyl substituents the two components in each mixture could not be separated by gas chromatography. The component of lower mass in S35DM is an isomer of the heavier component of S35, and it was hoped to use metastable mapping to distinguish them. The samples were all viscous liquids, and both electron (EI) and chemical ionization (CI) were used to produce the ions.

7.2.1 Electron Ionization Maps

The samples were introduced into the EI source of the MS-50 via a reservoir probe and maps were taken using ten lead-in scans and a step size of 0.235%. The molecular weights of the components lie between 199 and 255 Dalton, and this step size would ensure that a peak resulting from any decomposition would be detected at

least once, even if no kinetic energy were to be released. The ions were accelerated by a potential of 8 kV and the unimolecular decomposition products examined. The most intense peaks in the EI spectra were found to be those due to α-cleavage, and the molecular ions of S35M and S35DM were very small. The only map which could be interpreted was that of S35, where the most intense transitions were those due to the losses of the terminal amine groups to give the corresponding alkene ions i.e. $199^+ \rightarrow 182^+$ and $227^+ \rightarrow 210^+$. All other significant peaks represented losses of alkene or alkyl groups from 182^+ and 210^+.

7.2.2 Chemical Ionization Maps

The reservoir probe could not be used under CI conditions because of problems with the electrical insulation, and the samples were introduced into the CI source of the MS-50 from a drawn-out glass capillary placed in the end of a solids probe. Methane and ammonia were used as the reagent gases, although it was found that the molecules would protonate themselves at high source pressures. It was found that the decomposition products of the protonated molecules were largely independent of the means of ionization. All of the maps were taken using air as a collision gas, typically with 30-50% beam transmission ratios.

Maps taken using ammonia as the reagent gas are presented as Figure 7.4 (for S35), 7.5 (for S35M), and

Figure 7.4 Part of a metastable map of S35

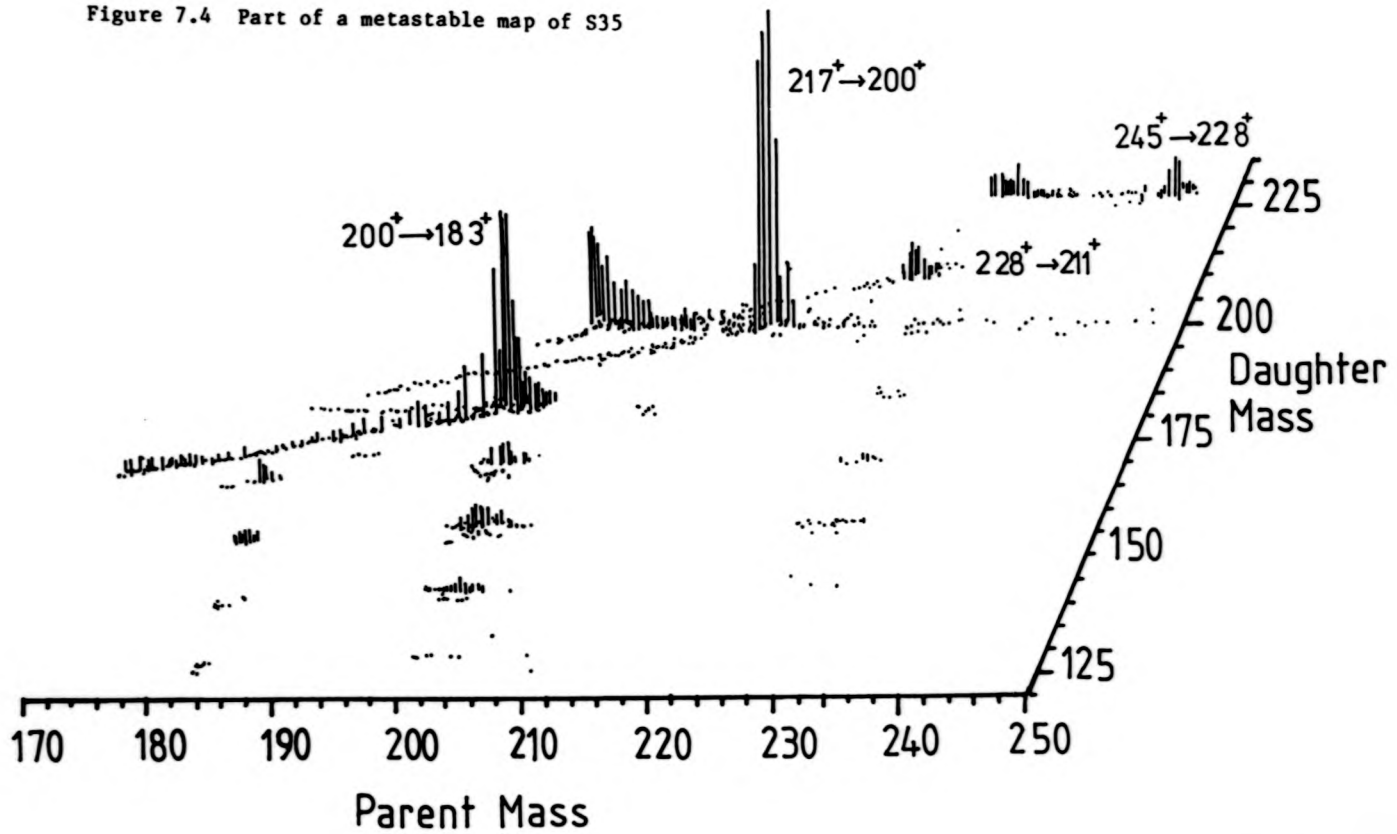

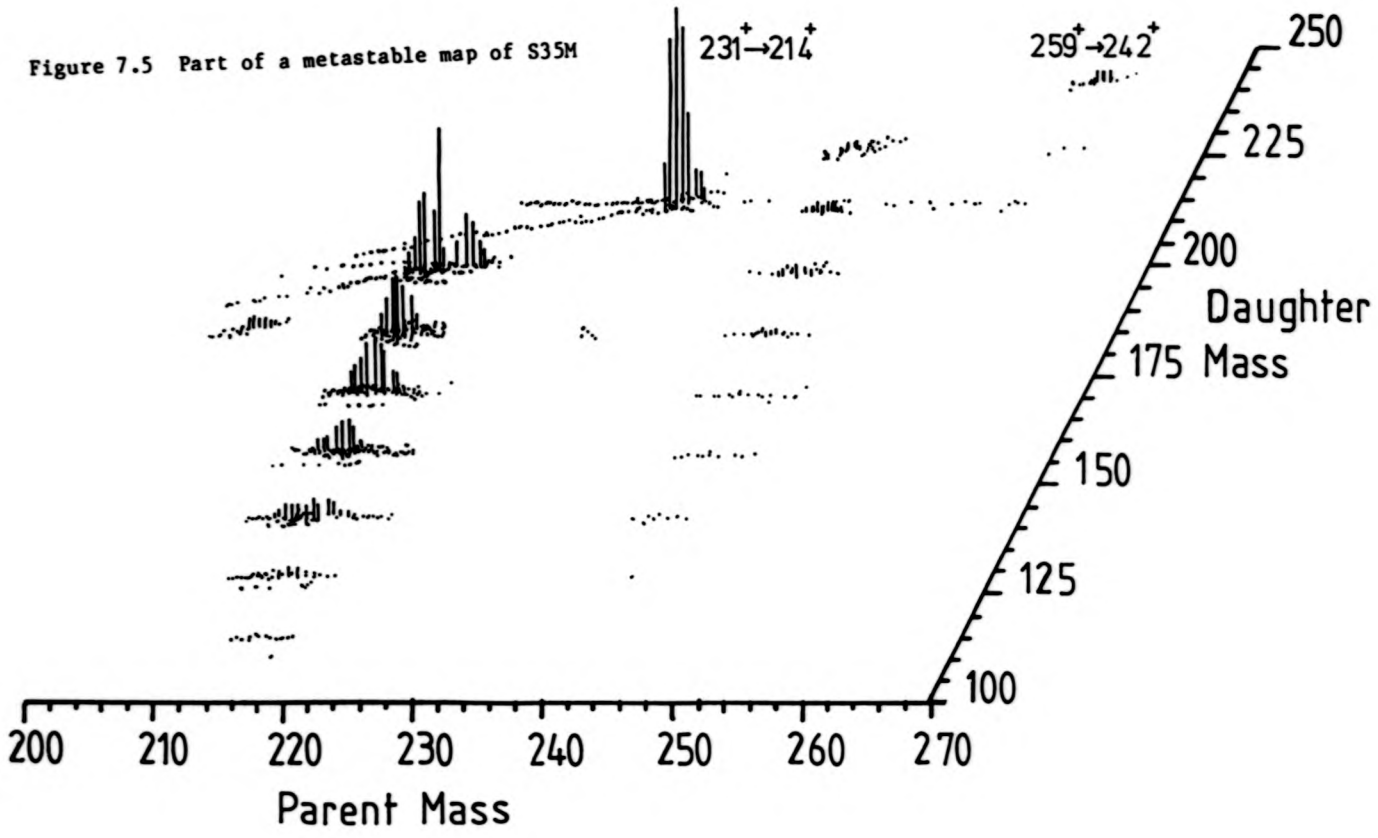

Figure 7.5 Part of a metastable map of S35M

Figure 7.6 Part of a metastable map of S35DM

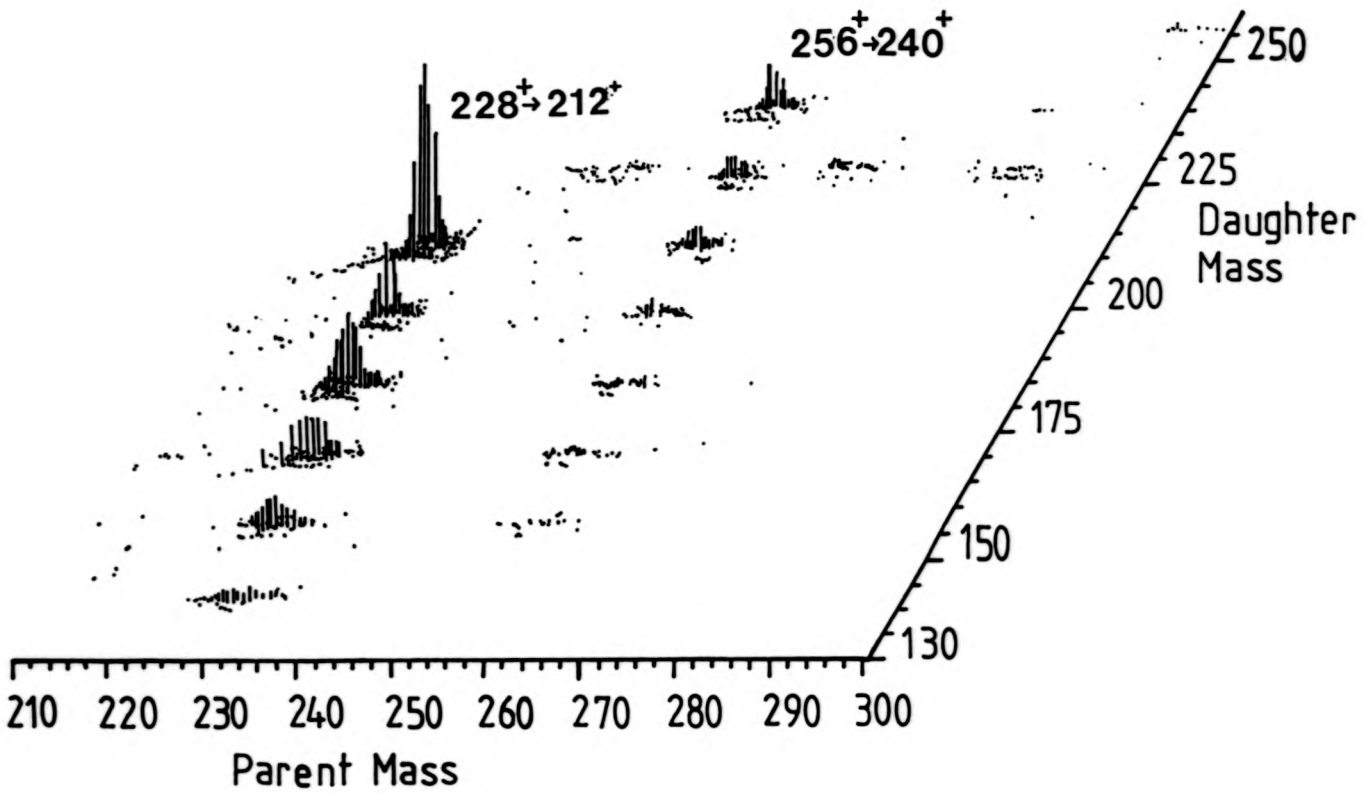

7.6 (for S35DM). For the mixture of the primary amines, S35, the largest transitions on the map were due to the loss of ammonia from the protonated and adduct ions, although no such adduct ions were observed in the mass spectra. Much smaller peaks due to the losses of alkyl-NH_2 groups could also be seen. Peaks due to the transitions from other ions (e.g. 182^+ or 210^+) were small compared to those of their parent ions. For the mixture of secondary amines, S35M, almost all of the transitions arose from the protonated molecular ions, and were typically losses of alkenes. Similar losses occured from the protonated molecular ion of S35DM.

It should be noted that the component of mass 227 in S35 preferentially lost ammonia while the corresponding isomer from S35DM was observed to lose methane, and it would thus be possible to distinguish them by a linked scan of the protonated molecular ions.

7.3 Some Proprietary Headache Cures

This section describes the use of metastable mapping to identify a minor component in a mixture of both biological and commercial interest. All of the maps were taken using 10 lead-in scans and a step size of 0.25%. Caffeine was introduced into the EI source of the MS-50 via a standard solids probe and a metastable map was acquired and is shown in Figure 7.7. A map for asprin (Acetylsalicylic acid) was also obtained (Figure 7.8). A water-soluble headache tablet commercially available in

Figure 7.7 Part of a metastable map of caffeine

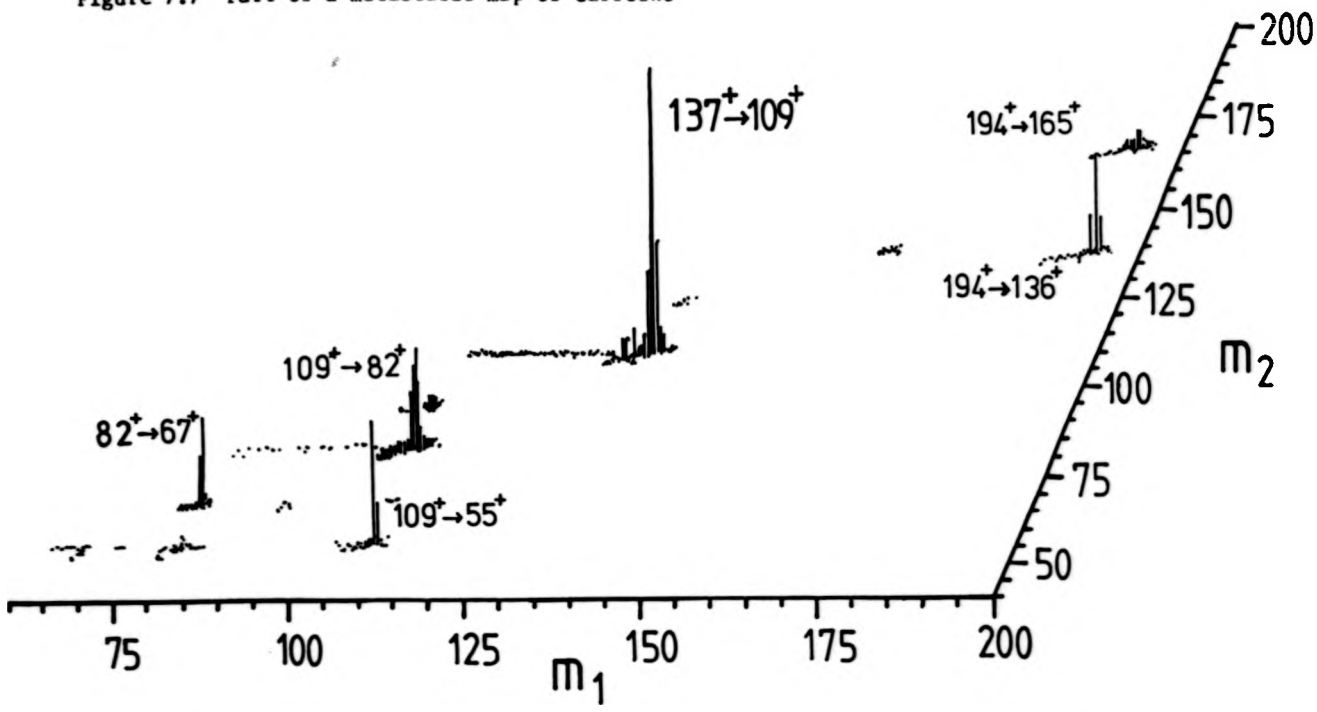

Figure 7.8 Part of a metastable map of acetylsalicylic acid

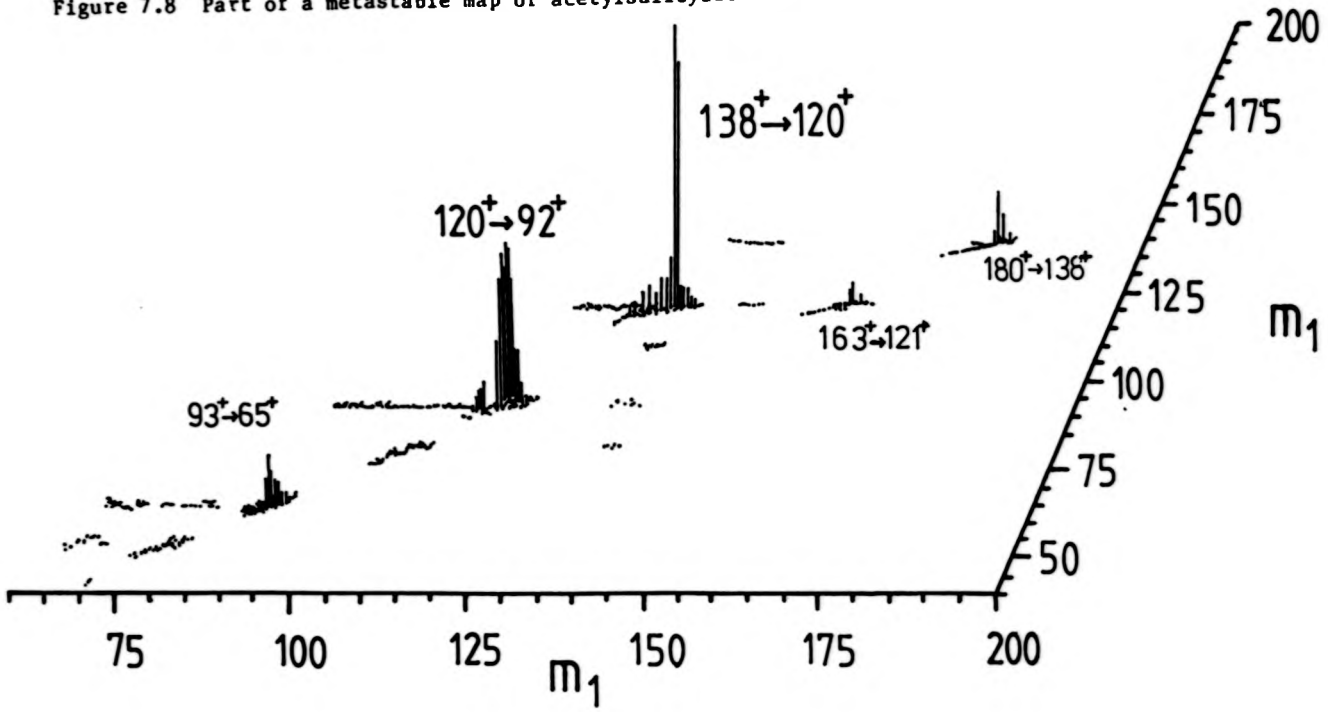

Australia ("Solprin", manufactured by Recketts, Australia) was ground up, and its metastable map showed only transitions which could be attributed to asprin. A popular British tablet ("Anadin", manufactured by the International Chemical Co. London) was similarly treated, and its metastable map is shown in Figure 7.9. Caffeine is introduced into the tablet at a concentration of 3.5% to act as a stimulant and the corresponding peaks, labelled 'C', can be seen on the map. Metastable maps are useful for the identification of components of mixtures because such identifications have the advantage of being made on the basis of several transitions.

7.4 Phthalate Plasticizers

This section describes the investigation of a set of phthalate esters manufactured by I.C.I. Petrochemicals and Plastics Division. They are viscous involatile liquids whose purpose is to soften paints, varnishes, plastics etc. The components of the mixture were not separable by GC because of the extreme involatility of the sample: phthalate isomers have been used as GC stationary phases and as diffusion pump oils. Two sets of results will be presented: those for a six-component mixture and those for a pair of isomers. The CI spectra of these phthalates showed a considerable degree of fragmentation in spectra obtained on both the MS-50 and the MS-80 using either ammonia or methane as reagent gases. The EI spectra showed no ions present above m/z 149.

Figure 7.9 A metastable map of an "Anadin" tablet, showing peaks due to the presence of caffeine

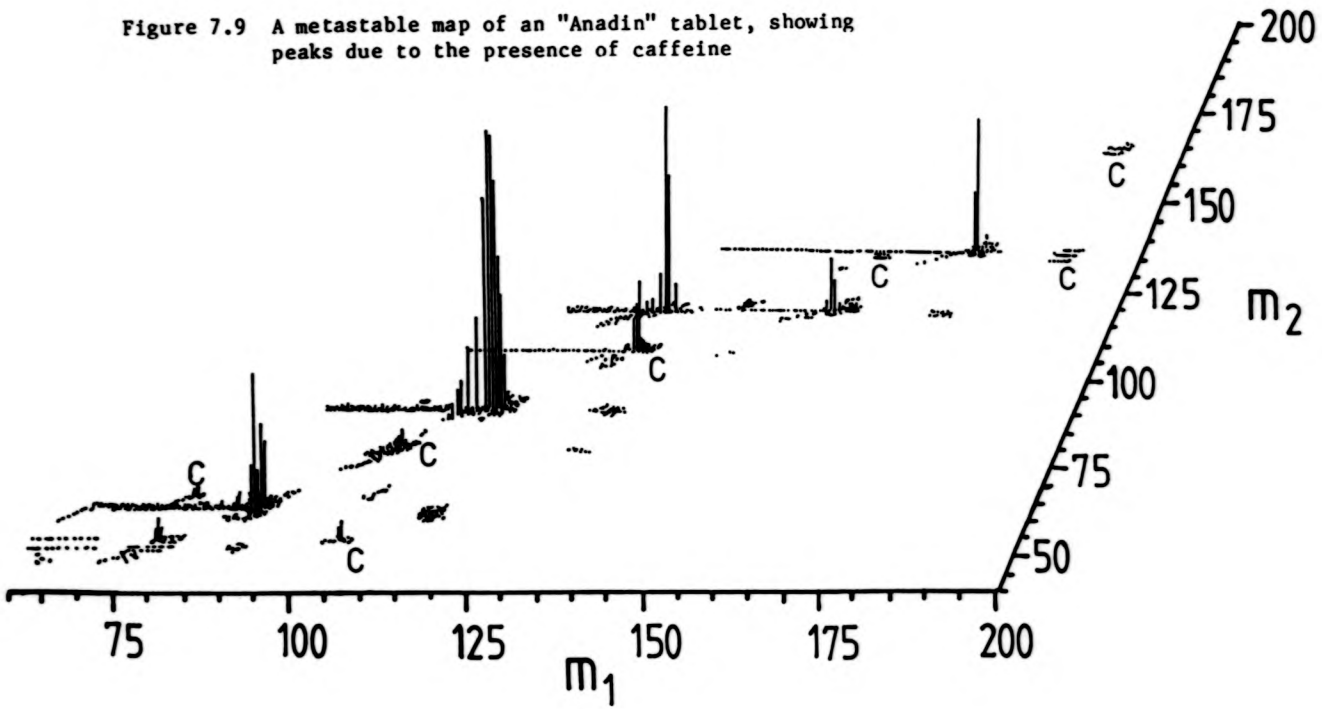

7.4.1 Analysis of a Phthalate Mixture

The liquid under study was suspected to be a set of phthalate esters whose side chains were straight-chain heptyl, octyl or nonyl groups. Each of the possible components of the mixture is shown below. The structures are :-

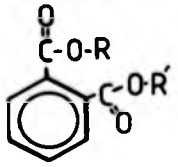

where	R=	R'=	MWt.
	heptyl	heptyl	362
	heptyl	octyl	376
	heptyl	nonyl	390
	octyl	octyl	390
	octyl	nonyl	404
	nonyl	nonyl	418

An ammonia CI spectrum of the mixture contained peaks at m/z 363, 377 and 391 and 405. A metastable map of the sample was acquired (10 lead-in scans, step size 0.166%), part of which is reproduced in Figure 7.10.

An ion at m/z 149 is common to the spectra of all phthalates, and a simulated B^2/E linked scan of all of the parents of this ion is shown in Figure 7.11. The peak at m/z 167 corresponds to a protonated phthalic acid ion, and peaks at m/z 363, 377, 391, 405 and 419 correspond to the suspected components of the mixture. Simulated B/E spectra of the protonated molecular ions of the components were produced, which showed that they lost predominantly alcohols and alkenes from the side chains. For example, the protonated heptyloctylphthalate ion was observed to lose heptanol, octanol, heptene and octene. These transitions produced the ions at m/z 247, 261, 265, 275, 279 and 293. These daughter ions lose the

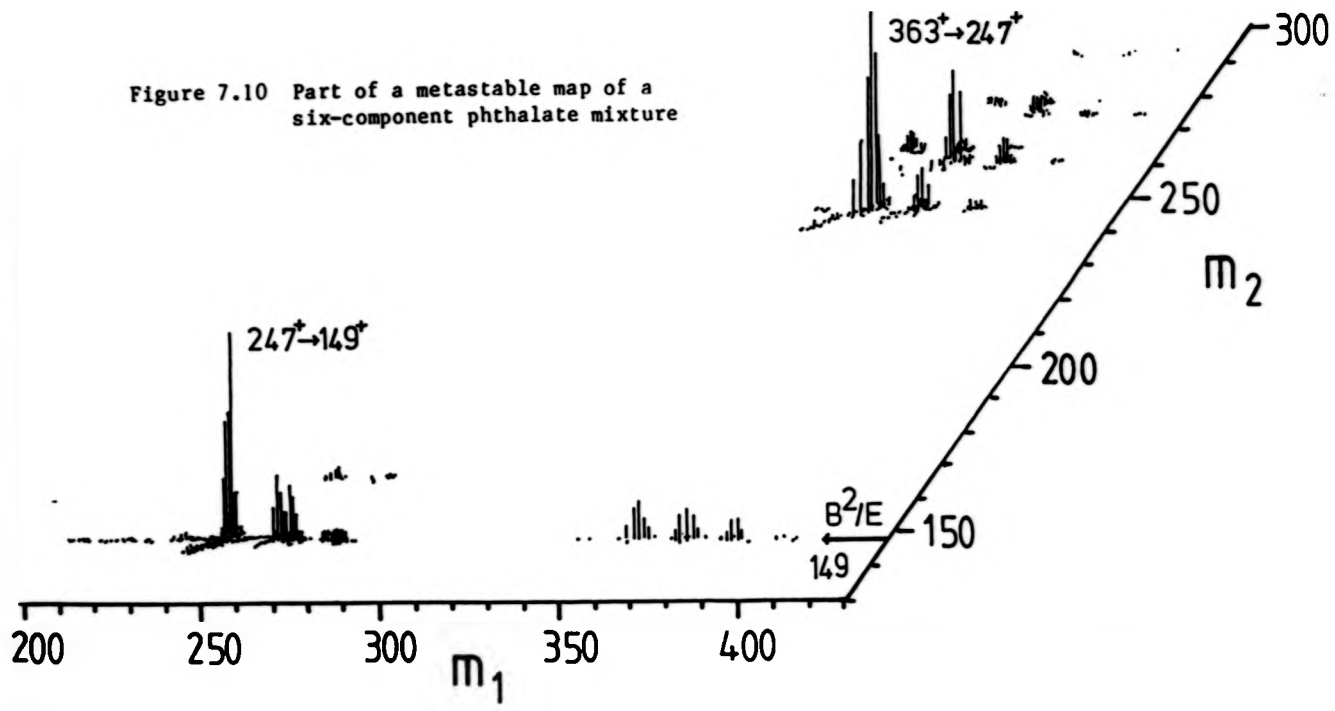

Figure 7.10 Part of a metastable map of a six-component phthalate mixture

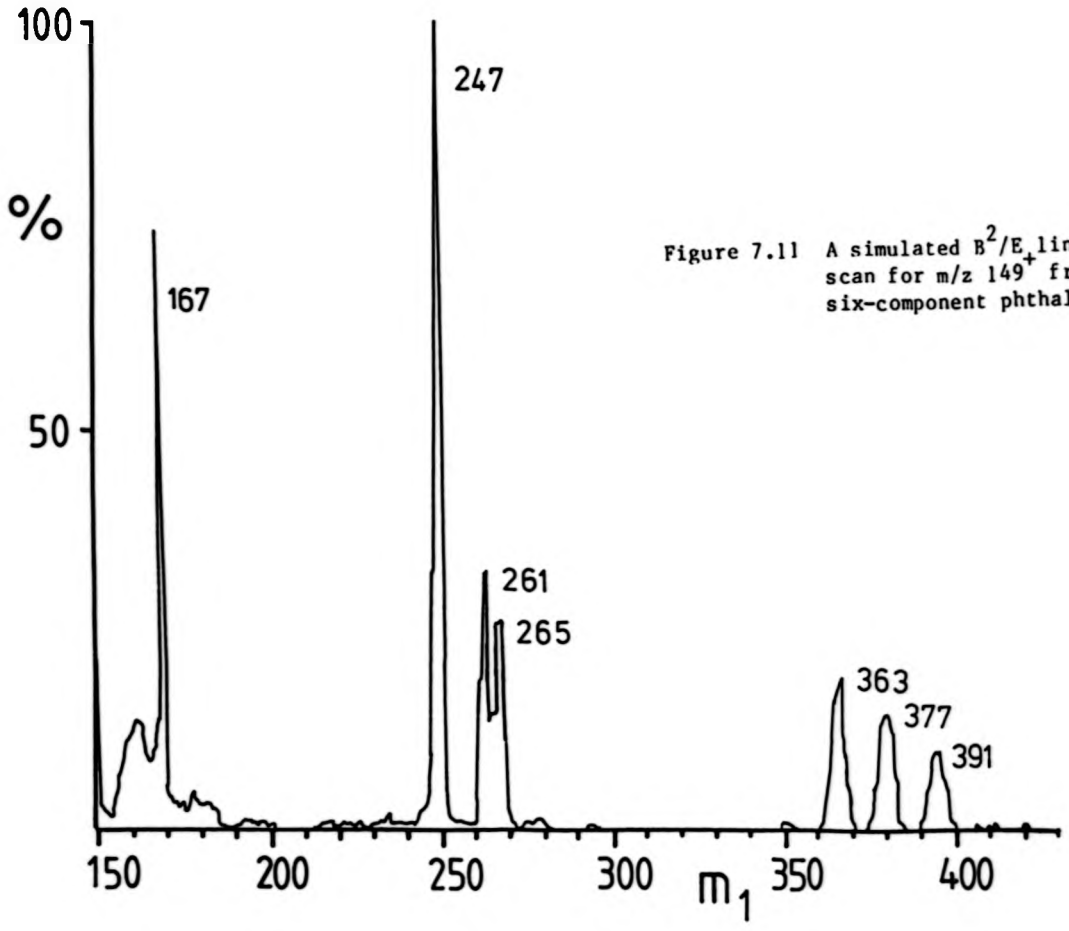

Figure 7.11 A simulated B^2/E_+ linked scan for m/z 149^+ from a six-component phthalate mixture

complementary alkenes or alcohols to give the ion at m/z 149. For example, the ion at m/z 265 is formed by the loss of octene from the protonated heptyloctylphthalate ion and heptene from the protonated diheptylphthalate ion (confirmed by simulated B/E linked scans of the ions at 363^+ and 377^+), and it loses heptanol to give 149^+. The ion at m/z 391 was found to lose heptanol, octanol, nonanol and the corresponding alkenes and so is formed from both the dioctyl- and heptylnonyl- isomers.

7.4.2 Distinguishing Between Phthalate Isomers

Two dioctylphthalate isomers with similar CI spectra (see Figure 7.12) were considered. Metastable maps, using the conditions specified for the map of the mixture, were obtained for the isomers, di(2-ethylhexyl)phthalate (DOP) and di(1,1,3,3-tetramethylbutyl)phthalate (DIOP), whose structures are shown in Figure 7.13. Their ammonia CI spectra and a simulated B^2/E linked scan of m/z 149 showed that both samples gave a protonated molecular ion at m/z 391. Simulated B/E linked scans of these ions are shown in Figure 7.14. As can be seen, the loss of an octene predominates for DOP (to form the ion at m/z 279) whereas the loss of an octanol predominates for its isomer. If we consider the loss of the alcohol from the protonated molecular ions, it can be seen that the 2-ethylhexyl isomer, DOP, will lose a primary alcohol, whereas the other isomer, DIOP, will lose a more stable tertiary alcohol. The activation energy for the latter

complementary alkenes or alcohols to give the ion at m/z 149. For example, the ion at m/z 265 is formed by the loss of octene from the protonated heptyloctylphthalate ion and heptene from the protonated diheptylphthalate ion (confirmed by simulated B/E linked scans of the ions at 363^+ and 377^+), and it loses heptanol to give 149^+. The ion at m/z 391 was found to lose heptanol, octanol, nonanol and the corresponding alkenes and so is formed from both the dioctyl- and heptylnonyl- isomers.

7.4.2 Distinguishing Between Phthalate Isomers

Two dioctylphthalate isomers with similar CI spectra (see Figure 7.12) were considered. Metastable maps, using the conditions specified for the map of the mixture, were obtained for the isomers, di(2-ethylhexyl)phthalate (DOP) and di(1,1,3,3-tetramethylbutyl)phthalate (DIOP), whose structures are shown in Figure 7.13. Their ammonia CI spectra and a simulated B^2/E linked scan of m/z 149 showed that both samples gave a protonated molecular ion at m/z 391. Simulated B/E linked scans of these ions are shown in Figure 7.14. As can be seen, the loss of an octene predominates for DOP (to form the ion at m/z 279) whereas the loss of an octanol predominates for its isomer. If we consider the loss of the alcohol from the protonated molecular ions, it can be seen that the 2-ethylhexyl isomer, DOP, will lose a primary alcohol, whereas the other isomer, DIOP, will lose a more stable tertiary alcohol. The activation energy for the latter

Figure 7.12 The ammonia CI mass spectra of DOP and DIOP

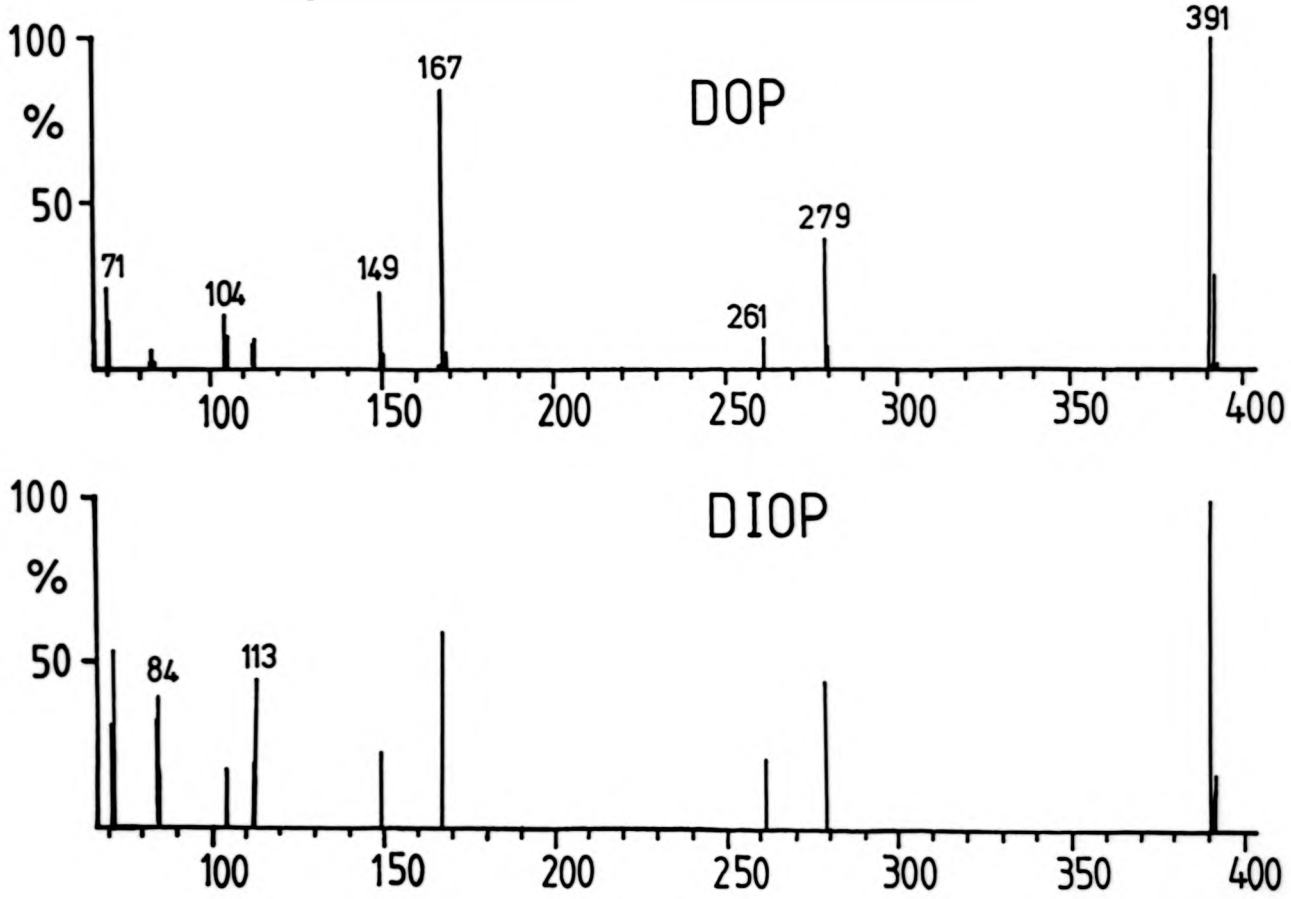

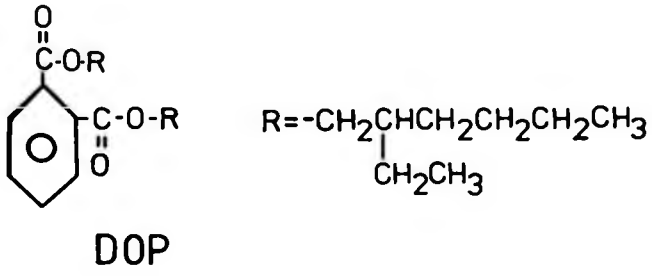

DOP

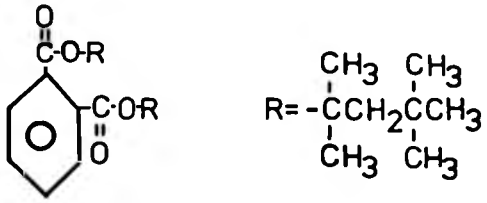

DIOP

Figure 7.13 The structures of the phthalate isomers DOP and DIOP

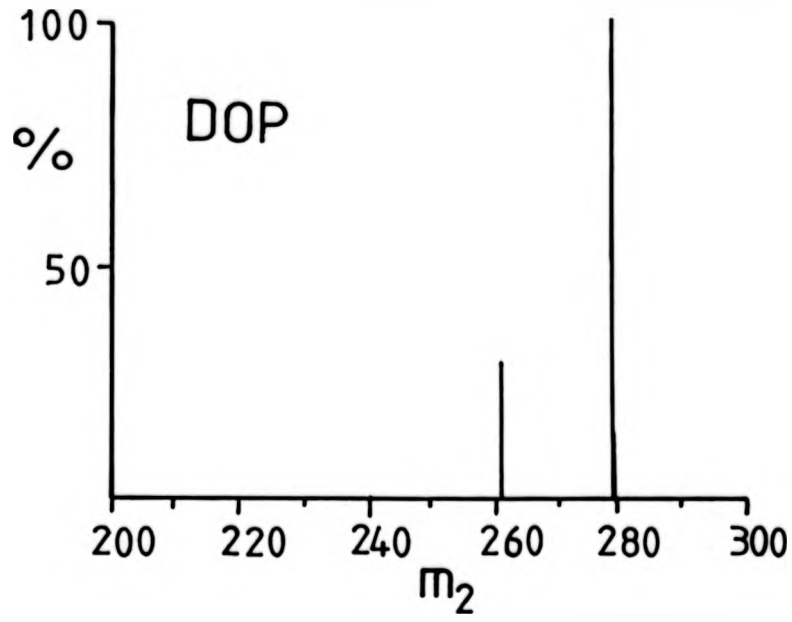

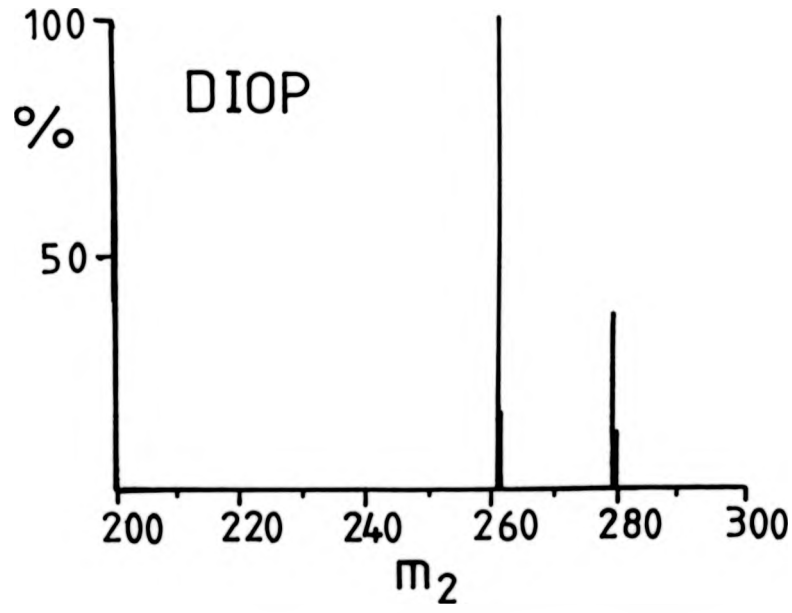

Figure 7.14 Simulated B/E linked scans for m/z 391 from DOP and DIOP

rearrangement would presumably be lower and and the resulting metastable peak more intense: this is reflected in the relative intensities of the octene and octanol losses from the isomers.

It is thus possible to identify which components, if any, of a mixture are phthalates by a B^2/E linked scan for all the parents of the m/z 149^+ ion, and to determine the structure of these ions by B/E linked scans. It is also possible to distinguish between dioctylphthalate isomers by examining the relative intensitites of the octene and octanol losses from their protonated molecular ions.

7.5 Peptide Sequencing

Much interest has been shown in recent years in methods of determining the structure of the peptides and their polymers, the proteins, by mass spectrometry. The latter have traditionally been sequenced, because of their large molecular weights, by breaking them down into smaller fragments with an enzyme and analysing the mixture of peptides produced {116-119}. Derivitization (e.g. acetylation and permethylation {116}) has been used to increase the volatility of peptides, so that EI mass spectra can be obtained, and recently special methods of ionization, such as negative chemical ionization {62,120,121}, Secondary Ion Mass Spectrometry {122,123}, Field Desorption {124-127} and Fast Atom Bombardment (FAB) {123,128-130} have reduced the need for pretreatment of the sample. An increase in sensitivity can be obtained by

studying negative ions {62}.

Both MIKE spectra {121,129,131,132} and linked scans {124,127,131,132} have been used to study the decomposition of selected peptide ions in field-free regions. Experiments performed in a triple quadrupole instrument {123} have also been used to sequence peptides: the mass range of such instruments is limited, however, especially when compared to that of double-focussing instruments equipped with high field magnets {133}.

Metastable maps have been used to sequence three N-acetyl peptide methyl esters: Ac-Trp-Ala-Leu-OMe, Ac-Glu(OMe)-Ala-Leu-OMe, and Ac-Val-Ile-Gly-Leu-OMe, where Ac is an acetyl fragment, OMe is a methoxy group, Glu(OMe) is a methoxyglutamate group, and Trp, Ala, Val, Ile, Leu, and Gly are the tryptophan, alanine, valine, isoleucine. leucine and glycine groups respectively. The samples were supplied by Dr. U.P. Schlunegger (University of Berne).

Approximately 2 mg of sample in methanolic solution was introduced into a glass capillary tube inserted into the tip of a standard solids probe. The probe was introduced into an EI source held at approximately 450 K and the probe temperature was increased from about 375 K to 525 K over a period of about fifty minutes. The EI mass spectra of the peptides are shown in Figure 7.16.

Ten lead-in scans and a step size of 0.167% were used for the metastable maps discussed in this section. The step

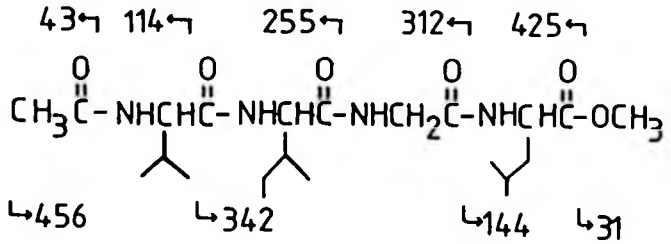

Ac-Val-Ile-Gly-Leu-OMe

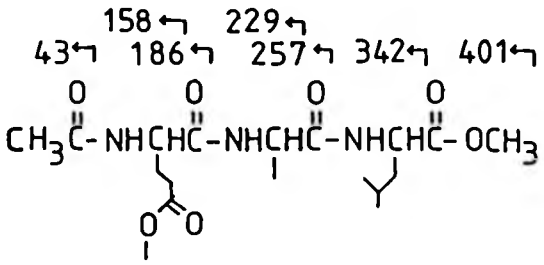

Ac-Glu(OMe)-Ala-Leu-OMe

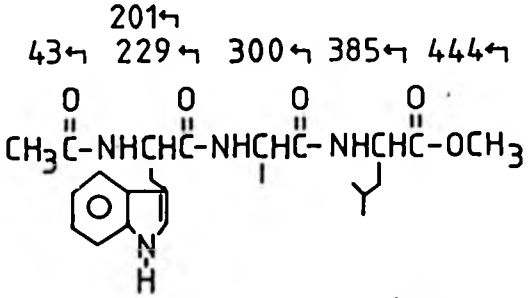

Ac-Trp-Ala-Leu-OMe

Figure 7.15 The structures of the peptides and the masses of some of their possible fragment ions

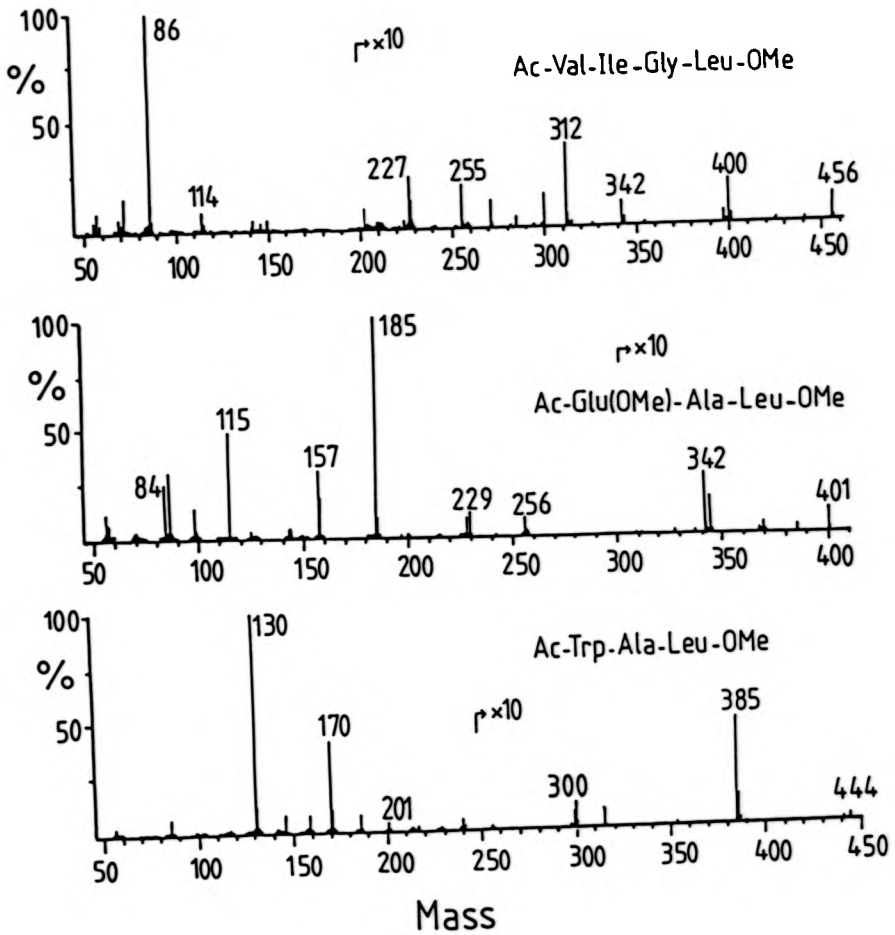

Figure 7.16 The EI mass spectra of the peptides

size was sufficently small to ensure that daughter ions of each fragmentation would be collected in at least one scan. A total of about 400 scans were acquired for each sample.

The metastable map of one of the peptides, Ac-Trp-Ala-Leu-Ome, was taken after argon had been introduced into the collision chamber so that the intensity of the ion beam was reduced to about 30% of its original value. The maps of the other peptides were not taken under CID conditions because structurally more revealing maps were obtainable from observing products of metastable transitions.

Peptides consist of chains of amino acid residues of the form (-NH-CHR-CO-). After ionisation by electron impact they tend to fragment at the peptide bond (to form the so-called sequence ions) or at the C-C bond. For a peptide of known composition but whose sequence is unknown, the various structures and their appropriate fragmentation patterns can be postulated and compared with the transitions shown on a metastable map of the sample. The structures of the peptides studied here are shown in Figure 7.15., together with the masses of some of the daughter ions which they might give rise to.

It is possible to deduce the sequence of the peptides from the fragments observed in the normal mass spectra. For example, the ions observed at m/z 312, 255 and 114 in the spectrum of Ac-Val-Ile-Gly-eu-OMe (Figure 7.16.) correspond to sequence ions and the order of the amino acid residues

can be deduced from these. It is not possible, however, to say with certainty from which ions these fragments were formed, and the additional information given by a MIKE spectrum or linked scan is necessary before the origin of the ions observed can be unambiguously determined.

Part of the metastable map of Ac-Val-Ile-Gly-Leu-OMe is shown in Figure 7.17. The presence of a methoxy terminal group can be deduced from the loss of methanol by the molecular ion (m/z 456). The ions at m/z 312 and 255 are sequence ions (see Figure 7.15.) and the transitions $425^+ \rightarrow 312^+$, $397^+ \rightarrow 312^+$ and $312^+ \rightarrow 255^+$ imply that the first two residues in the peptide are leucine (or isoleucine) and glycine respectively. A small peak from the transition $312^+ \rightarrow 142^+$ may indicate that the next residue is leucine (or isoleucine). The loss of a neutral fragment of mass 42 from the ion at m/z 114 (not shown) implies that the final fragment in the sequence is valine, because the loss corresponds to the expulsion of the protecting acetyl group as a ketene, $CH_2=C=O$. The sequence is confirmed by the transition $342^+ \rightarrow 146^+$, which is probably due to the loss of a CO-Leu-Gly or CO-Ile-Gly neutral fragment. It was not possible to distinguish between the isomers leucine and isoleucine from this map, although this might be possible if other methods of ionization and collision-induced decomposition were to be used.

The metastable map of Ac-Glu(OMe)-Ala-Leu-OMe is shown in Figure 7.18. The transitions $401^+ \rightarrow 342^+$ and

Figure 7.17 Part of a metastable map of Ac-Val-Ile-Gly-Leu-OMe

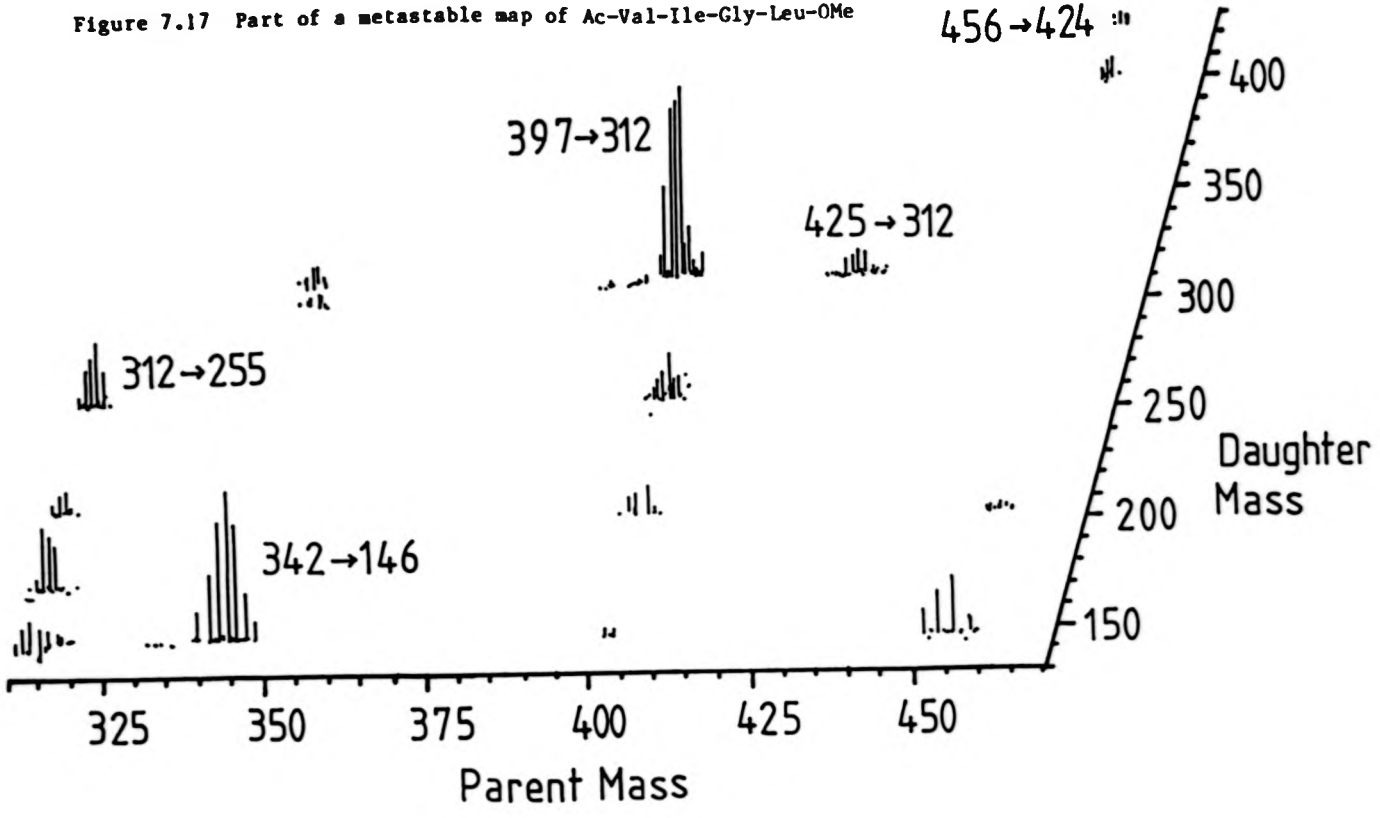

$370^{+} \rightarrow 342^{+}$ are sufficent to confirm the existence of the methoxy terminal group. The ion at m/z 342 is observed to lose a leucyl amine fragment to give an ion of m/z 256 (which corresponds to the Ac-Glu(OMe)-Ala sequence ion), which in turn loses an alanine residue to give the ion at m/z 185 (which corresponds to a Ac-Glu(OMe) sequence ion). The ion at m/z 115, which corresponds to a methoxyglutamate amine fragment, is observed to lose a methoxy radical from the side chain, thus confirming that the sequence of the peptide is Ac-Glu(OMe)-Ala-Leu-OMe.

The third peptide, Ac-Trp-Ala-Leu-OMe, proved much more difficult to sequence because it exhibited a greater degree of rearrangement than the other samples. The metastable map for this sample is shown in Figure 7.19. The residue adjacent to the acetyl group can be shown to be tryptophan because the ion at m/z 201 loses a neutral fragment of mass 42, which corresponds to the loss of the acetyl group as a ketene. The transition $300^{+} \rightarrow 229^{+}$ corresponds to the loss of alanine to give the Ac-Trp sequence ion. The mass difference between the molecular ion (m/z 444) and the ion at m/z 300 implies that the neutral fragment lost to give that daughter ion corresponds to either a Leu-OMe or an Ile-OMe group.

The samples used in this study were small peptides of known composition but, provided that suitable ionization methods (such as FAB) and a magnet capable of high mass range were used, the technique could be extended to sequence a small protein. Metastable mapping would also be

Figure 7.18 Part of a metastable map of Ac-Glu(OMe)-Ala-Leu-OMe

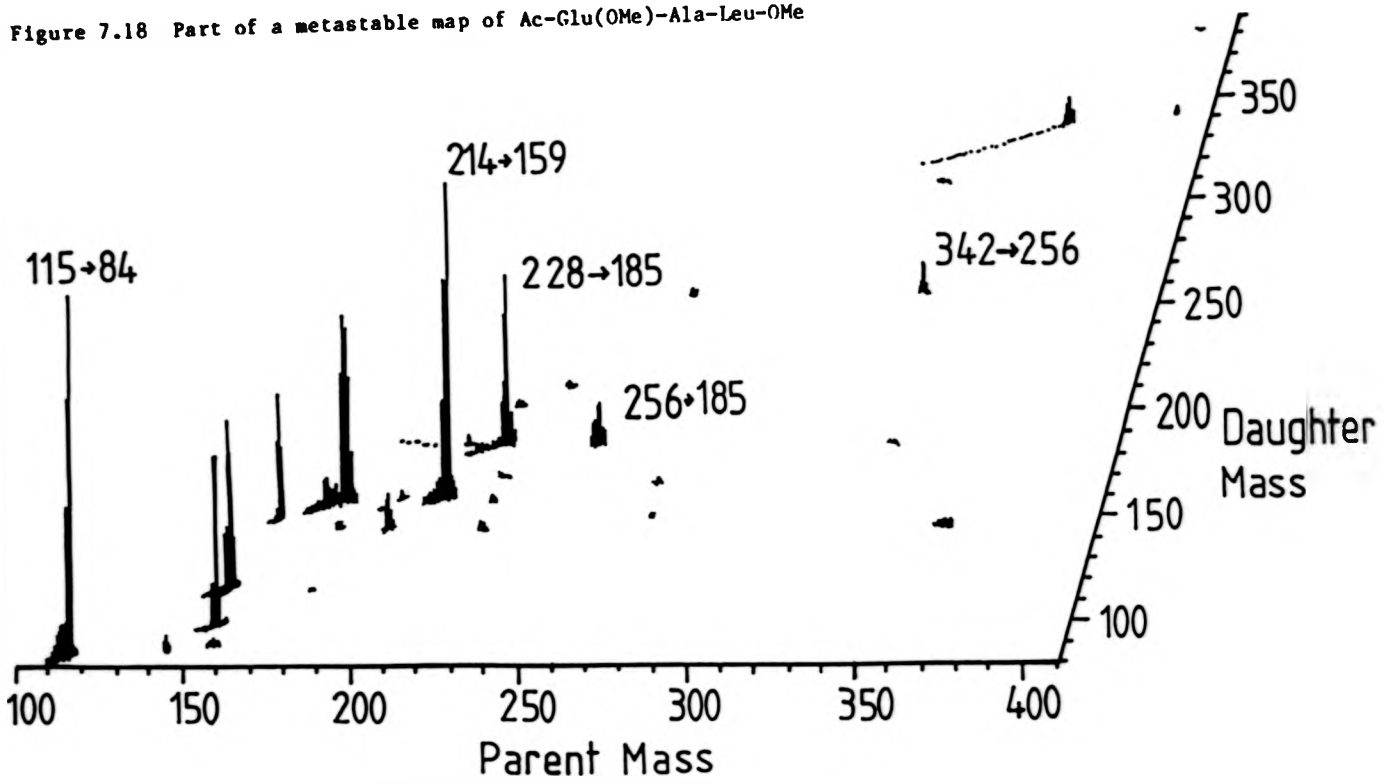

Figure 7.19 Part of a metastable map of Ac-Trp-Ala-Leu-OMe

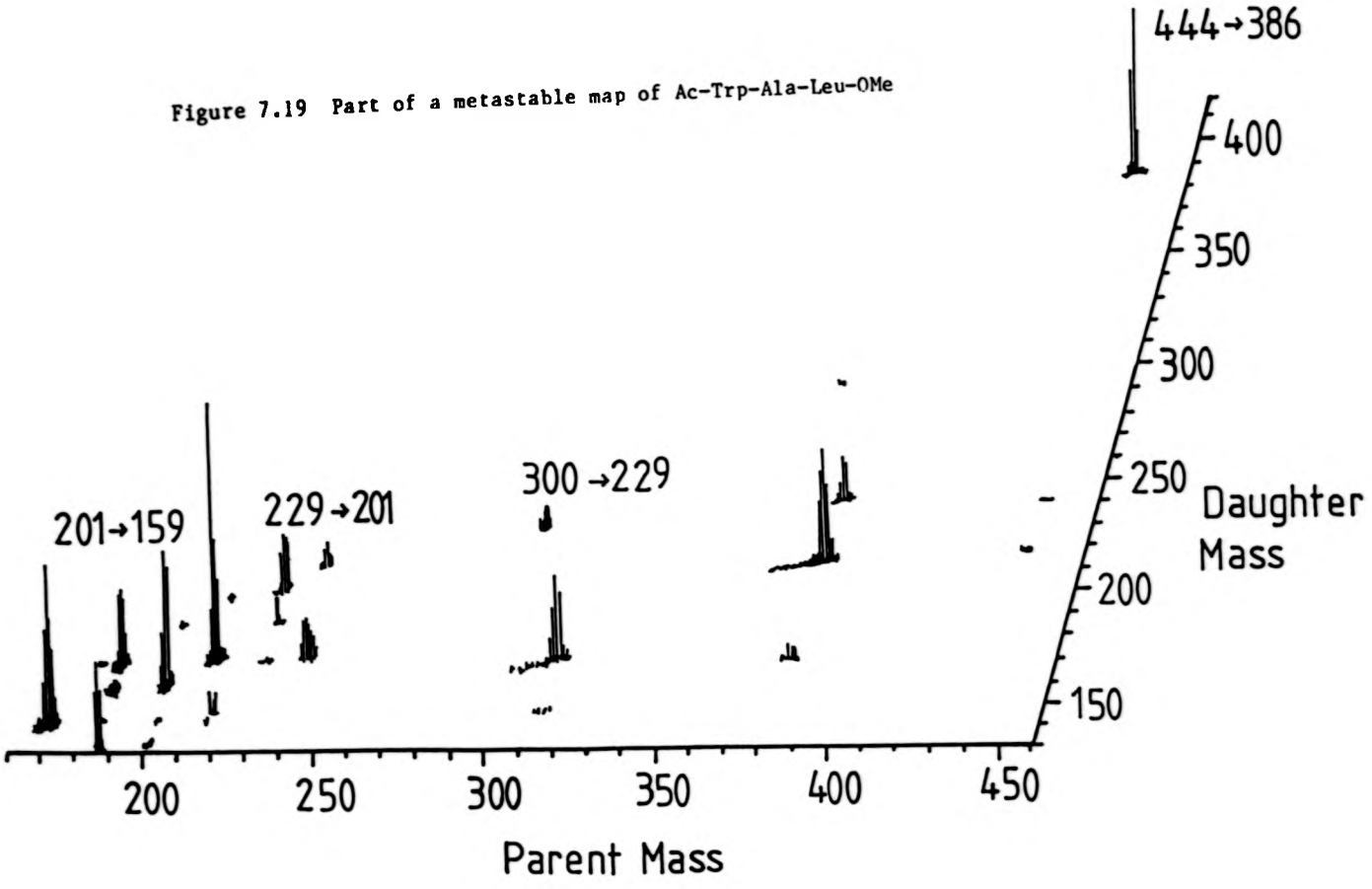

suitable for examining a mixture of fragments cleaved from a larger molecule by enzymic digestion because the mixture could be analysed without first separating the components. It would also be possible to program the data system so that it searches for losses of selected neutral fragments and thus sequences the peptide automatically.

7.6 Negative Ion Metastable Maps

It has been shown {68} that studying negative ions can be useful when trying to analyse mixtures by mass spectrometry: consequently, attempts were made to obtain negative ion metastable maps. Negative ions could be observed on the MS-50 by changing the amplifiers which provide the accelerating voltage and photomultiplier voltage, and by changing the polarity of the electric sector plates and the direction in which the current flows through the magnetic sector. A calibration obtained from positive ions was not found to be reliable when the instrument was so converted, and so it was necessary to calibrate the data system using a negative ion spectrum of a mixture of PFK and trichloromethane. A calibration range of 35 to 380 Dalton was obtainable with difficulty, although the calibration did not prove to be stable. Conversion from positive to negative ions on the MS-80 was achieved by means of a switch on the console of the instrument, and it was found that a calibration taken using a positive ion spectrum of PFK could be used to calibrate negative ion spectra. Maps of both unimolecular and collision-induced decompositions proved relatively

uninteresting, however, because little or no fragmentation could be observed.

7.7 An Assessment of Metastable Mapping

A recent review {76} has specified that there are eight factors to be considered when designing an instrument for the structural identification of organic compounds. These factors are useful criteria with which to judge metastable mapping. They are;

1) The instrument should be capable of isolating and identifying ions from the individual components of mixtures, particularly when the components of interest are at the parts per millon level.
2) It should be capable of generating a fragmentation map of the sample.
3) It should be able to examine both unimolecular and collision-induced decompositions.
4) It should have the highest possible resolution.
5) It should be capable of determining the magnitude of the kinetic energy released during the decompositions.
6) It should be able to produce constant daughter, constant parent and constant neutral loss spectra.
7) It as should be as simple and inexpensive as possible.
8) It should be capable of being scanned rapidly and under computer control.

Metastable mapping fulfils the second, third, fifth, sixth and eigth criteria. The seventh condition, that the instrument is to be as simple as possible, is well met by metastable mapping, as the forward-geometry instrument is

probably the most widely-used type of double-focussing mass spectrometer. Strictly speaking, metastable mapping does not fulfil the first criterion, because it does not isolate individual ions. The sensitivity and resolution of metastable maps, the detection of artifact peaks in simulated linked scans, are discussed at length below.

7.7.1 Resolution

Before discussing the resolution of metastable mapping, it may be useful to consider some other techniques. It has been shown {76} that the resolution of a MIKE spectrum is limited by the ability of the electric sector to separate daughter ions. This is dependent on the magnitude of the kinetic energy released during fragmentation and the daughter ion resolution of the technique is effectively about 100. The parent ion resolution can be as high as 3000. The magnitude of the kinetic energy released can also affect the daughter ion resolution of linked scans, as can the failure of the output of the device used to measure the magnetic field (usually a Hall probe) to vary linearly with the field. The kinetic energy released, however, has been found to be the limiting factor in the resolution of the B/E linked scan, although, for certain transitions a daughter ion resolution of 2000 can be obtained {135}. The accuracy with which one can select the parent ion in a linked scan is limited primarily by the energy resolution of the instrument and the degree of kinetic energy released during the decomposition.

The factors which influence the resolution of the metastable map will be similar to those which affect the resolution of linked scans. The mass resolution of the mass spectrometer was not found to be a problem in this work: the spectra composing the map were acquired at a resolution of 1000-2000. However, because of slight irreproducibilities in the magnetic field scans of the instruments (particularly the MS-50) and because Hites-Biemann correction could not be used, there was an error in the converted apparent mass of up to 0.5 Dalton for ions with a mass of about 400 Daltons. This occasionally made it difficult to exactly determine the parent and daughter ion masses from a transition.

The daughter ion masses of the peaks are well defined and the resolution of the peaks in simulated B/E spectra and CNL spectra is good. The resolution of peaks in simulated B^2/E spectra is limited by the kinetic energy released during fragmentation because it produces a significant spread in the apparent mass of the parent ions The problem is most acute for the decompositions of low-mass parent ions and for the loss of relatively large neutral fragments because of the form of the amplification factor (see section 2.5.1): for example, the peak for $363^+ \rightarrow 149^+$ in the phthalate mixture described earlier is very broad (see Figure 7.11), although the kinetic energy release is small (about 0.08 eV).

Another factor which will affect the resolution of

the peaks on a metastable map is the size of the step taken in the electric sector voltage. Each of the peaks observed on the map will probably be detected in several consecutive magnet scans because they will be broadened by kinetic energy release. It is usually wise, however, to choose a step size which ensures that the peak will be detected at least once, even if no kinetic energy were to be released. If the step is too coarse, it can be difficult to distinguish one peak from another. The step size must therefore be decreased as the mass of the heaviest ion increases, and so the map will take longer to acquire with consequently greater sample requirements.

7.7.2 Sensitivity

Unlike the single scan techniques (MIKES, linked scans etc.) metastable mapping is designed to detect the products of decompositions of many ions at once. It is not really suitable for the detection of components at the parts per million level because the data system suppresses small peaks in order to reduce the level of noise on the spectra. Algorithms could be designed which could differentiate between a small peak and a noise peak, but they would slow down the data acquisition considerably. Metastable mapping is not inherently less sensitive than other techniques which examine metastable or collision-induced decompositions, but more sample is needed because the experiment takes longer to perform. The length of time which an experiment takes obviously

places limitations upon the types of samples which can be run. However, when the sensitivity of the instrument is further reduced, for example, by studying CID transitions at non-zero scattering angles, the lack of sensitivity of the technique can become a problem.

The speed at which the magnetic sector field of the MS-50 was scanned was 3 seconds per decade of mass and so a typical scan on that instrument would take about seven seconds, including about a second to allow the magnet to reset. A good ion current can be obtained when using about 0.1 mg of sample per minute, and so if the map is composed of about four hundred scans, each taking seven seconds, about 5 mg of sample will be required. A faster scanning mass spectrometer would be able to reduce the time taken to acquire a map, and thus the amount of sample needed. For example, the magnet on the MS-80 is capable of scans of 0.5 seconds per decade of mass and can perform the scan mentioned in the example above in just under 2 seconds, reducing the amount of sample needed to a little over a milligram. However, less time would be spent on individual scans, thus reducing the likelihood of detecting the products of transitions of low intensity.

7.7.3 Artifact Peaks

In reversed-geometry mass spectrometers, peaks from decompositions occurring in both field-free regions fall on the metastable map (see Figure 3.1), and so a scan

designed to detect the products of decompositions in one field-free region might also detect products from decompositions in the other. For example, artifact peaks can occur in a MIKE spectum if the apparent mass of an ion from a first field-free region decomposition falls at approximately the same mass as the ion whose second field-free region decompositions are being studied. These artifacts will be narrower than the second field-free region peaks, however. Similarly, if a linked scan is being performed on a reversed-geometry instrument, and if a second field-free region decomposition falls at a value of apparent mass and E' which is crossed by the linked scan, then the product of that second field-free region decomposition will be detected. In addition, decompositions occurring in the accelerating region or the electric or magnetic sectors may all produce continua on metastable maps taken on reversed-geometry instruments and may produce artifact peaks in linked scans.

Linked scans simulated from a metastable map taken on a forward-geometry instrument do show artifact peaks caused by decompositions in the electric sector or in the region where the ions are accelerated, but these artifacts are easily detected by examining the metastable map (cf. Methanol). Peaks thus observed in a normal linked scan might not be correctly identified. An explanation given {136} for the origin of artifact peaks in linked scans, claiming that they are due to decompositions from ions of higher mass than the parent

ion, cannot be generally true as this would require parallel linked scan lines to cross. However, such interference can occur when decompositions from ions one mass unit either side of the peak of interest are accompanied by a very large kinetic energy release (vide infra).

Artifact peaks may occur in a linked scan generated from the metastable map for two other reasons: consecutive decompositions in two field-free regions and the incorrect use of the window parameter. If the product of a decomposition in the first field-free region further fragments in the second field-free region, the 'grand-daughter' ion so produced will appear on the metastable map {137}. In instruments of the type used here the value of E' at which the product of the first decomposition is transmitted will be determined by the ratio of the parent ion mass to the daughter ion mass, but the apparent mass at which the grand-daughter ion is detected is given by:-

$$m^* = m_3^2/m_1 \quad ,$$

where m_3 is the mass of the grand-daughter ion. Linked scans have been proposed {138} which can detect these ions and it has been shown that the peaks due to these consecutive decompositions can be observed in a metastable map {139,140}, and that they are broadened in two directions by kinetic energy release. These secondary decomposition products can appear as artifact peaks in linked scans designed to study other transitions {141}, although their intensity is low.

It is possible to generate artifact peaks in the linked scans extracted from a metastable map by an injudicious choice of the window parameter used by the simulation program. This parameter is designed to compensate for any errors in the time-to-mass calibration caused by the absence of Hites-Biemann correction. If too narrow a window is chosen, the product of the appropriate transition may not be detected, or its intensity may be incorrect. If too wide a window is chosen, however, a peak from another transition may be detected. For example, a B/E linked scan for the m/z 127^+ ion simulated from an EI metastable map of a dinonylphthalate showed, when a window of 1.0 Dalton was used, that the largest peak in the spectrum was due to the loss of butane, giving an ion at m/z 69. However, when the window was decreased to 0.1 Dalton, this peak almost disappeared (see Figure 7.20). This artifact peak is probably due to the loss of butane from the m/z 128^+ ion. Care should therefore be taken in choosing the value of the window parameter to be used when simulating linked scans from the metastable map.

7.8 Suggestions for Future Work

It has been suggested {145} that the volume of metastable peaks should be used when trying to determine quantitatively the composition of mixtures. It has been shown in chapter 5 that the peaks observed in metastable maps are essentially two-dimensional and so the areas of

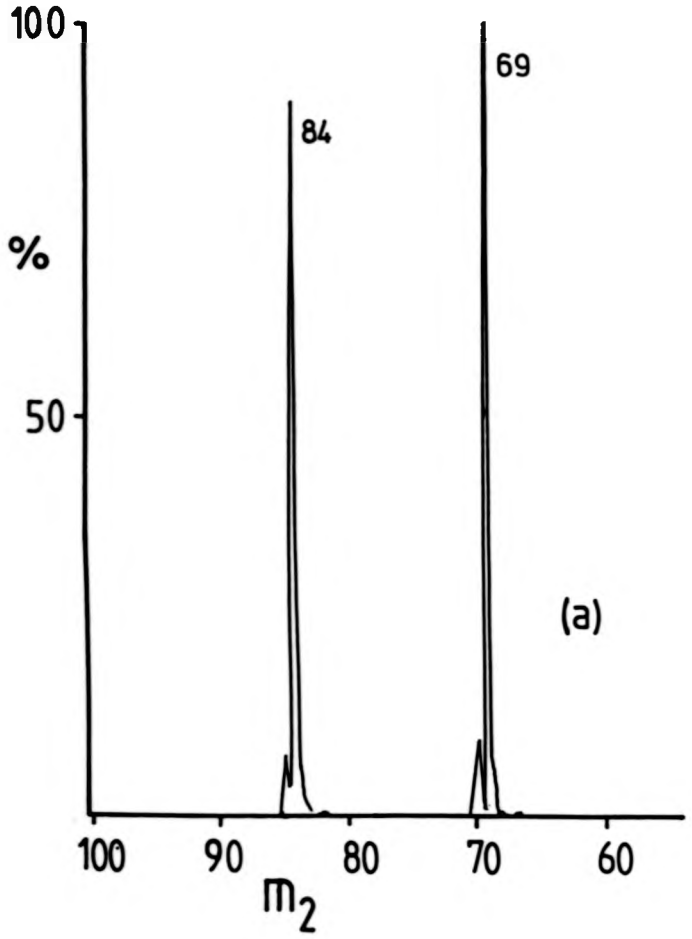

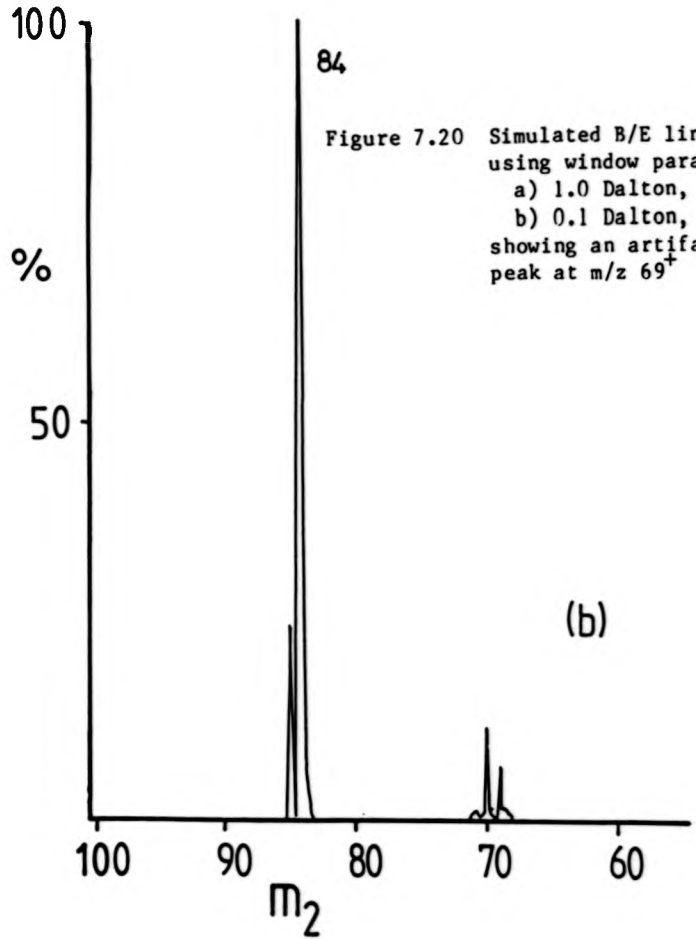

Figure 7.20 Simulated B/E linked scans using window parameters of
a) 1.0 Dalton, and
b) 0.1 Dalton,
showing an artifact peak at m/z 69^+

peaks obtained in a B^2/E linked scans would suffice. No attempt at quantitative analysis of the mixtures discussed above has been made, however, because of the difficulty of ensuring that the vapour pressure of the sample in the ion source remains constant throughout the experiment. An estimation of the ion current produced could be made by measuring the charge induced on a plate inserted into the edge of the ion beam before it passes into the electric sector. Such a charge could be amplified and measured by an A/D convertor on the data system while the data are being collected. Another modification which might be made to the instruments to improve the quality of the metastable maps obtained would be to install field control units, which would improve the reproducibility of the magnetic field scans and might remove the need for Hites-Biemann correction of the data and hence the use of window parameters in the linked scan simulation programs.

It has been shown that charge inversion sometimes occurs after collision-induced decomposition {146}, and it might prove more interesting to study the positively-charged fragments formed from a negative ion {147} than to study the negatively-charged ones because more ions are often present in the charge inversion spectrum than in the CID spectrum {148}. Preliminary experiments indicated that these transitions were of low intensity, however.

Some improvements might also be made to the data processing programs. The current method of storing the data

is inefficent in terms of both storage space and search times, and improvements on both counts could be made by storing the data as a set of parent and daughter ion masses and the corresponding intensities. The generation of the maps and linked scans would be made more efficent because the limitations, currently imposed by the limited core space of the NOVA, on the number of peaks which can be considered would be removed. The programs would also be much faster because the number of disk files to be opened, searched and closed would be reduced from (effectively) several hundred to one. Data presented in such a format would also allow the subtraction of one map from another, and possibly some form of library searching, to be performed.

8. Factor Analysis

8.1 Introduction

Peaks due to minor components in the EI mass spectrum of a mixture can often be obscured by peaks due to other components. Chromatographic methods such as GC-MS and LC-MS may be used to separate the components prior to analysis, and mass spectrometric methods such as MS/MS or metastable mapping, or 'soft' methods of ionization such as CI or FD can be used to identify them but these techniques are often difficult to perform or require special instrumentation. The analysis of mixtures by NMR is more difficult because the on-line chromatographic techniques extensively used in mass spectrometry are not generally available.

The mass spectrum and, under certain conditions, ^{13}C NMR spectrum of a mixture can be considered to be a linear sum of its component's spectra weighted by their relative concentrations; Factor analysis (FA) is a statistical technique which extracts these by expressing, as concisely as possible, the dissimilarity of the spectra. Techniques such as FA are being increasingly used in the physical sciences: for example in the analysis of infra-red spectra {149}, NMR solvent shifts {150-152} and chemical shifts {153}, GC peak deconvolution {154-157}, noise suppression {158} and, more recently, the analysis of mixtures by mass spectrometry {159-166}.

8.2 Theory of Factor Analysis

Factor analysis can be divided into two parts; the extraction of the factors and deciding on the number of components, and the rotation of the factors to obtain the most probable spectra.

8.2.1 Extracting the Factors

8.2.1.1 Differences Between the Spectra

The intensity of a peak in the spectrum of a mixture may be represented as the sum of a set of product terms involving pure component spectra and their concentrations. For example, if the intensity of the i^{th} peak in the spectrum of the j^{th} component is r_{ij}, and if the concentration of the component in mixture k is c_{jk}, the intensity of the corresponding peak in that mixture, d_{ik}, can be represented by

$$d_{ik} = \sum_{j=1}^{n} r_{ij} \cdot c_{jk} \qquad \langle 1 \rangle$$

where n is the number of components. If more mixtures of unique composition are considered than there are components in them FA may be used to extract the r_{ij} and c_{jk} terms, thus yielding the spectra and concentrations of the components. Such mixture spectra may be taken from individual mixtures, or from a single mixture where the concentrations of the

components vary with time, such as a distillation from a probe into the ion source or an unresolved GC peak.

The similarities of the spectra must first be calculated in the form of a correlation or covariance matrix {167} from which a set of independent factors which fully describe the data can be extracted. These factors are related to the components the mixtures. The data should consist of a set of intensities of the same peaks in the various mixture spectra, where each spectrum fills one column of a data matrix [D]. In abstract terms, the data matrix can be defined as the product of a row cofactor matrix [R] and a column cofactor matrix [C] by

$$[D] = [R].[C] \qquad <2>$$

The matrix [D] has dimensions (r)x(c), where c is the number of mixture spectra and r the number of peaks in each spectrum: [R] has dimension (r)x(n), where n is the number of components in the mixtures, and [C] is an (n)x(c) matrix.

The differences between the spectra in [D], from which FA will extract the cofactor matrices, may be expressed as either the correlation of the spectra or their covariance: the former normalizes the data to give equal statistical weight to all the variables regardless of their value, while covariance weights the variables in proportion to their absolute magnitude. Normalization is valid only when the

errors in the data are directly proportional to the absolute magnitude of the datum {159}: the errors in a mass (or ^{13}C NMR) spectrum should be relatively constant, however. The spectra cannot be normalized because the relative heights of the peaks are important (these would be destroyed by the normalization procedure), and so the covariance of the data must be considered instead.

The data may also be considered to be scattered 'about the mean', where each spectrum is expressed as a distribution about the average of the peak heights, or 'about the origin' where the data are left unaltered. Redistributing the data about the spectral mean is only of value when the data do not have a physically real zero value (e.g. temperatures expressed on the Fahrenheit scale).

The interrelationships of the data may thus be expressed in four ways; as the correlation about the mean (Rm) or about the origin (Ro), or as the covariance about the mean (Cm) or about the origin (Co). FA was originally developed for the social sciences, where the semi-quantatitive nature of the data and the lack of agreement on what is 'normal' meant that the most appropriate choice of measuring the variables' interrelationships was their correlation about the mean. The data considered here are of a special nature, where the data have a real zero (as a peak may be absent from the spectrum) and

may all be measured in terms of the same units. For such data, only the covariance about the origin matrix will retain all the information inherent in the spectra {161}.

Once one of the four methods (Cm, Rm, Co or Ro) has been chosen, and the data adjusted accordingly {161}, the relationships between the variables can be calculated by premultiplying the data matrix by its transpose

$$[Z] = [D]'.[D] \qquad \langle 3 \rangle$$

8.2.1.2 Extracting the Eigenvectors

The object of FA is the extraction of the cofactor matrices, [R] and [C], from the data matrix, and it has been shown {19} that this may be achieved by finding a matrix of eigenvectors, [Q], which reduces all of the off-diagonal elements in [Z] to zero. The correlation (or covariance) matrix is then represented by a set of orthogonal eigenvectors and associated eigenvalues.

i.e. $$[Q]^{-1}.[Z].[Q] = d_{jk}.\lambda_j \qquad \langle 4 \rangle$$

where d_{jk} is the Kronecker delta and λ_j is an eigenvalue of a set of equations having the form

$$[Z].Q_j = \lambda_j.Q_j \qquad \langle 5 \rangle$$

where Q_j is the j^{th} column of the eigenvector matrix [Q]. In general terms, equation 5 can be expressed as

$$[Z].[Q] = [\lambda].[Q]$$

where $[\lambda]$ is a diagonal matrix containing the eigenvalues. The eigenanalysis may thus be performed by finding values of [Q], [Z] and $[\lambda]$ for which this equation is valid.

The eigenvectors will be orthogonal and so the transpose of [Q] will be equal to its inverse :-

$$[Q]^{-1}.[Z].[Q] = [Q]^{-1}.[D]'.[D].[Q] \quad <6>$$

$$[Q]^{-1}.[Z].[Q] = [Q]'.[D]'.[D].[Q] \quad <7>$$

$$[Q]^{-1}.[Z].[Q] = [V]'.[V] \quad <8>$$

where $$[V] = [D].[Q] \quad <9>$$

$$[D] = [V].[Q]' \quad <10>$$

and $[V] = [R]$ and $[C] = [Q]'$ <11>

These matrices can be used (equation 10) to reproduce the data matrix. The eigenvectors stored in the columns of [Q] can be said to represent the factors and the eigenvalues represent their relative importance. Factor extraction can thus be reduced to the problem of diagonalizing [Z], either by the method of Jacobi {168}, where each off-diagonal element is reduced in turn to zero by a series of rotations, or by the Householder-Ortega-Wilkinson method {169}, where the rotation stops when a tridiagonal matrix is obtained and the eigenvectors are found by solving the resulting set of simultaneous equations.

8.2.1.3 Theory of Error

More mixtures must be considered in the analysis than there are components in them to ensure that enough information is present in the data to extract the factors and eigenvalues. If there were no experimental error in the data, however, only n of the eigenvalues would be greater than zero (where n is the number of components) because the corresponding factors would perfectly reproduce the data. Although this is most unlikely to occur when using real data, it can be seen that there will exist, when the errors are small, a distinct primary set of n eigenvectors, which represent the factors, and a secondary set, formed from the remaining (c-n) eigenvectors, which can be associated with the error (where c is the number of mixtures considered).

Determining the correct number of factors can be difficult, and Malinowski has developed {170,171} a theory of error for FA which can help. The theory states that there exist three kinds of error :-

1) Real error, RE, which accounts for all of the error in the data,
2) Extracted error, XE, which is the error that has been extracted by the eigenanalysis and which constitutes the secondary set of eigenvectors, and
3) Imbedded error, IE, which is a measure of the error left mixed in with the factors and which would be present in data reconstructed from only the primary

set of eigenvectors.

These functions are defined in Figure 8.1, and it may be observed that since the imbedded error is always less than the real error, reconstructing the data using only the primary set of eigenvectors will always lead to a data set containing fewer, and smaller, errors. Such a reconstruction has been used to improve the quality of FT-IR spectra {158}.

8.2.1.4 Finding the Number of Factors

If the value of the experimental error is known, the correct number of factors may be deduced by assuming that all the eigenvectors giving rise to values of the RE function greater than the error are true factors. Since the experimental error is frequently unknown, however, it is fortunate that the imbedded error function reaches a theoretical minimum when the correct number of eigenvalues are considered, provided that the errors are small and are evenly distributed throughout the data. Malinowski's 'indicator function' (IND) (see Fig 8.1) has also been observed {171} to reach a minimum at the correct point, although he has commented {4} that since the physical significance of the function is not understood, it should be used with caution. An additional property of the IND function is that it increases steadily if the data set is random, and can thus be used to identify cases where there are no underlying factors. When the scree function (see Fig

$$RE = \left[\frac{\sum_{j=n+1}^{c} \lambda_j}{r(c-n)} \right]^{\frac{1}{2}}$$

where

c = number of mixtures

r = number of peaks

n = number of factors

$\lambda_j = j^{th}$ eigenvalue

$$IE = \left(\frac{n}{c}\right)^{\frac{1}{2}} . RE$$

$$XE = \left(1 - \frac{n}{c}\right)^{\frac{1}{2}} . RE$$

Thus $RE^2 = IE^2 + XE^2$

$$IND = \frac{RE}{(c-n)^2}$$

$$\text{Scree function} = \frac{\sum_{j=n+1}^{c} \lambda_j}{\sum_{j=1}^{c} \lambda_j}$$

Figure 8.1 The RE, IE, XE, IND and Scree functions

8.1) is plotted against the number of factors used to construct the function, the resulting curve should show a sharp discontinuity at the correct value of n {172}, especially if data covariant about the origin were considered {161}. Gillette and Koenig {158} have recently used a discontinuity in a plot of log(eigenvalue) against the number of suspected components to indicate the number of factors.

8.2.2 Factor Rotation

Although knowing the number of components in a mixture and the accuracy of the measurements are both of use to the analytical chemist, his principal interest lies in determining what those components are. The factors have been extracted by the diagonalization procedure as orthonormal eigenvectors and they bear little resemblance to the true spectra because some of the elements will be less than zero. If the data were to be represented graphically, they would be distributed within an n-dimensional ellipsoid whose axes are the factors {167}. It is often possible to obtain spectra which give a better fit to the data by rotating the ellipsoid until the largest number of data lie close to an axis.

8.2.2.1 Thurstone's Criteria

The pattern of correlations between the data and the factors which represent them is called their

factor structure. The 'simple structure' criteria of Thurstone {173} attempt to provide some guidelines as to which of the infinite number of rotations to use. It is theoretically possible to rotate the eigenvectors so that each component of the mixture relates only to one factor, and although such a solution is unlikely in practice, it should always be possible to obtain a simpler solution than that produced by the diagonalization procedure. Thurstone's criteria can be expressed as:-

1) Each peak should be absent from the spectrum of at least one component.
2) Each factor should contain at least n elements with zero intensity.
3) For every pair of factors, there should be at least n elements with zero values in one factor but not in the other.

8.2.2.2 Orthogonal and Oblique Rotations

Thurstone's criteria are subjective and are rarely satisfied for real data, but they have been used to fit the factors to the data by rotating them to maximize the squares of the factor loadings. This has been referred to as a Quartimax rotation {174} and it may be regarded as a method where the first eigenvector is rotated until it lies close to the maximum number of data points followed by rotation of the other factors about the first until as much of the remaining variance as possible is accounted for.

The factors themselves are not changed, remaining orthogonal and uncorrelated, but their interpretation has been altered. Another common rotation is the 'Varimax' {175}, where the data, rather than the factors, are rotated.

Although both methods retain the orthogonality of the original eigenvectors, there is frequently no reason why the factors should be uncorrelated and the factors may sometimes be rotated to give a better fit to the data if their orthogonality is relaxed.

8.2.2.3 Target Transformation

Another method of interpreting the factors {160}, known as target transformation, involves the rotation of each factor in turn to give the best possible least squares fit to the spectrum of a suspected component of the mixture: if a fit is much better than that which would be expected from a random rotation, then that factor corresponds to the 'target'. This process has also been called Procrustian transformation because the factors are forced to resemble a particular model and it should be used with care. It would also be possible to confirm the presence of a component in the mixtures by including its spectrum in the original data set and seeing if subsequent analysis produces an extra factor.

8.2.2.4 Empirical Rotation

Because the [R] matrix contains the spectra of the pure components, and [C] their concentrations, obtaining these matrices is of some importance: Knorr and Futrell {165} have discussed the transformation of the [V] and [Q]' matrices, and have proposed that the [C] matrix is a oblique rotation of [Q]' given by

$$[C] = [Q]'.[A] \qquad \langle 12 \rangle$$

where [A] is a suitable (n)x(n) rotation matrix. [R] may then be found by multiplying [D] by the psuedo-inverse of [C] (it is not a square matrix, and so it does not have a true inverse).

$$[R] = [D].[C]'.([C].[C]')^{-1} \qquad \langle 13 \rangle$$

The matrix [Q]' may be built from the primary set of eigenvectors and [V], which contains the spectra in an orthogonal form, may be obtained from equation 9. When a suitable rotation matrix has been constructed, the concentrations and spectra of the components may be obtained.

Knorr has developed an empirical method of finding [A] which assumes that there exists a set of peaks which are each unique to one component, This assumption can be seen as an extension of Thurstone's simple structure criteria. According to Knorr, the 'pure peaks' correspond to those peaks in the unrotated spectra which are least like the average and least like each other. The first may be found by

normalizing the sum of the squares of each row of [V] to one and looking for the smallest element in the first column, and the rest of the pure peaks correspond to those peaks in successive columns of [V] which are least like the average value of the preceding pure peaks' contributions to that spectrum.

Malinowski has pointed out (176) that Knorr's method often fails for the fourth and succeeding factors and has proposed that the rotation matrix be constructed from the rows of [V] which are most orthogonal to the preceding ones. According to Malinowski the first pure peak is, as indicated by Knorr, the lowest member of the first column of [V], but the second lies in the row which has the smallest two-dimensional dot product with the row containing the first. The subsequent pure peaks can be obtained by finding those rows of the [V] matrix which give the largest dot product with the cross product of the rows containing the previous ones. For example, the cross product of the rows containing the first two pure peaks is a vector perpendicular to the plane formed by them and the row which is most unlike them is the one which is closest to the resultant.

The advantage of the Knorr rotation method is that it has been designed for mixture analysis and that it extracts the concentrations and spectra directly. The principal disadvantage is that each component must have at least one peak which is unique

to that spectrum: the technique is thus not suitable for compounds which give spectra which are very similar, such as the mass spectra of some isomers.

8.3 Experiments and Results

Knorr and Futrell's work on the extraction and oblique rotation of the factors of the mass spectra of mixtures has been used as the basis of a factor analysis program written for I.C.I. Petrochemicals and Plastics division. The program, written in BASIC for a CBM PET 4032 microcomputer, uses as its input the mass or ^{13}C NMR spectra of mixtures and determines the number of components in them and their spectra and concentrations.

8.3.1 Extracting the Factors

Because some of the information present in the spectra would be lost if the data were to be normalised or redistributed about the spectral means, only the Co (covariance about the origin) matrix was considered. There are two ways of preparing the data - with each spectrum occupying a row of the data matrix (known as R analysis) or occupying a column (Q analysis). The covariance matrix will be of dimension (k)x(k), where k is the number of columns in the data matrix, and as the number of peaks in each spectrum is likely to be greater than the number of spectra considered, Q analysis will be faster. In Rozett's study {161} of the 22 isomers of $C_{10}H_{14}$, 125 peaks were studied from each spectrum

and so Q analysis would give a 22x22 correlation matrix while R analysis would give a 125x125 matrix: as the latter has over fifteen thousand elements, certain practical problems are likely to be encountered in calculating it, especially as the matrix would exceed the memory capacity of most micro- and minicomputers. Since the results are similar {161}, Q analysis is thus to be preferred and has been used here. The eigenanalysis was performed by a subroutine using Jacobi's method {168}, translated into BASIC from a FORTRAN IV library package {177}.

8.3.2 Determining the Number of Factors

Several methods of determining the number of factors were tested by taking thirteen sets of data in which the number of components were known and comparing the answers given by the following tests:-

1) The imbedded error (IE) and the IND function function, both of which would be expected to reach a minimum when the correct number of factors was estimated.

2) The ratio between successive values of the scree test, the real error (RE), the IND and IE functions and the eigenvalues.

As can be seen from the results shown in Table 8.1, the imbedded error and scree functions, both recommended previously as methods of determining the number of factors {4}, were not found to be reliable, whereas the IND function gave the correct answer for about seventy

Table 8.1 The number of factors indicated by the results of some common tests.

Data Set	n	RE SR	IE	IE SR	IND	IND SR	EV SR	Scree Test
A	2	2	3	2	2	2	2	2
B	3	2	-	-	3	2	3	2
C	3	3	-	-	3	2	3	2
D	3	2	8	3	4	2	3	2
E	3	2	2	2	2	2	3	2
F	3	2	-	2	3	2	1	2
G	3	1	-	2	3	1	3	1
H	2	1	-	1	-	1	2	1
I	2	1	-	1	-	1	2	1
J	2	1	-	1	2	1	2	1
K	4	3	4	3	4	3	4	2
L	4	4	5	4	4	3	4	3
M	5	4	-	4	5	4	5	4
Correct		3	1	3	9	1	12	1

- Indicates that the function did not reach a minimum value.
Correct The number of correct answers in each column.

RE The Real error IE The imbedded error
EV The eigenvalues Scree The scree test
IND The IND function
SR The ratio of successive values of the function.

Data Sets :-

A Knorr and Futrell test data {165}
B Real NMR spectra of mixtures of benzil, benzophenone and flavone
C Artificial NMR spectra of mixtures of 2-hydroxy-3-naphthooic acid, 2-naphthol and 6-hydroxy-2-naphthoic acid
D Artificial NMR spectra of mixtures of benzil,benzophenone and flavone.
E Artificial NMR spectra of mixtures of benzil, flavone and benzophenone where each carbon is idealized to unit intensity.
F Heptane/Octane experimental data from Ritter et al. {159}
G Cyclohexane/hexane experimental data from Ritter et al. {159}
H Malinowski error-free test data {4}
I Malinowski test data with error added {4}.
J Cyclohexane/cyclohexene experimental data {159}
K Artificial mixtures of the mass spectra of mixtures of hexane, heptane, 2-methylheptane and 3-methyloctane.
L Artificial mixtures of the mass spectra of methylbenzene, chloropropane, 2-ethylmethylbenzene and chlorohexane.
M Malinowski 5-factor test data {176}.

per cent of cases. The most successful test, however, which has not been reported previously, was that of dividing each eigenvalue by the succeeding one and finding the value of n where this ratio reaches a maximum. The test works because the ratio between each eigenvalue and the next will reach a maximum at the boundary between the primary set of eigenvalues and the secondary set. For a data set free from error, the ratio at the boundary will be infinite or, allowing for rounding errors in the computer, very large. If the experimental error is large the dividing line will not be sharp and the test may fail. For example, for data set F (Table 8.1), the mixtures of heptane and octane taken from Ritter et al. {159}, the real error was found to be 0.16 on an average datum of 0.73 : this value was comparable to about twenty per cent of the data. Only one factor was indicated by the eigenvalue ratios, although a second 'maximum' occured for n=3 (the correct answer). All of the tests failed for an experimental set of mixtures of methylcyclohexane, methylbenzene and ethylbenzene because the spectra of the alkylbenzenes were too highly correlated to be distinguished.

If too few factors were used to construct the [Q]' matrix the spectra and concentrations will consist mostly of large peaks. If too many factors were chosen, and if the extra factor was due to one or two 'rogue' data, the corresponding column of the concentration matrix may be filled with very small values. If the experimental error is high, however, the extra factor

will not be so obvious and may be mistaken for a real component.

Ritter et al. have considered the mass spectra of four mixtures of cyclohexane/hexane {159} and found that three significant factors were produced. Elimination of the m/z 28 peak and subsequent re-analysis yielded only two factors, and Malinowski has demonstrated by target transformation {160} that the third factor was dinitrogen. Analysis of the Ritter data set by the method used here also indicated that there were three factors present in the data and identified m/z 28 as the pure peak for the third. The spectrum of this component contained only m/z 28, and the concentrations showed that the contaminant was present in the mixture spectra at an average value of 4 $\pm$ 1%.

8.3.3 Obtaining the Cofactor Matrices

Once the number of components in the mixtures had been determined, the eigenvectors associated with the appropriate number of factors could be used to build the [V] matrix. The rotation matrix, [A], was constructed from those rows of the [V] matrix which contained the pure peaks; in this work, the rows of [V] were used as the rows of [A] and the concentrations determined by:-

$$[C] = [A].[Q]' \qquad \langle 14 \rangle$$

This differs from the method published by Knorr {165}, who filled the columns of [A] with the rows of [V] containing the pure peaks and generated the

concentration matrix using equation 12: the rotation matrix used in this work is the transpose of Knorr's and the two methods are effectively the same. The spectra were then found by using equation 13, although it would be simpler to postmultiply [V] by the inverse of [A] (4)

i.e. $$[R] = [V].[A]^{-1} \quad . \qquad \langle 15 \rangle$$

8.3.4 What is a Pure Peak?

The program was altered so that the pure peaks could be selected manually, and it was found that a 'pure peak' can be said to be a peak which has a much greater intensity in the spectrum of one component than in the spectra of the others, although the intensity of the peak need not be great, nor need the intensities of the corresponding peaks in the other spectra be zero.

If a pure peak was not selected for one of the components it was found that the reproduced spectrum and concentrations of that component were better than those for which pure peaks were selected. There is no obvious explanation for this and the best results were obtained when pure peaks for all of the components were chosen.

It was found that small peaks adjacent to, or in the same row as, very large peaks were frequently overestimated in the extracted spectra, regardless of which pure peaks were chosen. Interchanging the order in which the pure peaks were specified only altered the

order in which the spectra were extracted, since the rows of the rotation matrix had been interchanged. Malinowski's view that Knorr's method sometimes finds the wrong pure peaks seems to be correct, because that method often chose more than one pure peak for a component.

8.3.5 Selecting the Pure Peaks

Malinowski's method of selecting the second pure peak is based on finding the smallest dot product between the first two values of each row of the [V] matrix and the first two values of the row containing the first pure peak. This was found to yield incorrect results for some of the data sets used in Table 8.1; the second pure peak was often found to occur in more than one component, or to be unique to the same component as one of the other pure peaks.

Both Knorr's and Malinowski's algorithms consider the first pure peak to be the smallest element of the first column of [V] - let us assume that this corresponds to element 'a' of the hypothetical [V] matrix shown in Figure 8.2. The second pure peak is given by Knorr to be that element of the second column which is most unlike 'b' while Malinowski takes it to be the second element of the vector which has the lowest dot product with (a.b); if this vector is (e.f), then the dot product will be given by (a.e + b.f). and the second pure peak will be 'f'.

```
m  n  o  p
a  b  c  d
i  j  k  l
e  f  g  h
u  v  w  x
q  r  s  t
```

Figure 8.2.

Part of a hypothetical [V] matrix

(See text for details)

The dot product described above did not always yield the correct results, but finding the mimimum value of the product of 'b' with the other elements in the second column did.

The third pure peak is given by the Knorr method to be the peak in the third column which is furthest from (c+g)/2, while the Malinowski method searches for the maximum value of a set of determinants where the top two rows in each are the first three elements of the rows of [V] containing the pure peaks which have already been determined and the bottom row represents the first three elements of each row in turn. Subsequent pure peaks are found in the same manner as the third in both algorithms: as the peak furthest from the mean of previous pure peaks' contributions in that spectrum by the Knorr method and as the maximum value of the set of NxN determinants by the Malinowski method. The routine for evaluating the determinant was translated from a FORTRAN IV library program {178}, and the adapted Malinowski subroutine gave the correct pure peaks for all the data sets in Table 8.1.

8.3.6 The Factor Analysis Program

The factor analysis program read the data either

from the keyboard or from a floppy disk, constructed the data matrix and calculated the Co matrix, which was then analysed to give the factors and eigenvalues. The user was presented with the real error, the IND function and the ratio of successive eigenvalues and was asked to choose the number of factors. The program created, filled and normalized the [V] matrix and the user was given the choice of either manual selection of the pure peaks or automatic selection using either the Malinowski or the Knorr algorithms (the latter has the advantage of being faster, even if it is not reliable for data sets containing more than three factors). Once the pure peaks had been chosen, the rotation matrix was constructed from the rows of [V] containing the pure peaks and the spectra and concentrations of the components were calculated. The rows of the concentration matrix were normalized to a sum of 100 to give percentage concentrations of the components in each mixture and the largest peaks in each spectrum were normalized to 100%. The program took about ten minutes to analyse a data set composed of the spectra of ten five-component mixtures, each containing about twenty peaks.

8.3.7 Testing the Program

It was found that the program analysed perfectly an artificial, error-free, data set containing two factors. The data sets commonly referred to in the literature are those of Ritter et al {159}, and the results of this work correspond to those quoted by Knorr {165} for their

cyclohexane/hexane and cyclohexane/cyclohexene mixtures, but the results for the heptane/octane mixtures {159} were poor because of the high experimental error in the data. The results for the data sets of Knorr {165} and Malinowski {176} were adequately reproduced.

8.3.7.1 Mass Spectral Data

A set of mixtures of methylcyclohexane, methylbenzene and 4-methylpentan-2-ol were evaporated into a three litre glass bulb and sampled through a leak by a Balzers QMG 511 quadrupole mass spectrometer. A program written for the PDP-11 data system controlling the mass spectrometer collected and averaged two spectra and subtracted a background spectrum. The spectra were taken under identical conditions of source temperature and tuning and at a constant electron energy. The mass spectra so obtained were subjected to FA, and the data and results are shown in Table 8.2. The ratios of successive eigenvalues and the IND function both indicated that there were three components in the mixtures. The experimental error was found (by the value of the RE function corresponding to three factors) to be about seven percent. The Knorr algorithm selected as the pure peaks m/z 100, 98 and 70, although the second pair are both unique to the same component. The adapted Malinowski algorithm selected m/z 100,91 and 70, each of which is unique to a different component. The extracted spectra are

Table 8.2 Mass spectral data for Methylcyclohexane, methylbenzene and 4-methylpentan-2-one. (Results obtained on Balzers QMG 511)

		Density
Component X	Methylcyclohexane	0.77 g/ml
Component Y	Methylbenzene	0.87 g/ml
Component Z	4-Methylpentan-2-one	0.80 g/ml

Spectra m/z	Expected X	Y	Z	Found X	Y	Z
100	-	-	25	-	-	22
98	25	-	-	18	8	-
92	4	59	-	6	56	-
91	4	100	-	8	100	-
85	-	-	21	9	9	21
83	71	-	-	57	7	-
71	-	-	24	3	-	20
70	16	-	-	17	-	-
69	11	-	-	9	1	1
65	6	27	-	5	27	-
63	3	14	5	8	16	6
62	3	10	-	5	8	-
58	-	-	100	30	8	100
57	8	-	17	21	18	25
56	33	2	-	33	1	4
55	100	-	-	100	16	-
51	1	15	-	9	15	7

Composition of mixtures

Volumes of liquid (ul) X	Y	Z	% by mass X	Y	Z	Determined by Program (%) X	Y	Z
100	0	0	100	0	0	98	0	2
0	100	0	0	100	0	0	100	0
0	0	100	0	0	100	7	0	93
0	200	200	0	52	48	0	76	24
100	0	100	49	0	51	66	6	28
100	100	100	32	36	33	28	54	18
50	100	100	19	42	39	12	61	27
100	50	100	38	22	40	38	34	29
100	100	50	38	43	20	33	64	4
100	50	50	48	27	25	47	38	14

very similar to the pure spectra but the reproduction of the concentrations of the components in the mixtures was poor, however.

Because of the large amount of experimental error in the data the spectra of the pure components could only be extracted from the mixtures if those spectra were included in the original data set. This was not considered satisfactory, and the spectra of seven mixtures of the samples, introduced into the heated inlet system of of a VG 7070 double-focussing forward-geometry mass spectrometer, were obtained and subjected to FA. Each of the mixtures contained all three components. The covariance matrix formed from these spectra was diagonalized and both the IND function and the ratios of successive eigenvalues indicted that there were three factors, implying a real error (RE) of 0.7%. Both the Malinowski and the Knorr/Futrell pure peak algorithms selected m/z 100, 70 and 63 as the pure masses, and the resulting rotation matrix produced fairly good results for the concentrations and spectra. Manual selection of the pure peaks (m/z 100, 98 and 92) produced much better spectra but slightly worse results for the concentrations. These results are shown in Table 8.3 and the spectra presented in Figure 8.3.

Table 8.3 Mass spectral data for Methylcyclohexane, methylbenzene and 4-methylpentan-2-one. (Results obtained on VG 7070)

		Density
Component X	Methylcyclohexane	0.77 g/ml
Component Y	Methylbenzene	0.87 g/ml
Component Z	4-Methylpentan-2-one	0.80 g/ml

Spectra	Expected			Found		
m/z	X	Y	Z	X	Y	Z
100	-	-	24	-	-	22
98	43	-	-	41	-	-
92	-	70	-	-	69	-
91	-	100	-	2	100	-
85	-	-	26	-	-	24
83	100	-	-	100	3	-
70	18	-	-	15	-	-
69	19	-	-	17	-	-
65	-	10	-	-	9	-
63	-	5	-	-	5	-
58	-	-	41	1	3	30
57	3	-	31	6	3	29
56	17	-	-	18	-	1
55	67	-	2	63	4	-
51	1	5	-	-	4	-
43	4	-	100	9	15	100
41	32	1	22	34	7	16
39	15	9	11	13	11	8

Composition of mixtures

Ratios			% by mass			Determined by program (%)		
X	Y	Z	X	Y	Z	X	Y	Z
1	1	1	32	36	33	23	59	18
2	1	1	24	27	49	19	48	33
1	1	2	48	27	25	39	50	11
1	2	1	23	53	24	14	78	8
2	1	2	38	22	40	33	41	26
1	2	2	38	43	20	27	67	6
2	2	1	19	42	39	11	69	20

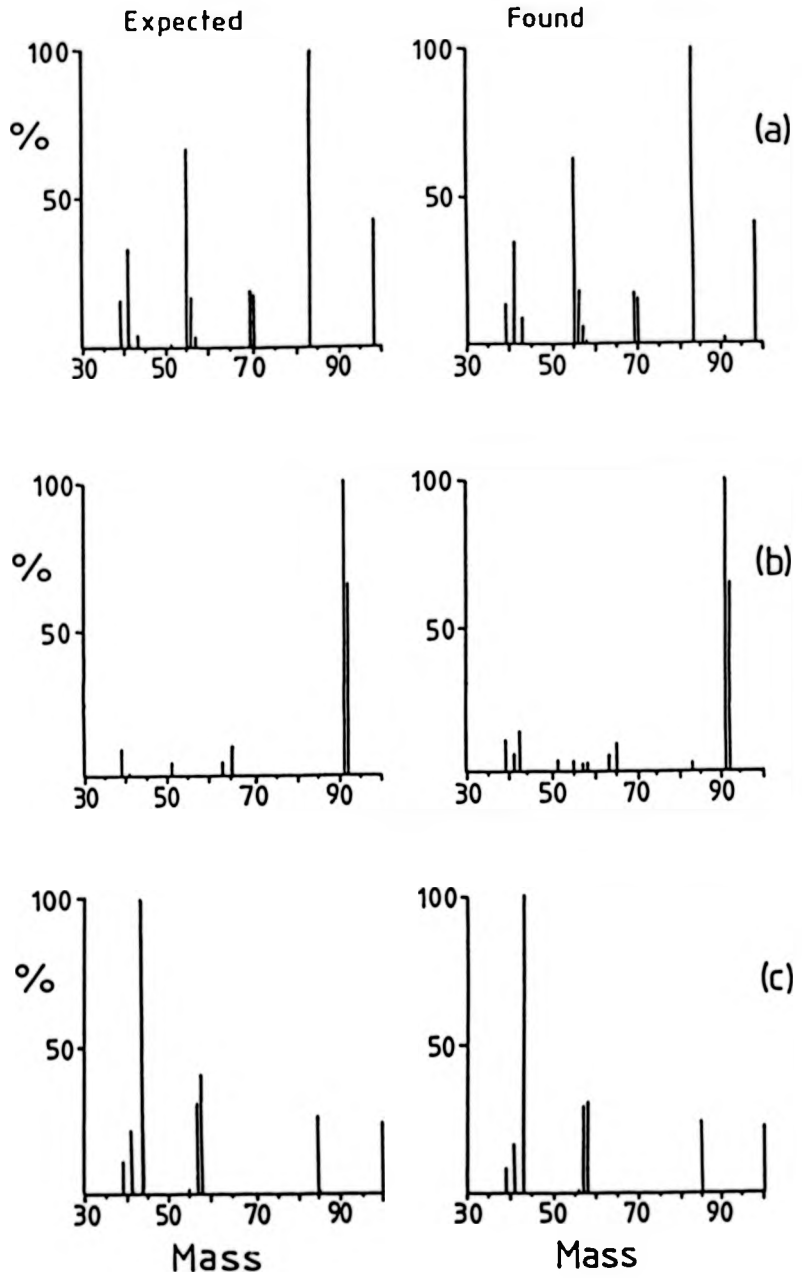

Figure 8.2 Predicted and extracted mass spectra of
a) Methylcyclohexane
b) Methylbenzene, and
c) 4-Methylpentan-2-one

8.3.7.2 Carbon NMR Data

The method used in this work rests on two assumptions: firstly that each component must have a unique peak, and secondly that the spectrum of each mixture must be a sum of the components' spectra weighted by their concentrations. The first of these assumptions requires that the spectra of the components are not too similar and this is more likely to be true for NMR data sets than for those from mass spectra. The validity of the second assumption, however, is dependent on the reproducability of the peak intensities and their chemical shifts, which are dependent on the experimental conditions. The spectra of the mixtures described below were taken on the same machine (a Jeol FX200), using the same probe, at room temperature and at about 50% concentration in the same solvent (deuterochloroform), thus keeping constant any shifts in the peak positions due to temperature, solvent or instrumental effects. All peaks occurring within bands of 0.5 ppm were added together to cope with small changes in the chemical shifts. In practice, however, the shifts were found to change by not more than 0.2 ppm.

Not only may the position of a peak change, but its intensity may not be directly proportional to the number of carbon atoms of that specific type if the Nuclear Overhauser Enhancement (NOE) factors or the

relaxation times for that atom differ significantly from the others in the molecule.

To prevent protons from splitting the carbon resonances and thus decreasing sensitivity, the sample is pumped with radiation to equalize the populations in the upper and lower hydrogen energy levels, thus removing carbon-proton interactions. The intensity of the carbon peaks are increased by up to a factor of almost three, For some carbon atoms which are not subject to strong proton-carbon couplings (e.g. those with no attached protons) this NOE factor will be much smaller.

In addition, for unprotonated carbon atoms the relaxation time needed to equate the population between the energy levels may also be of the order of seconds. After this spin-lattice relaxation time has elapsed, 1/e (36.8%) of the initial magnetization remains: it takes five times that period for greater than ninety-nine percent relaxation to occur. If complete relxation has not taken place before the next pulse, less than full absorbtion will be observed and the peak will be smaller than it would otherwise have been. Relaxation times can be shortened by a number of methods, such as the use of pulse angles of less than ninety degrees or allowing oxygen to remain dissolved in the sample which relaxes the atoms in the sample by a different route.

The carbon NMR spectra of ten mixtures of anisole, benzyl alcohol, and benzyl acetate were taken and submitted to FA. The experiments were run under quantitative conditions: a 30^{o} pulse angle, undegassed samples and 4.5 second pulse intervals to allow full relaxation of the atoms to the Boltzmann distribution. The NOE was suppressed by using a gated decoupling technique {179}. The results of the analysis are shown in Table 8.4. The ratios of successive eigenvalues again gave two maxima at n=1 and n=3, implying large experimental errors. The IND function gave the correct number of factors (n=3) and both the Knorr and the Malinowski algorithms produced correct pure peaks. The spectra of benzyl alcohol and benzyl acetate were successfully isolated, but the spectrum of anisole was poorly reproduced, as it contains a large spurious peak of 36% intensity (compared to the experimental error of 11%), but again this occurs in a row containing two large peaks, and might have been expected.

A set of ten mixtures of benzil, benzophenone and flavone were run under more normal conditions: the results are shown in Table 8.5. Both the successive ratios of the eigenvalues and the IND function implied three factors, giving a RE value of 12%. Both algorithms produced valid pure peaks. As can be seen from the spectra, spurious peaks do occur, but these are smaller than the experimental error: so, unfortunately, are some of the real peaks,

Table 8.4 Carbon-13 NMR data for Anisole, Benzyl Alcohol and Benzyl Acetate

Concentrations (%)

Expected			Found				
A	B	C	A	B	C		
33	33	33	26	44	30	A	Anisole
10	40	50	6	58	36		
20	30	50	13	48	39	C	Benzyl Alcohol
30	20	50	24	31	45		
40	10	50	36	14	50		
10	50	40	6	67	27		
20	50	30	13	63	25		
50	30	20	40	42	18		
50	40	10	33	66	1		
40	40	20	33	56	11		

Spectra (%)

Shift (ppm)	Expected			Found		
	A	B	C	A	B	C
168.5	-	8	-	4	8	-
157.8	25	-	-	28	-	1
138.9	-	-	19	-	-	32
134.2	-	8	-	9	10	-
127.5	98	-	-	100	-	-
126.3	-	100	72	36	100	72
125.1	-	-	100	12	11	100
118.7	49	-	-	50	-	1
112.0	100	-	-	99	-	-
64.1	-	16	-	4	18	-
62.3	-	-	34	-	3	38
52.8	43	-	-	38	3	-
18.9	-	10	-	1	12	-

Table 8.5 Carbon-13 NMR data for Benzil, Benzophenone and Flavone.

Concentrations (%)

Expected			Found			
A	B	C	A	B	C	
0	100	0	0	100	0	A Flavone
0	0	100	0	6	94	B Benzophenone
100	0	0	97	0	3	C Benzil
10	80	10	2	90	8	
10	10	80	0	9	91	
80	10	10	56	23	21	
33	33	33	13	52	35	
25	50	25	6	66	28	
25	25	50	14	40	46	
25	50	25	29	45	26	

Spectra (%)

Shifts (ppm)	Expected			Found		
	A	B	C	A	B	C
193.6	-	3	-	-	4	-
192.2	-	-	7	-	-	9
175.7	29	-	-	27	1	1
160.7	25	-	-	19	-	1
153.7	22	-	-	22	1	1
135.1	-	10	-	-	11	1
132.6	-	-	45	-	-	46
131.4	41	-	-	42	3	4
130.6	-	-	13	-	1	14
130.0	-	42	1	1	43	1
129.2	40	-	-	43	5	4
127.7	-	86	100	-	97	93
126.7	86	-	78	82	4	100
125.9	-	100	-	-	100	3
123.8	100	-	-	100	6	8
123.2	41	-	-	44	3	4
122.8	33	-	-	37	3	3
121.5	21	-	-	21	-	-
115.8	39	-	-	42	3	5
105.1	43	-	-	43	2	2

and it would be impossible to distinguish between the two. It may be concluded that running the spectra under quantitative conditions has the advantage of reducing the range of peak intensities, thus aiding interpretation of the isolated spectra but that it does not seem to improve the quality of the analysis, although the experiments take a great deal longer.

8.4 Conclusion

A simple method which isolates the spectra and concentrations of components in mixtures based on eigenanalysis and Knorr/Futrell/Malinowski rotation has been developed and used as the basis of a program for a laboratory microcomputer. In addition, a measure of the experimental error is obtained and it may be eliminated from the data if they are reconstructed from the factors. Although the method requires dissimilar spectra and constant experimental conditions, it analyses perfectly data free of error and adequately data sets containing relatively large errors. The reproduction of the concentrations is not, in general, as good as that of the spectra and spurious peaks sometimes occur next to, or in the same rows as, large peaks, but the results are generally acceptable.

References.

1) R.G.Cooks, NBS Special Publications 519, (1979)

2) G.L.Glish, V.M.Shaddock, K.Harman, R.G.Cooks, Anal.Chem., 52 (1980) 165

3) D.Henneberg, Adv.Mass Spectrom., 8B (1980) 1511

4) E.R.Malinowski, D.G.Howery, "Factor Analysis in Chemistry", Wiley-Interscience, New York, 1980

5) I.E.Frank, B.R.Kowalski, Anal.Chem., 54 (1982) 232R

6) K.Levsen, "Fundamental Aspects of Organic Mass Spectrometry", Verlag Chemie, Weinheim, 1975

7) J.Roboz, "Introduction to Mass Spectrometry", Wiley-Interscience, New York, 1968

8) E.G.Johnson, A.O.Nier, Phys.Rev. 91 (1953) 10

9) C.J.Drewery, G.C.Goode, K.R.Jennings, in "MTP International Review of Science: Vol. 5" ed. A.Maccoll, Butterworth, London, 1972

10) C.L.Wilkins, M.L.Gross, Anal.Chem., 53 (1981) 1661A

11) R.S.Lerhle, J.E.Parker, in ref 9.

12) I.Howe, D.H.Williams, R.D.Bowen, "Mass Spectrometry, Principles and Applications", 2nd ed., McGraw-Hill, New York, 1981

13) J.R.Chapman, "Computers in Mass Spectrometry", Academic Press, New York, 1978

14) J.D.Henion, Anal.Chem., 50 (1978) 1687

15) J.J.Brophy, D.Nelson, M.K.Withers, Int.J.Mass Spec.Ion Phys., 36 (1980) 205

16) W.H.McFaddon, H.L.Schwartz, S.J.Evans, J.Chromatog. 122 (1976) 389

17) E.D.Hardin, M.C.Vestal, Anal.Chem., 53 (1981) 1492

18) R.Kraft, A.Otto, A.Makower, G.Etzold, Anal.Biochem., 113 (1981) 193

19) S.E.Unger, A.Vincze, R.G.Cooks, R.Chrisman, L.D.Rothman,
Anal.Chem., 53 (1981) 976

20) A.Maccoll, Org.Mass Spectrom., 17 (1982) 1

21) M.S.B.Munson, F.H.Field, J.Am.Chem.Soc., 88 (1966) 2621

22) K.R.Jennings, in "Gas Phase Ion Chemistry: Vol. 2"
Ed M.Bowers, (1979) 123

23) D.F.Hunt, T.M.Harvey, W.C.Brumley, J.F.Ryan,
J.W.Russel, Anal.Chem., 54 (1982) 492

24) D.F.Hunt, Adv.Mass Spectrom., 6 (1974) 517

25) R.E.Mather, J.F.J.Todd, Int.J.Mass Spec.Ion Phys., 30 (1979) 1

26) R.C.Dougherty, Anal.Chem., 53 (1981) 625A

27) D.F.Hunt, F.W.Crow, Anal.Chem., 50 (1978) 1781

28) K.R.Jennings, Phil.Trans.Roy.Soc.Lond., A293, (1975) 125

29) H.D.Beckley, Angew.Chem.Int.Ed., 8 (1969) 623

30) H.D.Beckley, H.-R.Schulten, Angew.Chem.Int.Ed., 14 (1975) 403

31) R.D.Macfarlane, D.F.Torgenson, Science, 191 (1976) 920

32) M.A.Posthumus, P.G.Kistemaker, H.L.C.Meuzelaur,
M.C.Ten Noever de Brauw, Anal.Chem., 50 (1978) 985

33) A.F.Dillon, R.S.Lehrle, J.C.Robb,
Adv. Mass Spectrom., 4 (1968) 47

34) A.Benninghoven, D.Jaspers, W.Sichtermann,
Appl.Phys. 11 (1976) 35

35) F.M.Devienne, J.C.Roustan, Org.Mass Spectrom., 17 (1982) 173

36) M.Barber, R.S.Bordoli, G.J.Elliot, D.Sedgewick,
A.N.Tyler, Anal.Chem., 54 (1982) 645A

37) M.Barber, R.S.Bordoli, D.Sedgewick, A.N.Tyler,
Nature, 293 (1981) 270

38) J.A.Hipple, E.U.Condon, Phys.Rev., 68 (1945) 54

39) R.G.Cooks, J.H.Beynon, R.M.Caprioli, G.R.Lester,
"Metastable Ions", Elsever, Amsterdam, 1973

40) R.A.Yost, C.G.Enke, Anal.Chem. 51 (1979) 1251A

41) N.R.Daly, A.McCormick, R.E.Powell,
Rev.Sci.Instrum., 39 (1968) 1163

42) T.Wachs, P.F.Bente, F.W.McLafferty,
Int.J.Mass Spec.Ion Phys., 9 (1972) 333

43) J.H.Beynon, R.G.Cooks, J.W.Amy, W.E.Baitinger,
T.Y.Ridley, Anal.Chem., 45 (1973) 1023A

44) D.S.Millington, J.A.Smith, Org.Mass Spectrom. 12 (1977) 264

45) R.S.Stradling, K.R.Jennings, S.Evans,
Org.Mass Spectrom., 13 (1978) 429

46) M.J.Lacey, C.G.Macdonald, Chem.Commun. (1975) 421

47) A.F.Weston, K.R.Jennings, S.Evans, R.M.Elliott,
Int.J.Mass Spec.Ion Phys., 20 (1976) 317

48) M.Barber, R.M.Elliott,Proc.ASTM (E14), Montreal (1964)

49) K.R.Jennings, J.Chem.Phys., 43 (1965) 4176

50) J.H.Futrell, K.R.Ryan, L.W.Sieck,
J.Chem.Phys.,43 (1965) 1832

51) A.P.Bruins, K.R.Jennings, S.Evans,
Int.J.Mass Spec.Ion Phys., 26 (1978) 395

52) R.K.Boyd, C.J.Porter, J.H.Beynon,
Org.Mass Spectrom. 16 (1981) 490

53) K.R.Jennings, to be published

54) M.J.Lacey, C.G.Macdonald, Anal.Chem., 51 (1979) 691

55) W.F.Haddon, Org.Mass Spectrom., 15 (1980) 539

56) B.Shushan, R.K.Boyd, Anal.Chem., 53 (1981) 421

57) J.H.Beynon, A.E.Fontaine, Z.Naturforsch., 22A (1967) 334

58) J.H.Beynon, R.A.Saunders, A.E.Williams,
Z.Naturforsch., 20A (1965) 180

59) F.W.McLafferty, Trends in Anal.Chem. 1 (1982) 298

60) D.J.Burinsky, R.G.Cooks, E.K.Chess, M.L.Gross,

Anal.Chem., 54 (1982) 295

61) F.W.McLafferty, P.J.Todd, A.C.McGilvery, M.A.Baldwin, F.M.Bockofff, G.J.Wendal, M.R.Wixom, T.E.Niemi, Adv.Mass Spectrom., 8B (1980) 1589

62) F.W.McLafferty, Acc.Chem.Res., 13 (1980) 33

63) R.P.Morgan, J.H.Beynon, R.H.Bateman, B.N.Green, Int.J.Mass Spec.Ion Phys., 28 (1978) 171

64) R.A.Yost, C.G.Enke, J.Am.Chem.Soc. 100 (1978) 2274

65) R.A.Yost, C.G.Enke, Int.J.Mass Spec.Ion Phys., 30 (1979) 127

66) P.H.Dawson, J.D.French, J.A.Buckley, D.J.Douglas, D.Simons, Org.Mass Spectrom., 17 (1982) 205

67) D.G.McGilvery, J.D.Morrison, Int.J.Mass Spec.Ion Phys., 28 (1978) 81

68) D.F.Hunt, J.Shabanowitz, A.B.Giordani, Anal.Chem., 52 (1980) 386

69) A.Maquestiau, Y.Van Haverbeke, R.Flammang, M.Abrassant, D.Finnet, Bull.Chim.Soc.Belg., 87 (1978) 765

70) A.Maquestiau, P.Megrant, R.Flammang, Org.Mass Spectrom., 17 (1982) 96

71) D.H.Russel, D.H.Smith, R.J.Warmack, L.K.Bertram, Int.J.Mass Spec.Ion Phys., 35 (1980) 381

72) M.L.Gross, E.K.Chess, P.A.Lyon, F.W.Crow, S.Evans, H.Tudge, Int.J.Mass Spec.Ion Phys., 42 (1982) 243

73) D.J.Burinsky, R.G.Cooks, E.K.Chess, M.L.Gross, Anal.Chem., 54 (1982) 295

74) F.W.McLafferty, P.J.Todd, D.C.McGilvery, M.A.Baldwin, J.Am.Chem.Soc., 102 (1980) 3360

75) J.H.Futrell, C.D.Miller, Rev.Sci.Instrum., 37 (1966) 1521

76) J.H.Beynon, F.M.Harris, B.N.Green, R.H.Bateman, Org.Mass Spectrom., 17 (1982) 55

77) F.M.Alonso, E.J.Finn, "Fields and Waves", Addison-Wesley, Phillipines, 1967

78) W.F.Haddon, Anal.Chem., 51 (1979) 983

79) R.K.Boyd, J.H.Beynon, Org.Mass Spectrom., 12 (1977) 163

80) T.W.Shannon, T.E.Mead, C.G.Warner, F.W.McLafferty, Anal.Chem., 39 (1967) 1748

81) M.Barber, R.M.Elliot, Proc. ATSM(E14) Comm. 1964 Montreal

82) E.Tajima, J.Seibl, Int.J.Mass Spec.Ion Phys., 3 (1969) 245

83) F.W.McLafferty, J.Okomoto, H.W.Major, Org.Mass Spectrom., (1969) 751

84) R.W.Kiser, R.E.Sullivan, M.S.Lupin, Anal.Chem., 41 (1969) 1958

85) J.E.Coutant, F.W.McLafferty, Int.J.Mass Spec.Ion Phys., 8 (1972) 323

86) C-S.Hwang, R.W.Kiser, Int.J.Mass Spec.Ion Phys., 27 (1978) 209

87) A.Fraefel, J.Seibl, Org.Mass Spectrom., 17 (1982) 448

88) A.Fraefel, J.Seibl, Int.J.Mass Spec.Ion Phys., 46 (1983) 284

89) M.J.Lacey, C.G.Macdonald, Org.Mass Spectrom., 12 (1977) 587

90) M.J.Lacey, C.G.Macdonald, K.F.Donchi, P.J.Derrick, Org.Mass Spectrom., 16 (1981) 361

91) M.J.Lacey, C.G.Macdonald, Org.Mass Spectrom., 13 (1978) 243

92) M.J.Lacey, C.G.Macdonald, Aust.J.Chem., 31 (1978) 2161

93) M.J.Lacey, C.G.Macdonald, Int.J.Mass Spec.Ion Phys., 30 (1979) 359

94) M.J.Lacey, C.G.Macdonald, Org.Mass Spectrom., 15 (1980) 135

95) C.G.Enke, J.T.Stults, J.F.Holland, J.D.Pinkerton, J.Allison, J.T.Watson, Int.J.Mass Spec.Ion Phys., 46 (1683) 229
J.T.Stults, C.G.Enke, J.F.Holland, Anal.Chem., 55 (1983) 1323

96) M.J.Farncombe, R.S.Mason, K.R.Jennings, J.Scrivens,

Int.J.Mass Spec.Ion Phys., 44 (1982) 91

97) C.R.Warburton, R.S.Stradling, R.S.Mason, M.J.Farncombe, Org.Mass Spectrom., 16 (1981) 507

98) R.A.Hites, K.Biemann, Anal.Chem., 39 (1967) 965

99) KRATOS Programmers Guide, Kratos Analytical Instruments Ltd, Manchester, 1979.

100) J.H.Beynon, A.E.Fontaine, G.R.Lester, Int.J.Mass Spec.Ion Phys., 1 (1968) 1

101) R.G.Cooks, K.C.Kim, J.H.Beynon, Chem.Phys.Lett., 23 (1973) 190

102) P.H.Hemburger, J.A.Laramee, A.R.Hubik, R.G.Cooks, J.Phys.Chem., 85 (1981) 2355

103) E.E.Kingston, A.G.Brenton, R.K.Boyd, J.H.Beynon, Int.J.Mass Spec.Ion Phys., 47 (1983) 117

104) J.A.Laramee, P.H.Hemburger, R.G.Cooks, Int.J.Mass Spec.Ion Phys., 33 (1980) 231

105) D.J.Burinsky, G.L.Glish, R.G.Cooks, J.J.Zwinselman, N.M.M.Nibbering, J.Am.Chem.Soc., 103 (1981) 465

106) D.M.Fedor, R.G.Cooks, Anal.Chem., 52 (1980) 679

107) V.Franchetti, J.J.Carmody, D.A.Krause, R.G.Cooks, Int.J.Mass Spec.Ion Phys., 26 (1978) 353

108) J.A.Laramee, J.J.Carmody, R.G.Cooks, Int.J.Mass Spec.Ion Phys., 31 (1979) 333

109) T.Ast, D.T.Terwilliger, R.G.Cooks, J.H.Beynon, J.Phys.Chem., 79(1975) 708

110) R.S.Mason, unpublished work.

111) J.A.Laramee, P.H.Hemburger, R.G.Cooks, J.Am.Chem.Soc., 101 (1979) 6460

112) A.R.Hubik, P.H.Hemburger, J.A.Laramee, R.G.Cooks, J.Am.Chem.Soc., 102 (1980) 3997

113) P.J.Todd, R.J.Warmack, E.H.McBay,

Int.J.Mass Spec.Ion Phys., 44 (1982) 91

97) G.R.Warburton, R.S.Stradling, R.S.Mason, M.J.Farncombe, Org.Mass Spectrom., 16 (1981) 507

98) R.A.Hites, K.Biemann, Anal.Chem., 39 (1967) 965

99) KRATOS Programmers Guide, Kratos Analytical Instruments Ltd, Manchester, 1979.

100) J.H.Beynon, A.E.Fontaine, G.R.Lester, Int.J.Mass Spec.Ion Phys., 1 (1968) 1

101) R.G.Cooks, K.C.Kim, J.H.Beynon, Chem.Phys.Lett., 23 (1973) 190

102) P.H.Hemburger, J.A.Laramee, A.R.Hubik, R.G.Cooks, J.Phys.Chem., 85 (1981) 2355

103) E.E.Kingston, A.G.Brenton, R.K.Boyd, J.H.Beynon, Int.J.Mass Spec.Ion Phys., 47 (1983) 117

104) J.A.Laramee, P.H.Hemburger, R.G.Cooks, Int.J.Mass Spec.Ion Phys., 33 (1980) 231

105) D.J.Burinsky, G.L.Glish, R.G.Cooks, J.J.Zwinselman, N.M.M.Nibbering, J.Am.Chem.Soc., 103 (1981) 465

106) D.M.Fedor, R.G.Cooks, Anal.Chem., 52 (1980) 679

107) V.Franchetti, J.J.Carmody, D.A.Krause, R.G.Cooks, Int.J.Mass Spec.Ion Phys., 26 (1978) 353

108) J.A.Laramee, J.J.Carmody, R.G.Cooks, Int.J.Mass Spec.Ion Phys., 31 (1979) 333

109) T.Ast, D.T.Terwilliger, R.G.Cooks, J.H.Beynon, J.Phys.Chem., 79(1975) 708

110) R.S.Mason, unpublished work.

111) J.A.Laramee, P.H.Hemburger, R.G.Cooks, J.Am.Chem.Soc., 101 (1979) 6460

112) A.R.Hubik, P.H.Hemburger, J.A.Laramee, R.G.Cooks, J.Am.Chem.Soc., 102 (1980) 3997

113) P.J.Todd, R.J.Warmack, E.H.McBay,

Int.J.Mass Spec.Ion Phys., 50 (1983) 299

114) S.A.McLuckey, S.Verma, R.G.Cooks, M.J.Farncombe, R.S.Mason, K.R.Jennings, Int.J.Mass Spec.Ion Phys., 48 (1983) 423

115) C.J.Porter, C.J.Proctor, J.H.Beynon, Org.Mass Spectrom., 16 (1981) 62

116) H.R.Morris, Nature, 286 (1980) 447

117) H.H.Morris, Phil.Trans.Roy.Soc.Lond., A293 (1979) 39

118) H.E.Krutzch, J.J.Pisano, Meth.Enzymol., 47 (1977) 391

119) H.E.Krutzch, Biochem.J., 19 (1980) 5290

120) C.V.Bradley, I.Howe, J.H.Beynon, Chem.Commun., (1980) 562

121) C.V.Bradley, I.Howe, J.H.Beynon, Biomed.Mass Spectrom., 8 (1981) 85

122) J.B.Westmore, W.Ens, K.G.Standing, Biomed.Mass Spectrom., 9 (1982) 119

123) D.K.Hunt, W.M.Bone, J.Shabanowitz, J.Rhods, J.M.Ballard, Anal.Chem., 53 (1981) 1704

124) T.Matsuo, H.Matsuda, I.Katakuse, Y.Shimonishi, Y.Maruyama, T.Higuchi, E.Kubota, Anal.Chem., 53 (1980) 416

125) T.Matsuo, H.Matsuda, I.Katakuse, Y.Wada, T.Fujita, A.Hayashi, Biomed.Mass Spectrom., 8 (1981) 25

126) R.Weber, K.Levsen, Biomed.Mass Spectrom., 7 (1980) 314

127) O.M.Desiderio, J.Z.Sabbatini, Biomed.Mass Spectrom., 8 (1981) 56

128) H.R.Morris, M.Panico, M.Barber, R.S.Bordoli, R.D.Sedgewick, A.N.Tyler, Biochem.Biophys.Res.Commun., 101 (1981) 623

129) M.Barber, R.S.Bordoli, R.D.Sedgewick, A.N.Tyler, Biomed.Mass Spectrom., 9 (1982) 208

130) D.H.Williams, C.V.Bradley, S.Santikarn, G.Bojesen, Biochem.J., 210 (1982) 105

131) R.Steinaur, U.P.Schlunegger,

Biomed.Mass Spectrom., 9 (1982) 153

132) R.Steinaur, H.Walther, U.P.Schlunegger,
Helv.Chim.Acta, 63 (1980) 610

133) H.R.Morris, A.Dell, R.A.McDowell,
Biomed.Mass Spectrom., 8 (1981) 463

134) K.Levsen, H-K.Wipf, F.W.McLafferty,
Org.Mass Spectrom., 8 (1973) 117

135) C.J.Porter, A.G.Brenton, J.H.Beynon,
Int.J.Mass Spec.Ion Phys. 36 (1980) 69

136) J.H.Bilton, N.Kyriakidis, E.S.Waight,
Org.Mass Spectrom., 13 (1978) 489

137) R.P.Morgan, C.J.Porter, J.H.Beynon,
Org.Mass Spectrom., 12 (1977) 735

138) R.K.Boyd, B.Shushan, Int.J.Mass Spec.Ion Phys., 37 (1981) 355

139) M.J.Lacey, C.G.Macdonald, Org.Mass Spectrom., 13 (19789) 284

140) A.Fraefel, J.Seibl, Int.J.Mass Spec.Ion Phys., 51 (1983) 245

141) B.Shushan, R.K.Boyd, Int.J.Mass Spec.Ion Phys., 37 (1981) 369

142) L.Horner, H.Hoffmass, H.G.Wippel, Chem.Ber., 91 (1958) 61

143) J.Marsh, "Advanced Organic Chemistry", 2nd Ed.,
McGraw-Hill, Kogakusha, 1977

144) P.A.Cload, D.W.Hutchinson, Org.Mass Spectrom., 18 (1983) 57

145) M.A.Baldwin, F.W.McLafferty,
Int.J.Mass Spec.Ion Phys., 12 (1973) 86

146) T.Keough, J.H.Beynon, R.G.Cooks,
J.Am.Chem.Soc., 95 (1973) 1695

147) J.H.Bowie, T.Blumenthal, J.Am.Chem.Soc., 97 (1975) 2959

148) C.J.Porter, J.H.Beynon, T.Ast,
Org.Mass Spectrom., 16 (1981) 101

149) J.T.Bulmer, H.F.Shurvell, J.Phys.Chem., 77 (1973) 256

150) E.R.Malinowski, P.H.Weiner, J.Am.Chem.Soc., 92 (1970) 4193

151) E.R.Malinowski, P.H.Weiner, J.Phys.Chem., 75 (1971) 1207

152) K.B.Wiberg, W.E.Pratt, W.F.Bailey, Tet.Lett., 49 (1978) 4861

153) P.H.Weiner, E.R.Malinowski, A.Levinstone,
J.Phys.Chem., 74 (1970) 4537

154) P.H.Weiner, D.G.Howery, Anal.Chem., 44 (1972) 1189

155) P.H.Weiner, J.F.Parcher, Anal.Chem., 45 (1973) 302

156) D.Macnaughton, L.B.Rogers, G.Wernimont,
Anal.Chem., 44 (1972) 1421

157) H.B.Woodruff, P.Tway P., I.J.C.Cline Love,
Anal.Chem., 53 (1981) 81

158) P.C.Gillette, J.L.Koenig, App.Spectros., 36 (1982) 535

159) G.C.Ritter, S.R.Lowery, T.L.Isenhour,
Anal.Chem., 48 (1976) 591

160) E.R.Malinowski, M.McCue, Anal.Chem., 49 (1977) 284

161) R.W.Rozett, E.M.Petersen, Anal.Chem., 47 (1975) 1301

162) R.W.Rozett, E.M.Petersen, Anal.Chem., 47 (1975) 2377

163) R.W.Rozett, E.M.Petersen, Anal.Chem., 48 (1976) 817

164) J.M.Halket, R.I.Reed, Org.Mass Spectrom., 10 (1975) 808

165) F.J.Knorr, J.H.Futrell, Anal.Chem., 51 (1979) 1236

166) P.Burke, K.R.Jennings, R.P.Morgan, C.A.Gilchrist,
Anal.Chem., 54 (1982) 1304

167) H.H.Harman, "Modern Factor Analysis",
Univ. Chicago Press (1976)

168) J.Jacobi, J.Rein.Ang.Math. p51 (1846)

169) J.H.Wilkinson, Comp.J., 1 (1958) 90

170) E.R.Malinowski, Anal.Chem., 49 (1977) 606

171) E.R.Malinowski, Anal.Chem., 49 (1977) 612

172) R.B.Catell, Mult.Behav.Res., 1 (1966) 245

173) L.L.Thurstone, "Vectors of the Mind",
Univ.Chicago Press, (1935)

174) J.D.Neuhaus, C.Wrigley, J.Stat.Psych., 7 (1954) 81

175) H.F.Kaiser, Psychomet., 23 (1958) 187

176) E.R.Malinowski, Anal.Chim.Acta, 134 (1982) 129

177) Subroutine EIGEN IBM 1130 Sci.Sub.Lib. ICI Mond Div.

178) Subroutine MX02 Harwell Sub.Lib.
ICI Petrochem.&.Plastics. Div.

179) Abraham R.J., Loftus P., "Proton and Carbon-13 NMR Spectroscopy", Hayden London (1978)

180) I.W.Griffiths, E.S.Mukthar, R.E.March, F.M.Harris, J.H.Beynon, Int.J.Mass Spec.Ion Phys., 39 (1981) 125

181) S.Verma, J.D.Ciupek, R.G.Cooks, A.E.Schoen, P.Dobberstein, Int.J.Mass Spec.Ion Phys., 52 (1983) 311